AD-A192 489 THE COVARIANCE OF SCALAR FIELDS SCATTERED BY PRESSURE-RELEASE RANDOMLY RO..(U) PENNSYLVANIA STATE UNIV UNIVERSITY PARK APPLIED RESEARCH LAB.. 1/2

UNCLASSIFIED J M RESTREPO ET AL. DEC 87 F/G 20/1 NL

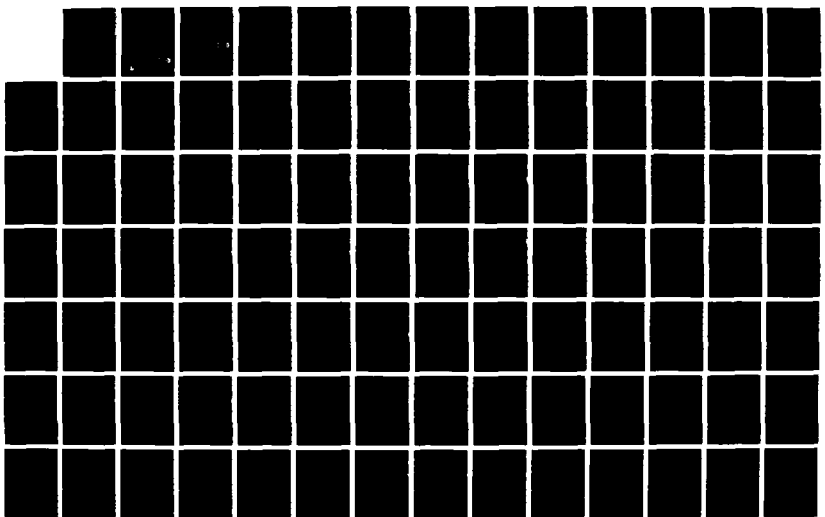

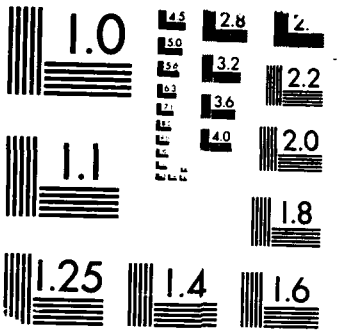

Applied Research Laboratory

Technical Report

THE COVARIANCE OF SCALAR FIELDS SCATTERED BY PRESSURE-RELEASE RANDOMLY ROUGH SURFACES

by

J. M. Restrepo, S. T. McDaniel

PENNSTATE

1855

The Pennsylvania State University
APPLIED RESEARCH LABORATORY
P. O. Box 30
State College, PA 16804

THE COVARIANCE OF SCALAR FIELDS SCATTERED BY PRESSURE-RELEASE RANDOMLY ROUGH SURFACES

by

J. M. Restrepo, S. T. McDaniel

Technical Report No. TR 87-015
December 1987

Supported by:
Office of Naval Research

L. R. Hettche, Director
Applied Research Laboratory

Unclassified
SECURITY CLASSIFICATION OF THIS PAGE

REPORT DOCUMENTATION PAGE

1a. REPORT SECURITY CLASSIFICATION Unclassified	1b. RESTRICTIVE MARKINGS
2a. SECURITY CLASSIFICATION AUTHORITY	3. DISTRIBUTION / AVAILABILITY OF REPORT (A) Unlimited
2b. DECLASSIFICATION / DOWNGRADING SCHEDULE	
4 PERFORMING ORGANIZATION REPORT NUMBER(S) TR-87-015	5. MONITORING ORGANIZATION REPORT NUMBER(S)
6a NAME OF PERFORMING ORGANIZATION Applied Research Laboratory The Penna. State University 6b. OFFICE SYMBOL (If applicable) ARL	7a. NAME OF MONITORING ORGANIZATION Office of Naval Research
6c ADDRESS (City, State, and ZIP Code) P. O. Box 30 State College, PA 16804	7b. ADDRESS (City, State, and ZIP Code) 800 N. Quincy St. Arlington, VA 22217
8a. NAME OF FUNDING / SPONSORING ORGANIZATION Office of Naval Research 8b. OFFICE SYMBOL (If applicable) ONR	9. PROCUREMENT INSTRUMENT IDENTIFICATION NUMBER
8c. ADDRESS (City, State, and ZIP Code) 800 N. Quincy St. Arlington, VA 22217	10. SOURCE OF FUNDING NUMBERS PROGRAM ELEMENT NO. / PROJECT NO. / TASK NO. / WORK UNIT ACCESSION NO.
11 TITLE (Include Security Classification) The Covariance of Scalar Fields Scattered by Pressure-Release Randomly Rough Surfaces	
12 PERSONAL AUTHOR(S) J. M. Restrepo, S. T. McDaniel	
13a TYPE OF REPORT M.S. Thesis 13b. TIME COVERED FROM _____ TO _____ 14. DATE OF REPORT (Year, Month, Day) December 1987 15. PAGE COUNT 172	
16 SUPPLEMENTARY NOTATION	
17 COSATI CODES FIELD / GROUP / SUB-GROUP	18. SUBJECT TERMS (Continue on reverse if necessary and identify by block number) Acoustic fields, Acoustic Scattering, Acoustic spectrum analysis, Acoustic wave coherence, surface wave acoustic devices

19 ABSTRACT (Continue on reverse if necessary and identify by block number)

Expressions for the spatial covariance of the scattered scalar field are presented. The scatterer is a randomly rough pressure-release surface with either Gaussian or Pierson-Stacy wavenumber spectrum.

Three different models are presented: the Standard Model, which utilizes the Helmholtz-Kirchhoff integral as a starting point and uses an integration-by-parts technique to compute the random

20 DISTRIBUTION / AVAILABILITY OF ABSTRACT ☒ UNCLASSIFIED/UNLIMITED ☐ SAME AS RPT ☐ DTIC USERS	21. ABSTRACT SECURITY CLASSIFICATION Unclassified
22a NAME OF RESPONSIBLE INDIVIDUAL	22b. TELEPHONE (Include Area Code) / 22c. OFFICE SYMBOL

DD FORM 1473, 84 MAR — 83 APR edition may be used until exhausted. All other editions are obsolete.

SECURITY CLASSIFICATION OF THIS PAGE
Unclassified

cont'd → normal gradient; the Slope-Operator Model, developed using the Fresnel and Fraunhofer phase approximation, begins with a double-layer potential integral and relies on an operator to compute the dot product of the random normal gradient. Finally, the Composite-Roughness Model, which in essence merges perturbation techniques with the tangent plane formulations of the scattering integral is considered. This last model is presented using the Slope-Operator as well as the integration-by-parts technique. The models are applied to the prediction of scattering strength and coherence so that qualitative comparisons can be made.

→ keywords:)

ABSTRACT

Expressions for the spatial covariance of the scattered scalar field are presented. The scatterer is a randomly rough pressure-release surface with either Gaussian or Pierson-Stacy wavenumber spectrum.

Three different models are presented: the Standard Model, which utilizes the Helmholtz-Kirchhoff integral as a starting point and uses an integration-by-parts technique to compute the random normal gradient; the Slope-Operator Model, developed using the Fresnel and Fraunhofer phase approximation, begins with a double-layer potential integral and relies on an operator to compute the dot product of the random normal gradient. Finally, the Composite-Roughness Model, which in essence merges perturbation techniques with the tangent plane formulations of the scattering integral is considered. This last model is presented using the Slope-Operator as well as the integration-by-parts technique. The models are applied to the prediction of scattering strength and coherence so that qualitative comparisons can be made.

TABLE OF CONTENTS

TABLE OF CONTENTS (Continued)

TABLE OF CONTENTS (Continued)

LIST OF FIGURES

LIST OF FIGURES (Continued)

LIST OF FIGURES (Continued)

LIST OF FIGURES (Continued)

LIST OF FIGURES (Continued)

LIST OF TABLES

LIST OF SYMBOLS

I. Latin Symbols

a_1	argument related to the Fresnel covariance expression 3.45
$\bar{a}_1$	argument related to the Fresnel intensity expression 3.50
a_2	argument related to the Fresnel covariance expression 3.45
$\bar{a}_2$	argument related to the Fresnel intensity expression 3.50
a_2'	argument related to the Fresnel covariance expression 3.45
$\bar{a}_2'$	argument related to the Fresnel intensity expression 3.50
A	ensonified area ($A=\pi UV$). Gaussian source beampattern
$A(\chi)$	spectral amplitude 1.9
$\tilde{A}$	factor related to covariance expression. Standard Model 3.19
$\bar{A}$	factor related to intensity expression. Standard Model 3.20
$A_{1,2}$	factors related to covariance expression. The Slope-Operator Model 3.44
$B_{1,2}$	factors related to covariance expression. Standard Model 3.30
b	factor related to covariance expression. The Slope-Operator Model 3.45
$\bar{b}$	factor related to intensity expression. The Slope-Operator Model 3.50

LIST OF SYMBOLS (Continued)

C	autocorrelation function
C_L	autocorrelation function (large-scale surface)
C_S	autocorrelation function (small-scale surface)
$\langle\ \rangle_{coh}$	coherent component
D	component in difference coordinates of source function 3.4
$\bar{D}$	component in center-of-mass coordinates of source function 3.4
D"	source function in double prime coordinates 2.6
f(θ)	Geometrical function related to the Standard Model (2.21)
$\langle\ \rangle^{Fn}$,$\langle\ \rangle^{Fh}$	Fresnel and Fraunhofer superscripts for the Slope-Operator Model
F(U)	significant component in the integration-by-parts procedure in the Standard Model 2.18
$F(\kappa,\Omega)$	direction function related to the ocean spectrum
g	roughness paramaters ($-k^2\gamma^2\sigma^2$) Intensity
G	roughness parameter ($-k^2\gamma_1\gamma_2\ \sigma^2$) Covariance
G(s)	Normalization function related to the Ocean Spectrum

LIST OF SYMBOLS (Continued)

h_c, h_I	factors related to the covariance and intensity expressions respectively. Slope-Operator Model-Fresnel $\begin{cases} 3.45 \\ 3.50 \end{cases}$
H_c, H_I	factors related to the covariance and intensity expressions respectively. Slope-Operator Model-Fraunhofer $\begin{cases} 3.44 \\ 3.49 \end{cases}$
$\mathbf{k}$	source wavevector with wavenumber k
$k_{1,2}$	wavevector corresponding to double and triple prime coordinates, from surface to receivers
$\mathbf{k}_o$	source wavevector in the Method of Small Perturbations
$\ell_{1,2}$	inverse of the autocorrelation lengths squared
$L_{1,2}$	autocorrelation lengths in the perpendicular and parallel to source directions
$< >_M$	radiation scattered by mirror surface
$M_{1,2}$	arguments related to the Standard Model 3.14
$\hat{n}$	outward normal at the surface
N	normalization constant 4.11
$N_{1,2}$	arguments related to the Standard Model 3.14. Covariance

LIST OF SYMBOLS (Continued)

$N_{1,2}$	arguments related to the Standard Model 3.20. Intensity
P	scattered radiation
P_M	pressure radiation scattered by mirror surface
P	constant related to the Fresnel phase expansion. Intensity expression
P_{total}	source plus scattered pressure at r
P_o	source contribution to the field at r
$P_{1,2}$	constants related to the Fresnel phase expansion
P^+	the sum of P_1 and P_2
P^-	the difference of P_1 and P_2
Q_L	large-scale surface contribution in composite-roughness model 3.61
$Q_{1,2}$	constants related to Fresnel Slope-Operator covariance 3.42
r	general receiver position
r'	source to center of insonified surface area vector
r_1	vector spanning the origin to receiver location 1
r_2	vector spanning the origin to receiver location 2
r'', r'''	vector spanning the origin to general location on the ensonified surface

LIST OF SYMBOLS (Continued)

$r_\perp$	difference coordinates vector
R	Rayleigh parameter
$R_\perp$	center-of-mass coordinates vector
$R_{1,2}$	constants related to composite-roughness model 3.64
R'	distance from a point on ensonified surface to source
$R_{1,2}$	distance from a point on ensonified surface to receiver 1 and 2 respectively
s	parameter of the directional ocean spectrum 4.30
$\mathbf{s}$	vector with components α,β
$\bar{\mathbf{s}}$	vector with components $\bar{\alpha},\bar{\beta}$
S	scattering strength 4.1
$S(\kappa)$	non-directional Pierson-Stacy ocean spectrum
$S(r'')$	shadowing conditional probability distribution function
T	time autocorrelation length
T_o	$=(\gamma_1-\gamma_2)^2/2\gamma_1\gamma_2$. Related to the high frequency asymptote of the Standard Model 3.29
$T_{1,2}$	second order terms from -the expansion of the exponential involving the autocorrelation function in the Standard Model
u	heaviside function and autocorrelation group velocity

LIST OF SYMBOLS (Continued)

U	semimajor axis of the ensonified area 2.6
v	autocorrelation phase velocity
V	semininor axis of the ensonified area 2.6
$W(\chi)$	surface elevation spectrum
x	difference coordinate perpendicular to source normal
$\bar{x}$	center-of-mass coordinate perpendicular to source normal
y	difference coordinate parallel to source normal
$\bar{y}$	center-of-mass coordinate parallel to source normal
$\hat{z}, \hat{z}'$	component orthogonal to r, r' in the Method of Small Perturbation

II. Greek Symbols

$\alpha_1 = - \cos\theta_1 \cos\phi_1$

$\alpha_2 = - \cos\theta_2 \cos\phi_2$

$\alpha = \alpha_1 - \alpha_2$

$\bar{\alpha} = (\alpha_1 + \alpha_2)/2$

$\beta_1 - \cos\theta - \delta_1$

$\beta_2 - \cos\theta - \delta_2$

$\beta = \beta_1 - \beta_2$

$\beta = (\beta_1 + \beta_2)/2$

$\gamma_1 = \sin\theta + \sin\theta_1$

LIST OF SYMBOLS (Continued)

γ_2 $= \sin\theta + \sin\theta_2$

γ_o vertical component of k_o 1.7

γ $= (k^2 - (\xi_o + \chi)^2)^{1/2}$ 1.10

γ' $= (k^2 - (\xi_o + \chi')^2)^{1/2}$ 1.11

γ_{12} complex degree of coherence

Γ $= G(\gamma_1^2 + \gamma_2^2)/(2\gamma_1\gamma_2)$

Γ_{ij} second order moment. When $i \neq j$ it is covariance, otherwise it represents intensity.

δ_1 $= +\cos\theta_1 \sin\phi_1$

δ_2 $= +\cos\theta_2 \sin\phi_2$

ϵ_1 $= -\alpha_1$

ϵ_2 $= -\alpha_2$

ζ'', ζ''' random variable describing the surface in double and triple prime coordinates

θ, θg source grazing angle (see Fig. 2)

θ_1 polar angle of r_1

θ_2 polar angle of r_2

Θ argument of $f(\Theta)$ symbolizing geometrical functional dependence

κ radial component of surface spectrum wavenumber

κ_L cutoff surface spectrum wavenumber

ξ_o horizontal component of k_o in the Method of Small Perturbation

LIST OF SYMBOLS (Continued)

σ	rms height of surface
σ_L	rms height of large scale surface
σ'_x, σ'_y	rms slope of large scale surface
$\sum, \sum'$	range of integration representing the ensonified portion of the scattering surface in TPM theory. Range of integration in the MSP
T	Slope-Operator
ϕ_1	azimuthal angle of r_1
ϕ_2	azimuthal angle of r_2
$\phi(r,r'')$	Green's Function 2.1
Φ	Aperture. Source beamwidth
χ	surface wave vector in cartesian coordinates, with components χ_x, χ_y
$\psi(r'')$	surface dipole distribution
$\omega(\zeta'', \zeta''')$	surface bivariate probability distribution
Ω	angular component of the surface spectrum wavenumber

ACKNOWLEDGMENTS

I wish to express my sincere appreciation to Dr. Suzanne McDaniel, whose thorough knowledge of the subject is a source of inspiration and expert guidance.

Dr. Diana McCammon kindly provided me with the material related to the Pierson-Stacy Spectra. I wish to thank Ms. Pat Green for her patience and expediency in the typing of this report.

Very special thanks goes to Mr. Charles Konzelman, fellow graduate student and friend, who very patiently checked some of the calculations presented in this work and offered his support during times of especially difficult personal circumstances.

This research was performed at the Applied Research Laboratory of The Pennsylvania State University under the support of the Office of Naval Research.

INTRODUCTION

The purpose of this study is to develop an expression for the spatial covariance for the scattered radiation when a randomly rough surface acts as a scatterer. Several properties of the covariance suggest some of the reasons for the development of such an expression. Some of these properties include the following:

1. The normalized covariance is the optimum test of similarity between a pair of field points by the least-squares criterion.
2. The covariance is the Fourier transform pair of the power spectrum density.
3. It responds to field fluctuations.
4. It is less sensitive to inhomogeneities in the propagating medium when compared to the intensity.
5. If the covariance is only a function of coordinate differences, then it follows that there is a uniquely determined fictitious incoherent source, which if placed at infinity, would produce the same coherence across the ensonified scatterer.
6. The correlation function obeys two Helmholtz equations (two wave equations when the disturbance time difference at each receiver is larger than the coherence time) since both the field disturbance as well as the correlation

between these disturbances propagate in the form of waves (1, p. 532).

7. It will enable the computation of the complex degree of coherence.

$$\gamma = \frac{\Gamma_{12}}{\sqrt{\Gamma_{11}}\ \sqrt{\Gamma_{22}}} \qquad (1)$$

where the spatial covariance is $\Gamma_{12} = \langle p(r_1)p^*(r_2)\rangle$

and the intensity is Γ_{ii} , i = 1 or 2, = $\langle p(r_i)p^*(r_i)\rangle$

Thus, this study presents a useful tool in the study of field fluctuations, source localization, and the determination of some physical properties of the scattering surface.

Since Issakovitch (2), Eckart (3), and Rice (4) published their formulations of the intensity of the scattered field some 35 years ago, a considerable number of researchers have made improvements or discussed particulars of the two basic methods that the above-mentioned researchers developed. The two methods are the Tangent-Plane method (or Helmholtz-Kirchhoff diffraction integral) and the Method of Small Perturbations. These have surface-roughness ranges of validity that hardly overlap.

Several alternative models have been proposed, among them the Composite-Roughness Model (5,6,7) which in essence merges the above-mentioned methods by applying the Kirchhoff method and the

perturbation method to the range in which they are valid. This method assumes that the height spectrum can be partitioned, a situation which turns out to be possible in such cases as the sea-surface spectrum. Most of the work in this area done by the acoustics community concerns the sea surface or the sea floor which are assumed to have near-Gaussian roughness distributions, so that most studies involve ideal pressure-release or rigid Gaussian surfaces. The problem of multiple scatter, realistic boundary conditions, surface movement, etc., can make computations exceedingly difficult so it has been customary to present these problems somewhat isolated for the purpose of study.

At present, interest exists in the development of correlation and higher-order moments so that inhomogeneities and fluctuations of the field scattered by the rough surface can be studied. So far in the acoustics literature, one finds relatively few studies on correlation and coherence, most of them being experimental (8,9,10,11,12). Among the theoretical, Bass and Fuks present in their monograph (13) a comprehensive but general discussion on field fluctuations; Clay and Medwin (14) develop approximate expressions for spatial and temporal correlation involving Gaussian surfaces and include the case of a moving surface autocorrelation function. Gulin (15,9,10) uses the Method of Small Perturbations and Parkins (16) arrives at an expression for spatial and temporal correlation using the Neumann-Pierson wave spectrum. Kinney and Clay (17) use

the facet-ensemble method to compare with laboratory data and Eckart's theory.

Three methods are presented in this study. The Method of Small Perturbations (MSP), the Tangent Plane Method (TPM), and the Composite-Roughness Model (CRM). The MSP is presented for completeness and to emphasize its simplicity and the lack of the need to revert to the Kirchhoff approximation. MSP is useful when the surface features are small compared to the source wavelength. It relies on a small parameter expansion (the roughness parameter) of the surface to translate the boundary conditions on the rough surface to the (flat) mean-value plane.

The TPM is presented in two different ways: the Standard Model and the Slope-Operator Model. Both use the Kirchhoff approximation and have the same validity range - the small source wavelength limit - and require that the surface slope change slowly. The standard model begins with the Helmholtz integral and relies on an integration-by-parts procedure in order to eliminate the dependence of the resulting integral on the surface slope terms. The angular dependence is expressed as a function and is taken as nearly constant so that it can be removed from the integral. This model requires the receiver angles be always very close to the specular direction.

The Slope-Operator model begins with the first term in the iterative solution to the double-layer potential integral. It uses

Gaussian properties and analyticity in the surface autocorrelation to change the order of averaging and differentiation in a systematic way, so that the end result is an operator that when applied to the autocorrelation provides the integral with slope corrections.

Lastly, the CRM begins with the usual Helmholtz integral. The surface autocorrelation is split into a part corresponding to the large-scale surface contribution to which the standard method applies, and a part from the small-scale surface contribution on which the MSP works well. The problem is that not all naturally occurring surfaces can be split into two roughness regimes. Another problem had been the choice of the cut-off surface wavenumber, but the implementation of diffractive corrections circumvented (7) adequately the problem and improved the model's behavior. In this study the Fraunhofer phase approximation will be employed for the CRM and the diffractive corrections will be implemented.

This study presents expressions for the covariance and intensity using the Composite Roughness theory, and two formulations of the Tangent Plane Theory. The surfaces in question are stationary Gaussian pressure-release with either Gaussian or Pierson (18) ocean spectrum. Expressions for the mirror-like surface scatter are developed as well so that the coherent and incoherent components may be studied separately. Table 1 provides the reader with an aid in understanding the organization of this study. The

Table 1. Diagram of the organization of this study. In parentheses is the section in which the covariance for each model is first discussed.

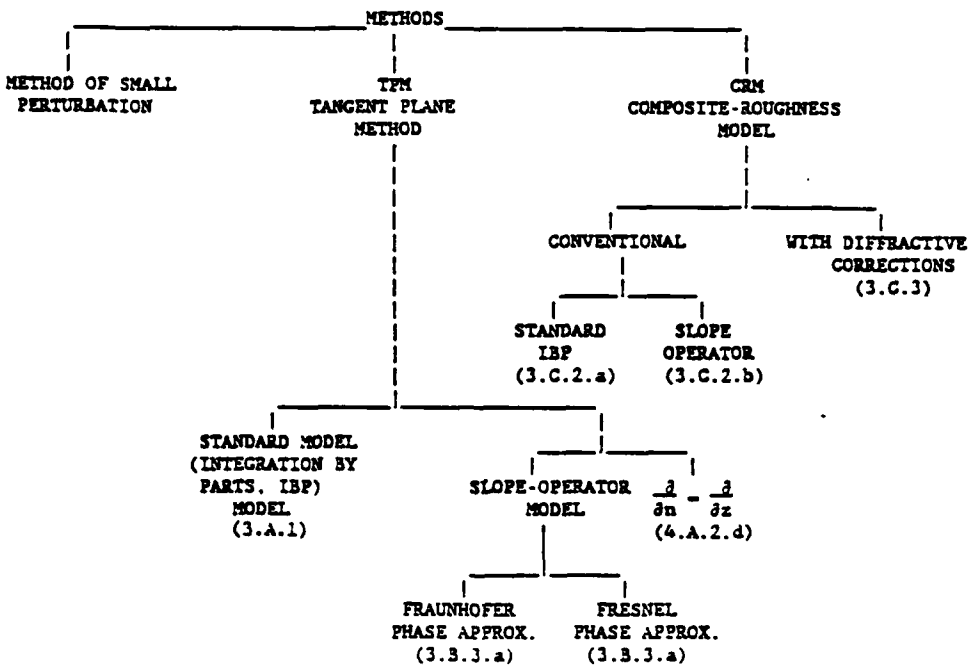

SPECTRUM OF GAUSSIAN SURFACES
- GAUSSIAN
- FLAT
- OCEAN (PIERSON SPECTRUM)

QUANTITIES COMPUTED AND DISPLAYED
- SCATTERING STRENGTH
- COHERENCE MAGNITUDE

table provides the equation numbers in parenthesis which correspond to each model. The intensity provides information about the surface elevation, while the covariance is more sensitive to surface spectrum and source position.

The perturbation approach is presented in the first chapter. The analysis illustrates the fact that this method applies to surfaces with small crest-to-trough elevation amplitudes but poses no restrictions to the steepness of the surface slope. Further, it supposes that the rough surface introduces "fuzziness" to the scattered sound beam. This is in contrast to the tangent-plane method, which proposes that the incident wave suffers Dali-like distortion once it impinges on the scatterer.

A survey of solutions to the Exterior Dirichlet Problem is included in order to emphasize that in TPM there are several alternatives in the formulation of the departing scattering integral. The Helmholtz-Kirchhoff integral lends itself to the integration-by-parts procedure on which the Standard Method is based. The Double-Layer Potential Integral lends itself to the slope-operator procedure. The latter integral leads naturally to a recipe for the study of multiply-scattered radiation problems.

The survey suggests the TPM is a solution in the geometrical acoustics frequency/roughness regime. Further, the Kirchhoff approximation is required, hence the surface may have large crest-to-trough amplitudes but gently changing slope. Lastly, the surface

must be at least twice differentiable and the solution to the scattering integral must satisfy Sommerfeld's radiation conditions.

Chapters 4 and 5 illustrate the scattering strength and coherence predictions of the Tangent-Plane models when a Gaussian, flat surface, or the ocean surface is involved. It is shown that near the specular direction the field is mainly determined by the coherent component and that the incoherent contribution becomes significant in the field strength predictions away from the specular direction. The scattering is better predicted by the Slope-Operator rather than the Standard Model since the latter model mispredicts for angles far away from the specular direction. Shown as well is the fact that when the normal gradient $\partial/\partial n$ is approximated by $\partial/\partial z$, the scattering formula will only display the coherent component of the field. This may be adequate when the surface is mildly rough and/or the autocorrelation lengths are very large.

The Slope-Operator Model is developed using the Fresnel and Fraunhofer phase approximations. Qualitative comparisons are made with regard to the behavior of the model when one or the other phase approximation is used, which show that the Fraunhofer approximation is adequate in the farfield. The plots for scattering strength show that for low grazing angles the Fresnel expression consistently predicts lower energy amplitudes as compared to the Fraunhofer expression and the Standard Model. The Fresnel phase approximation produces expressions for intensity and covariance with real and

imaginary parts. The author speculates, but never proves, that the imaginary part is less significant in the farfield and/or when both the autocorrelation lengths are large and grazing angles small. The coherence plots illustrate that the Standard Model and the Slope-Operator Model predict similar results. The phase is controlled in the farfield by the argument $k(r_1-r_2)$, that is, the wavenumber times the difference between the distances of the receivers to ensonified surface. It is shown as well that the horizontal coherence is insensitive to surface inhomogeneities when the random surface fluctuations are directed in the vertical direction.

CHAPTER I

PERTURBATION METHOD AND THE EXTERIOR DIRICHLET PROBLEM

A. THE METHOD OF SMALL PERTURBATION (MSP)

1. The Scattered Pressure Field

The method of Small Perturbation was applied by Rayleigh (19) to determine the field scattered by periodic surfaces and subsequently applied by such authors as Rice (20), Mandel'shtan (21) to slightly rough random surfaces. This technique, in its simplest form, is included here because it forms a basis for the Composite-Roughness Model.

Following Brekhovskikh (22) closely, the randomly rough pressure-release surface described by $z=\zeta(\mathbf{r})$ with mean value

$$\langle\zeta\rangle = \int_S \zeta(\mathbf{r})dS(\mathbf{r}) = 0 \qquad (1.1)$$

bounds the semi-infinite region $\mathfrak{R}$. This region contains a source generating a time-harmonic pressure field. For simplicity, assume the incident field to be plane waves. Further, assume that the total pressure at $(\mathbf{r},z)$ in $\mathfrak{R}$ satisfies

$$P_{total}(\mathbf{r},z,t)=P_o(\mathbf{r},z,t)+p(\mathbf{r},z,t) \qquad z>\zeta \qquad (1.2)$$

where P_o is the pressure disturbance in the absence of the rough surface. The boundary condition

$$P_{total}(r,\zeta(r)=0 \tag{1.3}$$

is expanded in a power series about z=0. We retain only terms up to 1st order (ζ is small):

$$P_{total} + \zeta \frac{\partial}{\partial z}\left[P_{total}\right] = 0. \tag{1.4}$$

Substituting (1.4) in (1.2) and matching orders we obtain the boundary condition at $z=\langle\zeta\rangle$:

$$P_o = 0 \tag{1.5}$$

$$p = -\zeta \frac{\partial}{\partial z}(P_o) \tag{1.6}$$

The solution to the reduced wave equation subject to Dirichlet boundary conditions is

$$P_o(r,z)=e^{i\xi_0 \cdot r}\{e^{-i\gamma_o z}-e^{+i\gamma_o z}\} \tag{1.7}$$

where $k_o^2 = \xi_o^2 + \gamma_o^2$

and $\xi_o \cdot \hat{r} = \xi_o$, ξ_o is the horizontal component of k_o

$\gamma_o \cdot \hat{z} = -\gamma_o$, γ_o is vertical component of k_o.

Substituting (1.7) in (1.6) and evaluating at z=0

$$P(\mathbf{r},0)=2i\gamma_o\zeta(\mathbf{r})e^{i\xi_o\cdot\mathbf{r}} . \qquad (1.8)$$

Let $A(\chi)$ be the surface spectral amplitude. It is the Fourier Transform of $\zeta(\mathbf{r})$

$$\zeta(\mathbf{r}) = \int_{-\infty}^{\infty} d\chi A(\chi)e^{i(\chi\cdot\mathbf{r})} . \qquad (1.9)$$

Utilizing this representation of $\zeta(\mathbf{r})$, we obtain

$$p(\mathbf{r}',z') = 2i\gamma_o \int_{\infty}^{\infty} d\chi A(\chi)e^{i(\xi_o+\chi)\cdot\mathbf{r}}e^{i\gamma z} \qquad (1.10)$$

$$\text{where } \gamma = (k^2-(\xi_o+\chi)^2)^{1/2} \quad \text{and } Im(\gamma)>0$$

as the final expression for the pressure at $(\mathbf{r},z)$.

2. Spatial Covariance and Intensity

The scattered pressure at $(\mathbf{r}',z')$ is

$$p(\mathbf{r}',z') = 2i\gamma_o \int_{-\infty}^{\infty} d\chi' A(\chi')e^{i(\xi_o+\chi')\cdot\mathbf{r}'+i\gamma' z'} \qquad (1.11)$$

$$\text{with } \gamma' = [k^2-(\xi_o+\chi')^2]^{1/2} .$$

The covariance is the expectation

$$\langle pp'^* \rangle = 4\gamma_o^2 \iint_{\Sigma\Sigma'} d\chi d\chi' \langle A(\chi)A^*(\chi')\rangle$$

$$e^{i\xi_o\cdot(\mathbf{r}-\mathbf{r}')+i(\chi\cdot\mathbf{r}-\chi'\cdot\mathbf{r}')+i(\gamma z-\gamma' z')} . \qquad (1.12)$$

The range of Σ and Σ' are determined by considering contributions from non-attenuating waves, for which the γ's are real.

Assume the surface to be stationary so that the surface correlation of $\zeta(\mathbf{r})$

$$C(\mathbf{r}_\perp) = \langle \zeta(\mathbf{r}_1)\zeta(\mathbf{r}_2)\rangle \tag{1.13}$$

depends only on the separation $\mathbf{r}_\perp = \mathbf{r}_2 - \mathbf{r}_1$.

In such a case $A(\chi)$ and $A^*(\chi')$ are delta correlated (13, p. 43)

$$\langle A(\chi)A^*(\chi')\rangle = W(\chi)\delta(\chi-\chi'), \tag{1.14}$$

where

$$W(\chi) = \frac{1}{(2\pi)^2}\int_{-\infty}^{\infty} d\mathbf{r}_\perp\, C(\mathbf{r}_1)e^{-i\chi\cdot\mathbf{r}_\perp} \tag{1.15}$$

is the spatial spectrum of roughness.

Substituting (1.14) in (1.12) and integrating with respect to χ',

$$\langle pp'^*\rangle = 4\gamma_o^2\int_\Sigma d\chi W(\chi)e^{i(\chi+\xi_o)\cdot\mathbf{r}_\perp+i(\gamma z-\gamma' z')} \tag{1.16}$$

is the covariance. When $(\mathbf{r},z)=(\mathbf{r}',z')$, the intensity

$$\langle pp^*\rangle = 4\gamma_o^2\int_\Sigma d\chi W(\chi) \tag{1.17}$$

is obtained.

3. Discussion

Equation (1.10) implies that to the first approximation each Fourier component of roughness acts as a virtual source giving rise to its own scattered plane wave propagating in the direction (ξ,r), which obeys Bragg's Law (22, p. 177):

$$\xi = \xi_o + \chi \ . \tag{1.18}$$

Equation (1.16) and (1.17) show that the scatter is mainly determined by the surface spectrum, not the height distribution, in the regime in which this method applies. The main feature of MSP is the translation of the boundary condition on $z=\zeta(r)$ to $z=<\zeta>=0$ by means of a Taylor series expansion. This fact restricts its applicability to wavelengths that are large compared to the correlation length ρ of the surface (13, p. 82), or more precisely, to the range

$$R = 2k_o\sigma\sin\theta_g << 1 \tag{1.19}$$

where R is the Rayleigh parameter

k_o is the source wavenumber

σ is the rms height of the surface

θ_g is the grazing angle of the incident wave.

Physically this amounts to each irregularity weakly distorting the field incident on it, and that in the frequency range of validity the roughness of the surface is shallow as seen by the incident wave.

Two alternatives to the MSP will be presented next, one being the popular "Tangent Plane Method" (TPM), which assumes that reflection takes place at each point on the surface according to geometric acoustics (the incoming wave sees a surface that very gradually changes and reflects from the tangent plane at each point of the surface). The problem with this method is that the Kirchhoff approximation is needed to predict the field at the boundary. The other model is a combination of the MSP and the Tangent Plane Method and it assumes that the surface is to be considered as the superposition of gently changing large-scale roughness with an overriding small-scale ripple.

The MSP has been presented, for simplicity, with an incident plane wave. However, the source could just as well generate spherical waves and have a beam pattern. In both the Tangent Plane method and the Composite-Roughness Models, source characterization will play an important role in the following presentation, but this need not be so in the general case (23).

Phenomenologically, it is interesting to note that the MSP and the TPM differ in their prediction of the effect the scattering

surface has on the incoming wave: MSP predicts that the incident wave becomes "fuzzy" or diffuse on reflection whereas TPM predicts a scattered field as a superposition of sharp images of the incident wave producing a "distorted" but well outlined incident wave. The composite-roughness result is a combination of both effects.

B. THE EXTERIOR DIRICHLET PROBLEM

1. Statement of the Problem

The total acoustic pressure at $\mathbf{r}$ in a semi-infinite region $\mathcal{R}$ of isotropic media will be assumed to be the point-wise superposition

$$P_{total}(\mathbf{r},t)=P_o(\mathbf{r},t)+p(\mathbf{r},t), \tag{1.20}$$

where P_o and p are the contributions from the source at $\mathbf{r}'$ and the boundary respectively (see Fig. 1). Our attention centers on the scattered field p, which in the time-harmonic case obeys

$$(\Delta+k^2)p(\mathbf{r})e^{-i\omega t} = 0 \text{ in } \mathcal{R} \tag{1.21}$$

the reduced wave equation, with Dirichlet boundary condition on the randomly rough interface

$$p(\mathbf{r}")=0 \qquad \mathbf{r}" \in S" \tag{1.22}$$

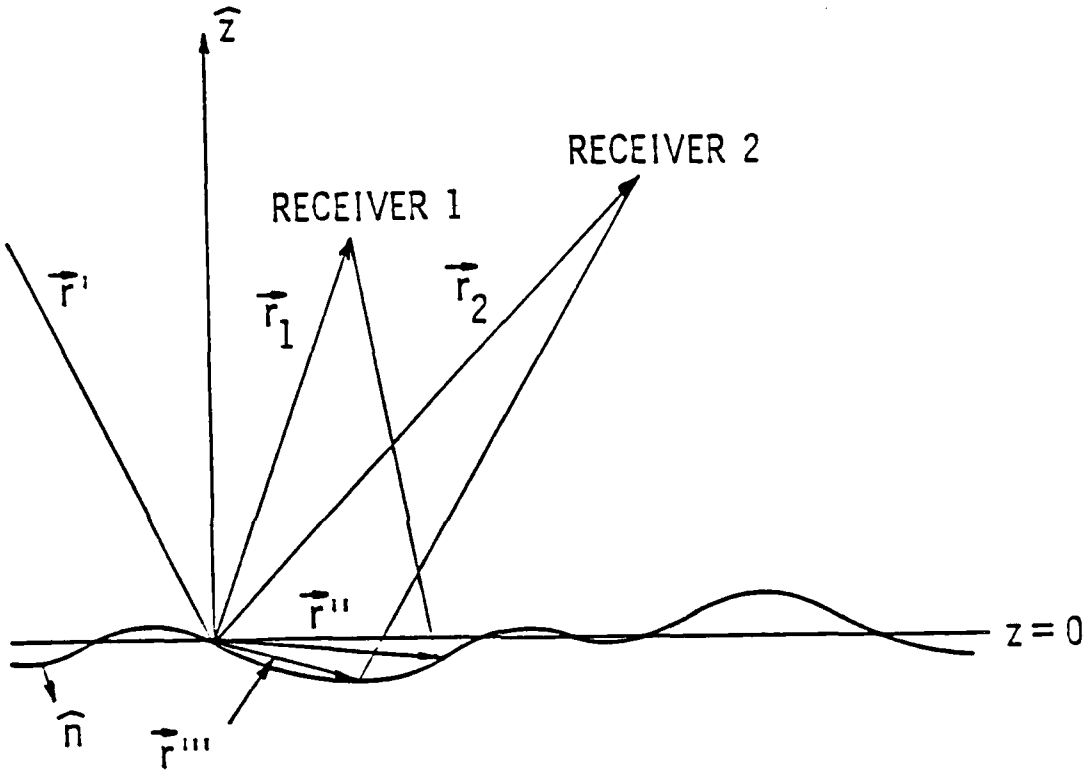

Figure 1. Scattering geometry. Two-dimensional view.

and Sommerfeld's Radiation conditions (24, p. 429)

$$\left(\frac{\partial}{\partial \mathbf{r}} - ik\right)p(\mathbf{r}) = o\left(\frac{1}{|\mathbf{r}|}\right) \tag{1.23}$$

as $|\mathbf{r}| \to \infty$, which guarantees no contribution from regions infinitely far away. This problem is known as the Exterior Dirichlet Problem.

2. Solutions-Survey

The double-layer potential integral (25, 26)

$$p(\mathbf{r}) = \int_{\Sigma} \psi(\mathbf{r}'')\hat{n}''\cdot\nabla''\phi(\mathbf{r},\mathbf{r}'')dS'' \qquad \mathbf{r}'' \in \sum,\ \mathbf{r} \in R \tag{1.24}$$

is known to be a solution. With $\sum$ the portion of the surface S" illuminated by the source,

$\psi(\mathbf{r}'')$ a (unknown) surface dipole distribution and

$\phi(\mathbf{r},\mathbf{r}'') = \frac{1}{4\pi}\frac{e^{ik|\mathbf{r}-\mathbf{r}''|}}{|\mathbf{r}-\mathbf{r}''|}$ is the Fundamental Green's Function with

$k = \frac{\omega}{c}$ the source wave number

The double-layer potential with continuous density ψ is a solution to the Exterior Dirichlet Problem (1.21) (1.22), provided ψ is a solution of the integral equation

$$2p(\mathbf{r}) = \psi(\mathbf{r}) + 2\int_{\Sigma} \psi(\mathbf{r}'')\hat{n}''\cdot\nabla''\phi(\mathbf{r},\mathbf{r}'')dS'' \quad \text{when } \mathbf{r} \in \sum \text{ and } \mathbf{r}'' \neq \mathbf{r}\,. \tag{1.25}$$

This equation, in turn, has a solution if the surface belongs to a class of Lyapunov surfaces (27) and if the density ψ is bounded everywhere on Σ. One important implication of this restriction is

that the correlation function must be analytic, and secondly the function $\zeta(r'')$ describing the surface must be Holder continuous (28).

Both p and ψ are unknown on the surface, but an approximate expression for the pressure for points on the surface is

$$p(\mathbf{r}) = -P_o(\mathbf{r}) \qquad \mathbf{r} \in \sum, \tag{1.26}$$

which is commonly known as the geometrical optics approximation (or one of the Kirchhoff approximations) because it is only approximately true for $k|\mathbf{r}-\mathbf{r}''|>>1$ -- the high frequency regime --. The physical intepretation of (1.26) is that at points corresponding to the surface, the field equals the incident pressure at those points in the absence of the surface. Further, when $\mathbf{r}$ is on the surface S", but not in Σ, the pressure is zero at $\mathbf{r}$. Thus specifying that shadows be infinitely sharp.

Substituting (1.26) in (1.25) and performing the iteration

$$\psi(\mathbf{r}\in\Sigma) = \psi_0 + \psi_1 + \psi_2 \ \ldots \ \psi_m \ \ldots ,$$

where

$$\psi_o(\mathbf{r}) = -\,2\,P_o(\mathbf{r}\in\Sigma) \qquad \mathbf{r}\in\Sigma$$

$$\psi_1(\mathbf{r}) = -\,2\int_{\Sigma_1} \psi_o(\mathbf{r}_1'')\hat{\mathbf{n}}_1''\cdot\nabla_1''\phi(\mathbf{r},\mathbf{r}_1'')\,dS_1'' \qquad \mathbf{r}_1''\in\Sigma_1$$

$$\vdots$$

$$\psi_m(\mathbf{r}) = -\,2\int_{\Sigma_m} \psi_{m-1}(\mathbf{r}_m'')\hat{\mathbf{n}}_m''\cdot\nabla_m''\phi(\mathbf{r},\mathbf{r}_m'')\,dS_m'' \qquad \mathbf{r}_m''\in\Sigma_m$$

$$\vdots \tag{1.27}$$

Retaining only the first two terms in (1.27) and substituting in (1.24)

$$p(\mathbf{r}) = -2\int_{\Sigma} P_o(\mathbf{r}'')\hat{n}''\cdot\nabla''\phi(\mathbf{r},\mathbf{r}'')dS''$$

$$+ 4\int_{\Sigma}\left\{\int_{\Sigma} P_o(\mathbf{r}_1'')\hat{n}_1''\cdot\nabla_1''\phi(\mathbf{r},\mathbf{r}_1'')dS_1''\right\} n''\cdot\nabla''\phi(\mathbf{r},\mathbf{r}'')dS'' - \ldots \qquad (1.28)$$

The first order contribution is recognized as the Rayleigh Diffraction Integral. Equation (1.28) states that the field at $\mathbf{r}$ is a linear combination of n-order multiple scatter terms. The first term represents the singly scattered contribution since the integration over Σ means that the contribution of every point $\mathbf{r}''$ is summed coherently to yield the first-order contribution. The second, that part of the disturbance at points $\mathbf{r}''$ in Σ_1, reradiates in the direction of $\mathbf{r}''$ in Σ, so that the second order contribution to the pressure at $\mathbf{r}$ is the integral over Σ of the coherent sum in Σ of the reradiation to every point $\mathbf{r}''$. Higher order terms in (1.28) represent even more complicated reradiation contributions. This method is particularly well suited for the study of multiple scattering, especially since iteration and superposition are in principle relatively easy to implement on a computer.

In principle it is also possible to formulate the solution to (1.21 and 1.22) by the use of a Single Layer (29) or Simple Source Distribution Integral

$$p(\mathbf{r}) = \int_{\Sigma} \psi(\mathbf{r}'')\phi_s(\mathbf{r},\mathbf{r}'')dS'' \quad \text{in } \mathfrak{R},\ \mathbf{r}'' \in S''. \tag{1.29}$$

Equation (1.29) is a solution to the Exterior Dirichlet Problem in question, provided ψ is a solution to the homogeneous integral equation

$$\int_{\Sigma} \psi(\mathbf{r}'')\phi_s(\mathbf{r},\mathbf{r}'')dS'' = 0 \ . \tag{1.30}$$

The task would be to find ϕ_s which is identically zero at the randomly rough boundary and that satisfies radiation conditions. This makes this formulation very unattractive and will not be discussed further.

Finally, we address the Helmholtz Integral formulation for the scattered field

$$p(\mathbf{r}) = \int_{\Sigma} \left\{ \phi(\mathbf{r},\mathbf{r}'')\mathbf{n}''\cdot\nabla''p(\mathbf{r}'') - p(\mathbf{r}'')\hat{\mathbf{n}}''\cdot\nabla''\phi(\mathbf{r},\mathbf{r}'') \right\} dS'' \quad \begin{matrix} \mathbf{r}'' \in \Sigma \\ \mathbf{r} \in \mathfrak{R}, \end{matrix} \tag{1.31}$$

This is the most frequent starting point for authors discussing the Tangent Plane Method. The formula may be derived using the divergence theorem and Green's identities (30, p. 803; 24, p. 40).

Equation (1.31) requires that the pressure and its normal derivative at each point of the surface be known. For a randomly rough surface this can only be determined approximately, for example, invoking the Kirchhoff approximations,

$$p(\mathbf{r}") = - P_o(\mathbf{r}") \tag{1.32}$$

$$\hat{n}"\cdot\nabla" p(\mathbf{r}") = 2\hat{n}"\cdot\nabla" P_o(\mathbf{r}") \tag{1.33}$$

part of which was used in connection with the dipole layer formulation. If these approximations are made, (1.31) is transformed into

$$p(\mathbf{r}) = 2 \int_{\Sigma} \frac{\partial}{\partial n"} (P_o \phi) dS", \tag{1.34}$$

P_o and ϕ are the doubly differentiable incident pressure and the Fundamental Green's Function respectively, $\hat{n}"$ is the outward normal of the randomly rough surface. This formulation could incorporate multiple scattering if the full integral equation that leads to the Kirchhoff approximations were implemented (29).

Alternatively, ϕ_h can be chosen to be the solution of

$$(\nabla^2 + k^2)\phi_h(\mathbf{r},\mathbf{r}") = - \delta(\mathbf{r}-\mathbf{r}") \tag{1.35}$$

which vanishes at the flat surface z=0. Under this condition (1.31) is

$$p(\mathbf{r}) = - \int_{\Sigma} p(\mathbf{r}") \frac{\partial}{\partial z} \phi_h(\mathbf{r},\mathbf{r}") \Big|_{z=0} dS" \tag{1.36}$$

The solution of (1.36) is arrived at by first making a Taylor series expansion for small σ, the rms height of the surface, much like in MSP, that would translate the boundary condition on the

rough surface back to the surface z=0. This technique is limited to wavelengths much greater than σ but does not rely on the Kirchhoff approximations.

3. Discussion

The previous section enumerates some of the less esoteric formulations of the solution to the Exterior Dirichlet Problem. Each one of these is used as a starting point for the development of different formulations of the TPM. Equation (1.34) and the first term of (1.28) (it is assumed that multiple scatter does not significantly perturb the scattered field) will be developed further in the next chapter. They both incorporate the Kirchhoff approximations, but differ in their starting points as well as in the evaluation of the quantity $\hat{n} \cdot \mathbf{k}$ and the phase in the exponential. Since Kirchhoff's approximations are invoked, diffraction shall be ignored. Thus, surfaces to which the Tangent Plane Method applies may have large crest to trough differences, but slope changes must occur very gradually. Furthermore, it is assumed that the source sees every point on Σ. Otherwise, eqs. (1.32) and (1.26) are replaced by

$$p(\mathbf{r}'') = -S(\mathbf{r}'')P_o(\mathbf{r}'') \qquad (1.37)$$

where S is a shadowing conditional probability function (31) that depends on the source depression angle as well as the height and

slopes of the surface. It is clear that this factor becomes more important for smaller source depression angles, but in this work we shall assume it is always equal to unity.

CHAPTER II

THE TANGENT PLANE METHOD

A. THE TANGENT PLANE METHOD

1. Preliminary

The starting point is the Rayleigh diffraction integral (1.28) and the Helmholtz Integral result (1.34)

$$p(\mathbf{r}_1) = -2 \int_{\Sigma} P_o(\mathbf{r}'')\hat{n}''\cdot\nabla''\phi(\mathbf{r}_1,\mathbf{r}'')dS'' \qquad \text{and} \qquad (2.1)$$

$$p(\mathbf{r}_1) = 2 \int_{\Sigma} \frac{\partial}{\partial n''} \left[P_o(\mathbf{r}'')\phi(\mathbf{r}_1,\mathbf{r}'')\right] dS'' \ . \qquad (2.2)$$

As illustrated in Figure 1, the source at $\mathbf{r}'$ generates spherically spreading waves, limited by the beam function D":

$$P_o = \frac{D''e^{ikR'}}{R'} \qquad (2.3)$$

$$\text{where} \quad R' = |\mathbf{r}'+\mathbf{r}''| \ .$$

The Fundamental Green's Function is

$$\phi(\mathbf{r}_1,\mathbf{r}'') = \frac{1}{4\pi|\mathbf{r}_1-\mathbf{r}''|} e^{ik|\mathbf{r}_1-\mathbf{r}''|} = \frac{1}{4\pi R_1} e^{ikR_1} \qquad (2.4)$$

and has a gradient with normal projection

$$\hat{n}'' \cdot \nabla''\phi(\mathbf{r},\mathbf{r}'') = i\hat{n} \cdot R_1 \left(1 - \frac{1}{ikR_1}\right) \frac{k}{R_1}\phi(\mathbf{r}_1,\mathbf{r}'') \quad \text{where } R_1 = \mathbf{r}_1-\mathbf{r}'' \qquad (2.5)$$

Assume that $kR_1 >> 1$ so that expression (2.5) can be approximated

$$\hat{n}'' \cdot \nabla''\phi(r_1, r'') \doteq \hat{in}'' \cdot k_1 \, \phi(r_1, r'') \qquad (2.6)$$

$$\text{with} \quad k_1 = \frac{kR_1}{R_1}$$

2. The Source Illumination Function

The use of most realistic beam patterns D in equation (2.3) will make the evaluation of (2.1) extremely difficult. Two reasonable approximations for the main lobe of highly directional sources are the aperture type and the Gaussian beam pattern, both absent of sidelobes. Here we assume a Gaussian source with directivity function (32, P. 198)

$$D'' = \exp\left\{ - \left[\frac{x''^2}{V^2} + \frac{y''^2}{U^2} \right] \right\} \qquad (2.7)$$

where $U = \left(\frac{20\log_{10} e}{3} \right)^{1/2} \frac{r' \tan(\frac{\phi}{2})}{\sin\theta}$ is the semimajor axis

$V = \left(\frac{20\log_{10} e}{3} \right)^{1/2} r' \tan(\frac{\phi}{2})$ is the semiminor axis

ϕ is the half-power beamwidth

θ is the source depression angle

so that the surface area A illuminated by the source is simply given by

$$A = \int_{-\infty}^{\infty} dx \int_{-\infty}^{\infty} dy \; e^{-\left(\frac{x^2}{V^2} + \frac{y^2}{U^2}\right)} = \pi UV \qquad (2.8)$$

Further, the source is assumed to have a narrow beamwidth so that the approximations

$$\begin{cases} R' \doteq r' \\ R_1 \doteq r_1 \end{cases} \quad \text{are valid.} \qquad (2.9)$$

Another convenient change that can be made on (2.1) by this choice of D is to change the limits of integration so that the integration is performed over the whole surface. It is this assumption that makes it evident that the choice of source beampattern plays an important role in the development presented here.

3. Fraunhofer and Fresnel Phase Approximations

Both ϕ and P_o (ignoring the source function D) in (2.3) and (2.4) represent spherically spreading waves. The phase in (2.3) and (2.4) is found to be (see Fig. 2)

$$ikR' = ik[x''^2 + (r'\cos\theta + y'')^2 + (r'\sin\theta - \zeta'')^2]^{1/2}$$

$$ikR = ik[r_1\cos\theta_1\cos\phi_1 - x'')^2 + (r_1\cos\theta_1\sin\phi_1 - y'')^2 +$$

$$(r_1\sin\theta_1 - \zeta'')^2]^{1/2} \quad . \qquad (2.10)$$

These can be approximated, retaining the first two terms of the binomial expansion, by

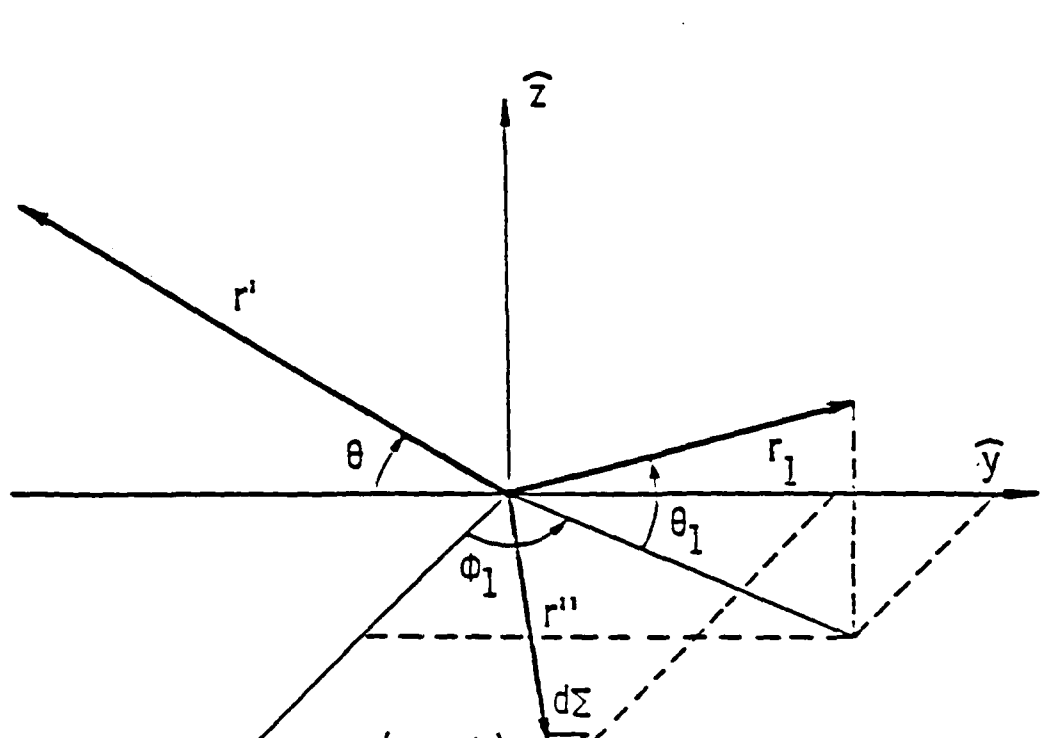

Figure 2. Scattering geometry. Three-dimensional view.

$$ikR' \doteq ik\left[r'+y''\cos\theta-\zeta''\sin\theta + \frac{1}{2r'}\,(x''^2+y''^2)\right] \qquad (2.11)$$

and

$$ikR \doteq ik\left[r_1-(\cos\theta_1\cos\phi_1 x''+\cos\theta_1\sin\phi_1 y''+\sin\theta_1\zeta'') + \frac{1}{2r_1}(x''^2+y''^2)\right]. \qquad (2.12)$$

In the future these two phase appear added

$$ik(R'+R) \doteq ik[r_1+r'+\alpha_1 x''+\beta_1 y''-\gamma_1\zeta''] + ikP_1(x''^2+y''^2), \qquad (2.13)$$

where $\alpha_1 = -\epsilon_1 = -\cos\theta_1\cos\phi_1$

$\delta_1 = -\cos\theta_1\sin\phi_1$

$\beta_1 = (\cos\theta-\delta_1)$

$\gamma_1 = \sin\theta + \sin\theta_1$

$P_1 = \dfrac{r_1+r'}{2r_1r'}$

This expansion is valid when $r'^{-2}\{x''^2+y''^2+2r'(y''\cos\theta-\zeta''\sin\theta)\} < 1$ and $r_1^{-2}\{x''^2+y''^2-2r_1(\epsilon_1 x''+\delta_1 y''+\sin\theta\zeta'')\} < 1$, which physically implies that the source and receivers are far enough so that the largest dimension of the insonified area is still smaller than the source/receiver-to-surface distance. An alternative to the binomial expansion is the replacement of R+R' by a power series in r" about the origin (33,34). The binomial expansion is admittedly poorer than the series expansion, but it is considerably easier to implement.

When the source is far away so that kR' >> 1 then the wave fronts of P_o are locally nearly plane and P_o can be approximated

$$P_o \doteq \frac{D'' e^{ik' \cdot (r' + r'')}}{R'} \tag{2.14}$$

$$\text{with} \quad k' = k \frac{r'}{r'}$$

Similarly ϕ can be approximated if $kR_1 \gg 1$ so that

$$\phi \doteq \frac{1}{4\pi R_1} e^{ik_1 \cdot (r_1 - r'')} \tag{2.15}$$

When the phases of (2.14) and (2.15) are combined, the term in square brackets in (2.13) is obtained. This is labeled the Fraunhofer phase approximation and physically suggests the assumptions made on the shape of the wavefronts. When the approximations in (2.14) and (2.15) are not made, i.e., the wavefronts are allowed to have some curvature, then at least second order terms must be included. When second order terms are retained, as in (2.13), the Fresnel phase approximation is being made. This approximation somewhat complicates computations of the moments of the pressure and shall only be given some attention here when the Slope-Operator Model is discussed.

Before proceeding, (2.1) and (2.2) are restated incorporating the changes discussed so far:

$$p(r_1) = \frac{e^{ik(r_1 + r')}}{2\pi i r_1 r'} \int_{-\infty}^{\infty} dS'' \hat{n}'' \cdot k_1 D e^{ik(\alpha_1 x'' + \beta_1 y'' - \gamma_1 \zeta'' + P_1 [x''^2 + y''^2])} \tag{2.16}$$

$$p(\mathbf{r}_1) = \frac{e^{ik(r_1+r')}}{2\pi i r_1 r'} \int_{-\infty}^{\infty} dS'' \hat{n}'' \cdot (\mathbf{k}-\mathbf{k}_1) D e^{ik(\alpha_1 x'' + \beta_1 y'' - \gamma_1 \zeta'')} \qquad (2.17)$$

$$\text{with } \hat{n}'' = \frac{(\frac{\partial \zeta''}{\partial x''})\hat{x} + (\frac{\partial \zeta''}{\partial y''})\hat{y} - \hat{z}}{[(\frac{\partial \zeta''}{\partial x''})^2 + (\frac{\partial \zeta''}{\partial y''})^2 + 1]^{1/2}}$$

and $dS'' = |\nabla \zeta''| dx'' dy''$.

Equation (2.16) corresponds to the Rayleigh Diffraction Integral expressed so that either Fraunhofer or Fresnel phase approximations can be considered. Equation (2.17) is the Helmholtz integral result and has the Fraunhofer phase approximation.

The evaluation of (2.1 and 2.2) shall be performed in two different ways. One approach shall be labeled "Standard Model" and starts with (2.17). The "Slope Operator Model" uses (2.16) first, with Fraunhofer, and later with the Fresnel phase approximation. The latter model does not make a large grazing angle approximation as will be the need in the Standard Model in order to permit the evaluation involving the normal $\hat{n}''$.

B. DERIVATION OF THE INSTANTANEOUS AND MEAN SCATTERED PRESSURE

1. Standard Method

a. Development

This approach has been preserted with slight variants a great many times. Among the earliest researchers to apply it to the computation of intensity are Issakovitch (2), Eckart (3), and

Brekhovskikh (35). Here we follow the approach presented by Tolstoy and Clay (32) and use the geometry of Figure 2.

Using the Fraunhofer approximation, the difference in the wave-vectors is

$$\frac{1}{k}(\mathbf{k}'-\mathbf{k}_1) = -\epsilon_1\hat{x} + (\cos\theta-\delta_1)\hat{y} - \gamma_1\hat{z} \tag{2.18}$$

with $\epsilon_1 = \cos\theta_1\cos\phi_1$

$\delta_1 = \cos\theta_1\sin\phi_1$

$\gamma_1 = \sin\theta + \sin\theta_1$

so that

$$p(\mathbf{r}_1) = -\frac{e^{ik(r'+r_1)}}{2\pi i r' r_1} k \int_{-\infty}^{\infty} dy'' \int_{-\infty}^{\infty} dx'' D''$$

$$(\alpha_1\zeta''_x+\beta_1\zeta''_y-\gamma_1)e^{ik(\alpha_1 x''+\beta_1 y''-\gamma_1\zeta'')} \tag{2.19}$$

with $\alpha_1 = -\epsilon_1$

$\beta_1 = (\cos\theta-\delta_1)$

ζ''_x, ζ''_y are respectively partials with respect to x" and y" of ζ'' .

The first two terms can be simplified using integration by parts. The first term gives

$$k\int_{-\infty}^{\infty} dx''\alpha_1 D'' e^{ik\alpha_1 x''}(e^{-ik\gamma_1\zeta}\zeta_x'' dx'') = -\frac{\alpha_1}{i\gamma_1} De'' e^{ik(\alpha_1 x''-\gamma_1\zeta'')}\Big|_{-\infty}^{\infty}$$

$$+ k\int_{-\infty}^{\infty} dx'' D'' \frac{\alpha_1^2}{\gamma_1} e^{ik(\alpha_1 x''-\gamma_1\zeta'')} + \int_{-\infty}^{\infty} dx'' \frac{\alpha}{i\gamma_1}\frac{\partial D''}{\partial x''} e^{ik(\alpha_1 x''-\gamma_1\zeta'')}. \tag{2.20}$$

Substituting the explicit form of $\frac{\partial D''}{\partial x''}$ and D'' gives the following result:

$$k\int_{-\infty}^{\infty} dx''\alpha_1 D'' e^{-ik\alpha_1 x''}(e^{-ik\gamma_1\zeta''}\zeta_x'' dx'') = 0$$

$$+ k\int_{-\infty}^{\infty} dx'' \frac{D''\alpha_1^2}{\gamma_1} e^{ik(\alpha_1 x''-\gamma_1\zeta'')} - 2k\int_{-\infty}^{\infty} \frac{dx'' x'' D''\alpha_1}{i\gamma_1 U^2} e^{ik(\alpha_1 x''-\gamma_1\zeta'')}$$

$$= F(U)+G(U) \tag{2.21}$$

For large kU, G(U) falls off faster than F(U). By Schwarz inequality

$$\frac{|G(U)|}{|F(U)|} \propto \frac{1}{kU}$$

so that G(U) is negligible if $kU \gg 1$ is enforced. The procedure is used to perform the y'' integration, yielding

$$p(r_1) \doteq \frac{ie^{ik(r'+r_1)}}{2\pi r' r_1} k\int_{-\infty}^{\infty} dy'' \int_{-\infty}^{\infty} dx'' D'' \frac{(\alpha_1^2+\beta_1^2+\gamma_1^2)}{\gamma_1} e^{ik(\alpha_1 x''+\beta_1 y''-\gamma_1\zeta'')} \tag{2.22}$$

provided that $kV \gg 1$ as well.

Finally, substituting (2.18) in (2.22) and imposing the restriction that changes in the incident and receiver grazing angles be restricted to a small range so that the angular dependence may be removed from the integral, the final result is

$$p(r_1) \doteq ik \frac{e^{ik(r'+r_1)}}{2\pi r_1 r'} f_1(\theta) \iint_{-\infty}^{\infty} D'' e^{ik(\alpha_1 x''+\beta_1 y''-\gamma_1 \zeta'')} dx''dy'' \quad , \tag{2.23}$$

where

$$f_1(\theta) = \frac{1+\sin\theta\sin\theta_1-\cos\theta\cos\theta_1\sin\phi_1}{\sin\theta+\sin\theta_1} \quad . \tag{2.24}$$

(2.23) is valid for angles in the neighborhood of the specular direction and $kU, kV \gg 1$.

If the surface is flat $\zeta''=0$ and the scattered pressure from a flat pressure-release surface or a "mirror" is obtained:

$$p_M(r_1) = \frac{ike^{ik(r'+r_1)}}{2\pi r_1 r'} f_1(\theta) \iint_{-\infty}^{\infty} D'' e^{ik(\alpha_1 x''+\beta_1 y'')} dx''dy'' \tag{2.25}$$

b. <u>The Mean Scattered Pressure</u>

The surfaces to be dealt with will be random stationary, described by $\zeta''(x'',y'')$. $\zeta''(x'',y'')$ is a sample of a stochastic process and the scattered pressure is therefore a random quantity. The ensemble average or "mean" pressure is

$$\langle p(r_1)\rangle = \frac{ike^{ik(r'+r_1)}}{2\pi r_1 r'} f_1(\theta) \iint_{-\infty}^{\infty} D'' e^{ik(\alpha_1 x''+\beta_1 y'')} \langle e^{-ik\gamma_1 \zeta''}\rangle dx''dy'' . \tag{2.26}$$

The interchange between the expectation and integrations is possible when there is uniform convergence. The expression $\langle e^{-ikr_1\zeta''} \rangle$ is recognized as the characteristic function of the random quantity $\zeta''(x'',y'')$

$$\langle e^{-ik\gamma_1\zeta''} \rangle = \int_{-\infty}^{\infty} d\zeta'' \omega(\zeta'') e^{-ik\gamma_1\zeta''} \tag{2.27}$$

where $\omega(\zeta'')$ is the probability density function of heights ζ''. As a special case, consider the Gaussian probability function

$$\omega(\zeta'') = \frac{e^{-\zeta''^2/2\sigma^2}}{\sqrt{2\pi\sigma^2}} \tag{2.28}$$

Substituting (2.28) in (2.27) we obtain

$$\langle e^{-ik\gamma_1\zeta''} \rangle = e^{-g/2} \tag{2.29}$$

where g is the roughness parameter, defined(*) as $g = k^2\gamma_1^2\sigma^2$

The mean scattered pressure for a Gaussian distributed surface is thus

$$\langle p(r_1) \rangle = e^{-g/2} P_M \tag{2.30}$$

* Readers familiar with acoustics literature that deals with scattering from rough surfaces will recognize the quantity $k^2\gamma_1^2\sigma^2$ as defined by g^2. In this study the square is omitted so that $g = k^2\gamma_1^2\sigma^2$.

The factor $e^{-g/2}$ is proportional to the degree of coherence in the scattered radiation. It tends to one for mirror surfaces and to zero as the roughness increases. It is worth noting that (2.30) implies that the average pressure is independent of the spectral composition of the surface.

2. Slope-Operator Model

The slope operator itself will be presented in the context of higher order computations. Described here is the derivation of the field using Rayleigh's diffraction formula. The result presented here will be used later when the operator is derived. This approach appears a few times in the acoustics literature, notably in Welton's report (25), as well as in Boyd and Deavenport's paper (36).

a. Development

The dot product in eq. (2.16) has components

$$(\hat{n}'' \cdot \mathbf{k}_1)_i = \frac{k}{R_1} (r_1 \epsilon_1 - x'') \zeta_x'' \tag{2.31}$$

$$(\hat{n}'' \cdot \mathbf{k}_1)_j = \frac{k}{R_1} (r_1 \delta_1 - y'') \zeta_y'' \tag{2.32}$$

$$(\hat{n}'' \cdot \mathbf{k}_1)_z = \frac{k}{R_1} (r_1 \sin\theta_1 - \zeta'')(-1) \ . \tag{2.33}$$

Let $\Phi'' = \alpha_1 x'' + \beta_1 y'' - \gamma_1 \zeta'' + P_1 [x''^2 + y''^2]$

Equation (2.16) is therefore

$$p(r_1) = \frac{e^{ik(r_1+r')}k}{2\pi i r_1 r'} \int_{-\infty}^{\infty} dx'' \int_{-\infty}^{\infty} dy'' \frac{D'' e^{ik\Phi''}}{R_1}$$

$$\times \{(r_1\epsilon_1 - x'')\zeta_x'' + (r_1\delta_1 - y'')\zeta_y'' - (r_1\sin\theta_1 - \zeta'')\} \qquad (2.34)$$

Rearranging

$$p(r_1) = \frac{e^{ik(r_1+r')}k}{2\pi i r'} \left\{ \iint_{-\infty}^{\infty} dx''dy'' \frac{D'' e^{ik\Phi''}}{R_1} (\epsilon_1\zeta_x'' + \delta_1\zeta_y'' - \sin\theta_1) \right.$$

$$\left. - \iint_{-\infty}^{\infty} dx''dy'' \frac{D''}{R_1} e^{ik\Phi''} \left(\frac{x''\zeta_x'' + y''\zeta_y'' + \zeta''}{r_1} \right) \right\} \qquad (2.35)$$

The second term can be ignored if the beam is sufficiently narrow so that $x'' \ll r_1$ and $y'' \ll r_1$. Further, note that this term is of order r_1^{-1} smaller than the first term. Thus,

$$p(r_1) \doteq \frac{e^{ik(r_1+r')}k}{2\pi i r_1 r'} \iint_{-\infty}^{\infty} D'' e^{ik\Phi''} (\epsilon_1\zeta_x'' + \delta_y'' - \sin\theta_1) dx''dy''. \qquad (2.36)$$

The pressure reflected by a plane pressure-release surface is obtained by letting ζ approach zero:

$$P_M(r_1) = \frac{ike^{ik(r_1+r')}\sin\theta_1}{2\pi r_1 r'} \iint_{-\infty}^{\infty} D'' e^{ik(\alpha_1 x'' + \beta_1 y'' + P_1[x''^2+y''^2])} dx''dy'' \qquad (2.37)$$

In the farfield the Fraunhofer approximation applies, thus $P_1[x''^2+y''^2]=0$. Attention to the matter of phase approximations shall be left to later sections.

b. The Mean Scattered Pressure

Again, assume uniform convergence so that the expectation and spatial integration operations may be exchanged. Thus,

$$\langle p(r_1)\rangle = \frac{ike^{ik(r_1+r')}}{2\pi r_1 r'} \iint_{-\infty}^{\infty} D'' \sin\theta_1 e^{ik(\alpha_1 x''+\beta_1 y''+P_1[x''^2+y''^2])}$$

$$\times \left\langle e^{-ik\gamma_1\zeta''} \left(1- \frac{\epsilon_1 \zeta_x''}{\sin\theta_1} - \frac{\delta_1 \zeta_y''}{\sin\theta_1} \right) \right\rangle dx''dy'' \qquad (2.38)$$

When ζ'' is statistically stationary then the average can be separated from the integrations in x" and y" (25)

$$\langle p(r_1)\rangle = \left\langle e^{-ik\gamma_1\zeta''} \left(1-\frac{\epsilon_1 \zeta_x''}{\sin\theta_1} - \frac{\delta_1 \zeta_y''}{\sin\theta_1} \right) \right\rangle P_M \qquad (2.39)$$

For the special case of Gaussian random process with zero mean height and slopes, (2.39) yields

$$\langle p(r_1)\rangle = e^{-g/2} P_M \qquad (2.40)$$

as before.

3. Discussion

So far the matter of evaluating the dot product involving $\hat{n}''$ has been illustrated. The results in sections 1 and 2 differ in the evaluation of the dot product because the integrals were different to begin with. These discrepancies are apparent when comparing (2.26) and (2.38) as well as the plane pressure release results.

Some authors choose to approximate the average of the random vector $\hat{n}$" by the $\hat{z}$ coordinate unit vector (3) when the slopes are gently changing and have zero mean value on surfaces for which the Tangent Plane Method applies. The slope corrections are increasingly important at lower grazing angles, far from the specular direction, and/or when the height surface spectrum content is high. In the Standard approach the approximation is reasonable since the model only applies to the neighborhood of the specular direction, but it is a severe restriction for the Slope-Operator Model since it is valid for a larger range of grazing angles and incorporates slope corrections.

CHAPTER III

SPATIAL COVARIANCE AND INTENSITY

The general expressions for covariance $\langle p(\mathbf{r}_1)p^*(\mathbf{r}_2)\rangle$ and intensity $\langle p(\mathbf{r})p^*(\mathbf{r})\rangle$ for the scattered pressure involving surfaces with stationary Gaussian height distributions will be presented using the Standard Slope-Operator and Composite-Roughness models.

A. STANDARD MODEL

1. Formulation

Using (2.23) with (2.24), the pressure at $\mathbf{r}_2$ is

$$p(\mathbf{r}_2) \doteq \frac{ike^{ik(r'+r_2)}}{2\pi r' r_2} f_2(\theta)\iint_{-\infty}^{\infty} D'' e^{ik(\alpha_2 x''+\beta_2 y''-\gamma_2 \zeta'')}\,dx''\,dy'' \tag{3.1}$$

$$f_2(\theta) = \frac{1+\sin\theta\sin\theta_2-\cos\theta\cos\theta_2\sin\phi_2}{\sin\theta+\sin\theta_2} \tag{3.2}$$

Hence, the spatial covariance is

$$\langle p(\mathbf{r}_1)p^*(\mathbf{r}_2)\rangle = \frac{k^2 f_1(\theta) f_2(\theta) e^{ik(r_1-r_2)}}{4\pi^2 r'^2 r_1 r_2} \iiiint_{-\infty}^{\infty} D'D''$$

$$e^{ik(\alpha_1 x'-\alpha_2 x''+\beta_1 y'-\beta_2 y'')}\cdot e^{-ik(\gamma_1\zeta'-\gamma_2\zeta'')}\,dx'\,dy'\,dx''\,dy''\rangle \tag{3.3}$$

As usual < > means ensemble average and * means conjugate. For brevity the symbol Γ_{12} shall replace $\langle p(\mathbf{r}_1)p^*(\mathbf{r}_2)\rangle$, the covariance, and Γ_{11} or Γ_{22} for the intensity at $\mathbf{r}_1$ and $\mathbf{r}_2$ respectively. Expediency in computations is improved by changing coordinates to center-of-mass and difference coordinates. Let

$$\bar{x} = \frac{x'+x''}{2} \qquad \bar{y} = \frac{y'+y''}{2}$$

and

$$x = x'-x'' \qquad y = y'-y''$$

Thus

$$\mathbf{r}_\perp = x\hat{i}+y\hat{j}$$

$$\mathbf{R}_\perp = \bar{x}\hat{i}+\bar{y}\hat{j}$$

Since $\left|\frac{\partial(x',x'')}{\partial(x,\bar{x})}\right| = 1$ and $\left|\frac{\partial(y', y'')}{\partial(y,\bar{y})}\right| = 1$ then

$$dx'dy'dx''dy'' = dxd\bar{x}dyd\bar{y}$$

Let $d\mathbf{r}_\perp = dxdy$

$$d\mathbf{R}_\perp = d\bar{x}d\bar{y}$$

Finally, let $\bar{\alpha} = \frac{\alpha_1+\alpha_2}{2}$ $\qquad \beta = \frac{\beta_1+\beta_2}{2}$

$$\alpha = \alpha_1-\alpha_2 \qquad \beta = \beta_1-\beta_2$$

$$\text{so that} \quad \bar{s} = \bar{\alpha}\hat{i}+\bar{\beta}\hat{j}$$

$$s = \alpha\hat{i}+\beta\hat{j}$$

Assuming uniform convergence, the expectation is taken inside the integral in (3.3). We adopt the changes in coordinates and notation to get

$$\Gamma_{12} = \frac{k^2 f_1(\theta) f_2(\theta) e^{ik(r_1 - r_2)}}{4\pi^2 r'^2 r_1 r_2} \int_{-\infty}^{\infty} dr_\perp \int_{-\infty}^{\infty} dR_\perp \, \bar{D} D e^{ik(R_\perp \cdot s + r_\perp \cdot \bar{s})}$$

$$\times \langle e^{-ik(\gamma_1 \zeta'' - \gamma_2 \zeta''')} \rangle \tag{3.4}$$

$$\text{where} \qquad \bar{D} = \exp\{-2[\frac{\bar{x}^2}{U^2} + \frac{\bar{y}^2}{V^2}]\}$$

$$D = \exp\{-\frac{1}{2}[\frac{x^2}{U^2} + \frac{y^2}{V^2}]\}$$

The expression in angular brackets is recognized as the characteristic function of the bivariate probability distribution function ω of the surface, defined as

$$\langle e^{-ik(\gamma_1 \zeta'' - \gamma_2 \zeta''')} \rangle = \int_{-\infty}^{\infty} d\zeta'' \int_{-\infty}^{\infty} d\zeta''' \omega(\zeta'', \zeta''') e^{-ik(\gamma_1 \zeta'' - \gamma_2 \zeta''')} . \tag{3.5}$$

Since it is assumed that the surface is Gaussian in distribution, homogeneous and stationary, the characteristic is computed by first expanding (3.5) in a Maclaurin series:

$$\langle e^{-ik(\gamma_1\zeta'' - \gamma_2\zeta''')}\rangle = \langle 1 - i(\ ) - \frac{k^2}{2!}[\gamma_1^2\zeta''^2 - 2\gamma_1\gamma_2\zeta''\zeta''' + \gamma_2^2\zeta'''^2] + i\frac{1}{3!}(\ )$$

$$+ \frac{k^4}{4!}[\gamma_1^4 y''^4 - 4\gamma_1^3 y''^3\gamma_2\zeta''' + 6\gamma_1^2 y''^2\gamma_2^2\zeta'''^2 - 4\gamma_1\zeta''\gamma_2^3 y'''^3 + \gamma_2^4 y'''^4]\ldots\rangle. \tag{3.6}$$

Following this, the expectation is computed term by term:

$$\langle e^{ik(\gamma_1\zeta'' - \gamma_2\zeta''')}\rangle = 1 - \frac{k^2}{2}(\gamma_1^2\sigma^2 - 2\gamma_1\gamma_2\sigma^2 C + \gamma_2\sigma^2)$$

$$+ \frac{k^4}{4!}(3\gamma_1\sigma_4^4 - 12\gamma_1\gamma_2^3\sigma_4 C + 18\gamma_1\gamma_2^2\sigma_4^2 C^2 - 12\gamma_1\gamma_2\sigma_4^3 C + 3\gamma_1\sigma_4^4)\ldots$$

$$= 1 - k^2\sigma^2\left[\frac{\gamma_1^2+\gamma_2^2}{2} - 2\gamma_1\gamma_2 C\right] + \frac{k^4\sigma^4}{2}\left[\frac{\gamma_1^2+\gamma_2^2}{2} - 2\gamma_1\gamma_2 C\right]^2 \ldots$$

$$= e^{-G\left(\frac{\gamma_1^2+\gamma_2^2}{2\gamma_1\gamma_2} - C\right)} \tag{3.7}$$

where $G = k^2\sigma^2\gamma_1\gamma_2$. If $\gamma_1 = \gamma_2$ then $G = g$ defined previously.

$\sigma = \sqrt{\langle\zeta^2(r_\perp)\rangle}$ is the rms height

$C = C(x,y)$ is the surface autocorrelation.

Substituting (3.7) in (3.4)

$$\Gamma_{12} = \frac{k^2 f_1(\theta) f_2(\theta) e^{ik(r_1 - r_2)} e^{-\Gamma}}{4\pi^2 r'^2 r_1 r_2} \int_{-\infty}^{\infty} dr_\perp D e^{ik(r_\perp \cdot \bar{s})} e^{GC(r_\perp)}$$

$$\times \int_{-\infty}^{\infty} dR_\perp \bar{D} e^{ik(R_\perp \cdot s)} \tag{3.8}$$

$$\text{with} \quad \Gamma = G\left(\frac{\gamma_1^2 + \gamma_2^2}{2\gamma_1\gamma_2}\right)$$

The integration in $R_\perp$ can be performed. From integral tables (37, p. 65.6A)

$$\int_{-\infty}^{\infty} dR_\perp D e^{ik(R_\perp \cdot s)} = \frac{A}{2} e^{-\frac{k^2}{8}(\alpha^2 U^2 + \beta^2 V^2)} \tag{3.9}$$

since $A = \pi UV$

Thus

$$\Gamma_{12} = \frac{Ak^2 f_1(\theta) f_2(\theta) e^{ik(r_1 - r_2)} e^{-\Gamma} e^{-\frac{k^2}{8}(\alpha^2 U^2 + \beta^2 V^2)}}{8\pi^2 r'^2 r_1 r_2}$$

$$\int_{-\infty}^{\infty} dr_\perp D e^{ik(r_\perp \cdot \bar{s})} e^{GC(r_\perp)} \tag{3.10}$$

2. Surface Autocorrelation

a. Gaussian Autocorrelation

The autocorrelation in this case is known to be (38)

$$C(x,y) = \exp\left\{-\frac{x^2}{L_1^2} - \frac{y^2}{L_2^2}\right\} \tag{3.11}$$

where L_1, L_2 are the surface autocorrelation lengths

The exponent involving the autocorrelation is expanded in a series

$$e^{GC} = \sum_{m=o}^{\infty} \frac{G^m}{m!} C^m \tag{3.12}$$

and substituted in (3.10). The summation and integration operations can be interchanged, provided the series is absolutely convergent, so that

$$\Gamma_{12} = \frac{Ak^2 f_1(\theta) f_2(\theta) e^{ik(r_1 - r_2)} e^{-\Gamma - \frac{k^2}{8}(\alpha^2 U^2 + \beta^2 V^2)}}{8\pi r'^2 r_1 r_2} \sum_{m=o}^{\infty} \frac{G^m}{m!}$$

$$\int_{-\infty}^{\infty} dr_\perp DC^m e^{ik(r_\perp \cdot \bar{s})} \quad . \tag{3.13}$$

Finally, the integration with respect to $r_\perp$ is performed

$$\int_{-\infty}^{\infty} dr_\perp DC^m e^{ik(r_\perp \cdot \bar{s})} = \frac{2A}{M_1 M_2} e^{-\frac{k^2}{2}\left[\frac{N_1^2}{M_1^2} + \frac{N_2^2}{M_2^2}\right]}$$

$$M_1 = \sqrt{1+2U^2 m/L_1^2} \qquad N_1 = \bar{\alpha} U$$

$$M_2 = \sqrt{1+2V^2 m/L_2^2} \qquad N_2 = \bar{\beta} V \tag{3.14}$$

M_1 and M_2 are the positive roots.

The covariance is therefore

$$\Gamma_{12} = \frac{A^2k^2f_1(\theta)f_2(\theta)e^{ik(r_1-r_2)}e^{-\Gamma-\frac{k^2}{8}(\alpha^2U^2+\beta^2V^2)}}{4\pi^2r'^2r_1r_2}$$

$$\cdot \sum_{m=o}^{\infty} \frac{(G)^m}{m!} \frac{e^{-\frac{k^2}{8}\left[\left(\frac{N_1}{M_1}\right)^2+\left(\frac{N_2}{M_2}\right)^2\right]}}{M_1M_2} \quad . \tag{3.15}$$

We shall call the m=o term the coherent component. It is equal to

$$\Gamma_{12} = \frac{A^2k^2f_1(\theta)f_2(\theta)e^{-\frac{k^2}{8}[U^2(\alpha^2+4\bar{\alpha}^2)+V^2(\beta^2+4\bar{\beta}^2)]+ik(r_1-r_2)}e^{-\Gamma}}{4\pi^2r'^2r_1r_2} \tag{3.16}$$

The same result is obtained using (2.25) and (2.40), calculating

$$\langle p(r_1)\rangle_M \langle p(r_2)\rangle_M^* e^{-\frac{(g_1+g_2)}{2}}.$$

If the surface is mirror-like, G approaches zero. Thus,

$$\Gamma_{12_M} = \frac{A^2k^2f_1(\theta)f_2(\theta)e^{-\frac{k^2}{8}[U^2(\alpha^2+4\bar{\alpha}^2)+V^2(\beta^2+4\bar{\beta}^2)]}e^{ik(r_1-r_2)}}{4\pi^2r'^2r_1r_2} \tag{3.17}$$

Consequently, (3.16) can be re-expressed:

$$\Gamma_{12_{coh}} = \langle p(r_1)p^*(r_2)\rangle_M e^{-\Gamma} \tag{3.18}$$

so that the degree of coherence can be measured by $e^{-\Gamma}$, and (3.15) is expressed in terms of the coherent and incoherent components

$$\Gamma_{12} = \Gamma_{12M} e^{-\Gamma} \left(1+\bar{A} \sum_{m=1}^{\infty} \frac{(G)^m}{m!} \frac{e^{-\frac{k^2}{2}\left[\left(\frac{N_1}{M_1}\right)^2+\left(\frac{N_2}{M_2}\right)^2\right]}}{M_1 M_2} \right), \qquad (3.19)$$

with a factor $\bar{A} = \exp\{\frac{k^2}{2}(\bar{\alpha}^2U^2+\bar{\beta}^2V^2)\}$.

The intensity is obtained from (3.19) when $r_1=r_2$. The few changes that occur in writing the intensity expression are worth enumerating, since they will be invoked a few times throughout this study:

$$r_1 = r_2 = r$$

$$\gamma_1 = \gamma_2 = \gamma$$

$$\Gamma = g$$

$$\alpha = 0 \qquad \bar{\alpha} = -\epsilon$$

$$\beta = 0 \qquad \bar{\beta} = \cos\theta - \delta$$

from the above, $f_1(\theta)=f_2(\theta)$ and the intensity at r

$$\Gamma_{11} = \Gamma_{11M} e^{-G} \left(1+\tilde{A} \sum_{m=1}^{\infty} \frac{(g)^m}{m!} \frac{e^{-\frac{k^2}{2}\left[\left(\frac{\tilde{N}_1}{M_1}\right)^2+\left(\frac{\tilde{N}_2}{M_2}\right)^2\right]}}{M_1 M_2} \right),$$

with $\tilde{N}_1 = -\epsilon U$ $\quad \tilde{N}_2 = (\cos\theta-\delta)V$ $\quad \tilde{A} = \exp\{\frac{k^2}{2}(\epsilon^2U^2+(\cos\theta-\delta)^2V^2)\}$

and $\Gamma_{11M} = \dfrac{A^2k^2f^2(\theta)e^{-\frac{k^2}{2}[U^2\bar{\alpha}^2+V^2\bar{\beta}^2]}}{4\pi^2(r'r)^2}$ $\qquad (3.20)$

Γ_{11M} resembles the intensity scattered by a mirror-like surface. In the limit, when U and V approach zero, the expression given above equals radiation scattered by an infinite plane surface in the far field -- see Chapter 4. The first term in (3.20) is the coherent component of the intensity:

$$\Gamma_{11coh} = \Gamma_{11M} e^{-g} \qquad (3.21)$$

2. Non-Gaussian Surface Autocorrelation

a. Slightly Rough Surface: or low frequency case, corresponds to GC<<1. The exponent involving G in (3.10) is expanded in a series

$$\Gamma_{12LF} = \frac{Ak^2 f_1(\theta) f_2(\theta) e^{ik(r_1 - r_2)} e^{-\Gamma_e} e^{-\frac{k^2}{8}(\alpha^2 U^2 + \beta^2 V^2)}}{8\pi^2 r'^2 r_1 r_2}$$

$$\times \int dr_\perp D e^{ik(\bar{r}\cdot s)} (1 + GC + \frac{1}{2} G^2 C^2 \ldots) \qquad (3.22)$$

The first term is familiar to us, since it is the coherent term that appears in (3.16). We shall be interested in the first two terms in (3.22). What remains therefore, is the computation of the first term in the incoherent part of the covariance

$$\int_{-\infty}^{\infty} dr_\perp D e^{ik(r_\perp \cdot s)} GC(r_\perp) \qquad (3.23)$$

where $C(r_\perp) = \frac{1}{2\pi\sigma^2} \int_{-\infty}^{\infty} d\chi\, W(\chi) e^{i\chi \cdot r_\perp}$

and W is the two-dimensional surface spectrum and the cartesian surface wavevector is

$$\chi = \chi_x \hat{i} + \chi_y \hat{j} \ .$$

Again, uniform convergence allows the integration with respect to $r_\perp$ be performed first

$$\int_{-\infty}^{\infty} d\chi \frac{GW(\chi)}{2\pi\sigma^2} \int dr_\perp D e^{ik(r_\perp \cdot \bar{s})} C(r_\perp) = \frac{2AG}{2\pi\sigma^2} \iint_{-\infty}^{\infty} d\chi_x d\chi_y W(\chi_x, \chi_y)$$

$$e^{-\frac{1}{2}[(k\bar{\alpha}+\chi_x)^2U^2+(k\bar{\beta}+\chi_y)^2V^2}} \qquad (3.24)$$

Substituting (3.24) and (3.16) into (3.22) we obtain

$$\Gamma_{12LF} \doteq \Gamma_{12coh}$$

$$+ \frac{GA^2k^2 f_1(\theta) f_2(\theta) e^{ik(r_1 - r_2)} e^{-\Gamma} e^{-\frac{k^2}{8}(\alpha^2U^2+\beta^2V^2)}}{8\pi^3\sigma^2 r_1 r_2 r'^2} \iint_{-\infty}^{\infty} d\chi_x d\chi_y W(\chi_x, \chi_y)$$

$$e^{-\frac{1}{2}[(k\bar{\alpha}+\chi_x)^2U^2+(k\bar{\beta}+\chi_y)^2V^2]} \qquad (3.25)$$

For the intensity, again we let $r_1 = r_2 = r$ and (3.25) transforms to

$$\Gamma_{11LF} = \Gamma_{11coh} + \frac{gA^2k^2 f^2(\theta) e^{-g_\infty}}{8\pi^3\sigma^2 (r'r)^2} \iint_{-\infty}^{\infty} d\chi_x d\chi_y W(\chi_x, \chi_y) e^{-\frac{1}{2}[(k\bar{\alpha}+\chi_x)^2U^2 (k\bar{\beta}+\chi_y)^2V^2]}$$

(3.26)

b. Very Rough Surface: or high frequency limit is applicable when GC>>1. The integral in (3.10) can be evaluated after approximating $C(r_\perp)$ by a power series about the origin and using saddlepoint integration.

$$C(x,y) = C(0,0)+x\frac{\partial C(0,0)}{\partial x}+y\frac{\partial C(0,0)}{\partial y}+\frac{1}{2}x^2\frac{\partial^2 C(0,0)}{\partial x^2}+\frac{1}{2}y^2\frac{\partial^2 C(0,0)}{\partial y^2}$$

$$+ xy\frac{\partial^2 C(0,0)}{\partial x \partial y}\ldots \qquad (3.27)$$

The saddle point is at the origin, the value of C(0,0) is one and the first order terms are zero. The surface has symmetry in x,y so that the second order cross term is zero. Impose the restriction that the surface must have at least second order derivatives. Thus

$$C(x,y) \doteq 1 + \frac{1}{2}\left(x^2\frac{\partial^2 C}{\partial x^2}\bigg|_{0,0}+y^2\frac{\partial^2 C}{\partial y^2}\bigg|_{0,0}\right) \qquad (3.28)$$

and $$e^{-\Gamma+GC} = e^{-\frac{G}{2}(T_0-T_1x^2-T_zy^2)} \qquad (3.29)$$

where $$T_0 = \frac{(\gamma_1-\gamma_2)^2}{\gamma_1\gamma_2}$$

$$T_1 = \frac{\partial^2 C(0,0)}{\partial x^2}$$

$$T_2 = \frac{\partial^2 C(0,0)}{\partial y^2}$$

Substituting (3.29) in (3.10) and integrating yields

$$\Gamma_{12HF} \doteq \frac{A^2k^2f_1(\theta)f_2(\theta)e^{ik(r_1-r_2)}}{4\pi^2r'^2r_1r_1B_1B_2}$$

$$\times e^{-\frac{k^2}{8}[U^2(\alpha^2+4\bar{\alpha}^2/B_1^2)+V^2(\beta^2+4\bar{\beta}^2/B_2^2)]}e^{-\frac{G}{2}T_o} \qquad (3.30)$$

for covariance,

where $B_1 = \sqrt{1-GT_1U^2}$ $\qquad$ $B_2 = \sqrt{1-GT_2V^2}$.

Note that T_1 and T_2 are negative, B_1 and B_2 are positive roots.

For intensity (3.30) gives

$$\Gamma_{11HF} \doteq \frac{A^2k^2f^2(\theta)e^{-\frac{k^2}{2}[(\bar{\alpha}^2/B_1^2)U^2+(\bar{\beta}^2/B_2^2)V^2]}}{4\pi^2(r'r)^2B_1B_2} \qquad (3.31)$$

B. THE SLOPE-OPERATOR MODEL

1. Formulation

This model shall be developed using both the Fresnel and Frauhofer approximation. Firstly, using (2.36) the pressure at some point r_2 is derived

$$p(r_2) \doteq \frac{ke^{ik(r_2+r')}}{2\pi ir'r_2}\iint_{-\infty}^{\infty} D\cdots e^{ik\Phi\cdots}(\epsilon_2\zeta\cdots+\delta_2\zeta\cdots-\sin\theta_2)dx\cdots dy\cdots \qquad (3.32)$$

Multiplying (2.36) by the complex conjugate of (3.32) yields

$$p(r_1)p^*(r_2) = \frac{k^2 e^{ik(r_1 - r_2)}}{4\pi^2 r'^2 r_1 r_2} \int\int\int\int_{-\infty}^{\infty} D'' D''' e^{ik(\Phi'' - \Phi''')}$$

$$\times [\epsilon_1 \zeta_x'' + \delta_1 \zeta_y'' - \sin\theta_1][\epsilon_2 \zeta_x''' + \delta_2 \zeta_y''' - \sin\theta_2] dx'' dy'' dx''' dy''' \tag{3.33}$$

and the expectation of (3.33), becomes

$$\langle p(r_1)p^*(r_2)\rangle = \frac{k^2 e^{ik(r_1 - r_2)}}{4\pi^2 r'^2 r_1 r_2} \int\int\int\int_{-\infty}^{\infty} D'' D''' \langle e^{ik(\Phi'' - \Phi''')}$$

$$[\epsilon_1 \zeta_x'' + \delta_1 \zeta_y'' - \sin\theta_1][\epsilon_2 \zeta_x''' + \delta_2 \zeta_y''' - \sin\theta_2]\rangle dx'' dy'' dx''' dy''' \tag{3.34}$$

The random quantity ζ is in the phase, therefore in the center-of-mass and difference coordinates

$$\langle e^{ik(\Phi'' - \Phi''')}\rangle = e^{ik[r_\perp \cdot \bar{s} + R_\perp \cdot s]} \langle e^{-ik(\gamma_1 \zeta'' - \gamma_2 \zeta''')}\rangle$$

$$\cdot e^{ik\left[P^-\left(\frac{x^2+y^2}{4} + \bar{x}^2 + \bar{y}^2\right) + P^+(xy + \bar{x}\bar{y})\right]} \tag{3.35}$$

where $P^+ = P_1 + P_2 \qquad P^- = P_1 - P_2$

The first two exponentials are the familiar Fraunhofer approximation and characteristic function. The third term is the correction necessary so that the Fresnel phase approximation can be presented. This term is the first in the expansion to show coupling among the orthogonal coordinates.

2. The Slope-Operator

Welton (25) and others (39,40) apply a theorem of mathematical statistics (41, p. 68) that postulates

$$\frac{\partial}{\partial q} \langle e^{-ikbz} \rangle = \langle \frac{\partial}{\partial q} e^{-ikbz} \rangle \tag{3.36}$$

where $z=z(q)$, provided the first- and second-order derivative of the autocovariance exist.

Thus,

$$\langle \zeta_x'' e^{-ik(\gamma_1\zeta'' - \gamma_2\zeta''')} \rangle = -\frac{1}{ik\gamma_1} \frac{\partial}{\partial x''} \langle e^{-ik(\gamma_1\zeta'' - \gamma_2\zeta''')} \rangle$$

$$\langle \zeta_x'' \zeta_x''' e^{-ik(\gamma_1\zeta'' - \gamma_2\zeta''')} \rangle = \frac{1}{k^2\gamma_1\gamma_2} \left[\frac{\partial}{\partial x''} \frac{\partial}{\partial x'''} \langle e^{-ik(\gamma_1\zeta'' - \gamma_2\zeta''')} \rangle \right] \tag{3.37}$$

etc.

Application of this theorem allows expressing the averaged quantity in (3.34) as

$$e^{ik[P^-(\frac{x^2+y^2}{4} + \bar{x}^2+\bar{y}^2)+P^+(xy+\bar{x}\bar{y})]} e^{ik[\mathbf{r}_\perp \cdot \bar{\mathbf{s}} + \mathbf{R}_\perp \cdot \mathbf{s}]} T \langle e^{-ik(\gamma_1\zeta'' - \gamma_2\zeta''')} \rangle \tag{3.38}$$

where the Slope-Operator is defined as

$$T(x'',x''',y'',y''')=\sin\theta_1\sin\theta_2+\frac{1}{k^2\gamma_1\gamma_2}\left\{\left[\epsilon_1\epsilon_2\frac{\partial}{\partial x''}\,\frac{\partial}{\partial x'''}+\right.\right.$$

$$+\delta_1\delta_2\,\frac{\partial}{\partial y''}\,\frac{\partial}{\partial y'''}+\epsilon_1\delta_2\frac{\partial^2}{\partial x''\partial y'''}+\delta_1\epsilon_2\frac{\partial^2}{\partial x'''\partial y''}\Big]$$

$$\left.\left.+\ ik\left[\gamma_1\sin\theta_1\left(\epsilon_2\frac{\partial}{\partial x'''}+\delta_2\frac{\partial}{\partial y'''}\right)-\gamma_2\sin\theta_2\left(\epsilon_1\frac{\partial}{\partial x''}+\delta_1\,\frac{\partial}{\partial y''}\right)\right]\right]\right\} \tag{3.39}$$

in the old coordinates. In the new coordinates

$$T(x,y)=\sin\theta_1\sin\theta_2-\frac{1}{k^2\gamma_1\gamma_2}\left\{\left[\epsilon_1\epsilon_2\frac{\partial^2}{\partial x^2}+\delta_1\delta_2\frac{\partial^2}{\partial y^2}+(\epsilon_1\delta_2+\epsilon_2\delta_1)\frac{\partial^2}{\partial x\partial y}\right]\right.$$

$$\left.+ik\left[\gamma_1\sin\theta_1\left(\epsilon_2\frac{\partial}{\partial x}+\delta_2\frac{\partial}{\partial y}\right)+\gamma_2\sin\theta_2\left(\epsilon_1\frac{\partial}{\partial x}+\delta_1\frac{\partial}{\partial y}\right)\right]\right\}\ . \tag{3.40}$$

Incorporating all these changes, as well as replacing the characteristic by eq. (3.7), transforms (3.34) into

$$\Gamma_{12}=\frac{k^2e^{ik(r_1-r_2)}e^{-\Gamma}}{4\pi^2r'^2r_1r_2}\int_{-\infty}^{\infty}dr_\perp\int^{\infty}dR_\perp\ D\bar{D}e^{ik\left[P^-\left(\frac{x^2+y^2}{4}+\bar{x}^2+\bar{y}^2\right)+P^+(xy+\bar{x}\bar{y})\right]}$$

$$\times\ e^{ik(\mathbf{r}_\perp\cdot\bar{\mathbf{s}}+\mathbf{R}_\perp\cdot\mathbf{s})}T_e^{GC(\mathbf{r}_\perp)} \tag{3.41}$$

The first exponential within the integral is identically unity when the Fraunhofer phase approximation is discussed. Since T is an operator in $\mathbf{r}_\perp$ then the integration with respect to $\mathbf{R}_\perp$ can be performed using the result from (3.9)

$$\Gamma_{12}^{FH} = \frac{Ak^2 e^{ik(r_1 - r_2) - \Gamma_e}}{8\pi^2 r'^2 \gamma_1 \gamma_2} e^{-\frac{k^2}{8}[\alpha^2 U^2 + \beta^2 V^2]} \int_{-\infty}^{\infty} dr_\perp \, De^{ikr_\perp \cdot s_{Te}} GC(r_\perp) \tag{3.42}$$

for the Fraunhofer approximation case. Henceforth the superscript Fh indicates Fraunhofer and the superscript Fn indicates the Fresnel result.

The Fresnel result is

$$\Gamma_{12}^{Fn} = \frac{Ak^2 e^{ik(r_1 - r_2)} e^{-\Gamma_e - (\frac{kU\alpha}{2Q_1})^2 - (\frac{kV\beta}{2Q_2})^2 (\frac{kU^2 P^+ \alpha}{\beta} - i2Q_1^2)^2}}{2\pi^2 r'^2 r_1 r_2 W_1}$$

$$\times \int_{-\infty}^{\infty} dr_\perp De^{ik[P^-(\frac{x^2+y^2}{4}) + P^+ xy]} e^{ikr_\perp \cdot \bar{s}_{Te}} GC(r_\perp) \tag{3.43}$$

with $Q_1 = \sqrt{2 - ikP^- U^2}$ $\qquad Q_2 = \sqrt{2 - ikP^- V^2}$

$$W_1 = \sqrt{4Q_1^2 Q_2^2 + (kUVP^+)^2} \quad , \text{ all positive roots}$$

3. Surface Autocorrelation

3.1 Surface with Gaussian Autocorrelation

The autocorrelation for this case appears in (3.11) and the result of the slope operator acting on (3.12) is

$$T\sum_{m=o}^{\infty}\frac{(G)^m}{m!}C^m=\sum_{m=o}^{\infty}\frac{(G)^m}{m!}\left\{-4m^2\left[\epsilon_1\epsilon_2\ell_1^2x^2+\delta_1\delta_2\ell_2^2y^2+(\epsilon_1\delta_2+\epsilon_2\delta_1)\ell_1\ell_2xy\right]\right.$$

$$+2m\left[\epsilon_1\epsilon_2\ell_1+\delta_1\delta_2\ell_2+ik\left\{\gamma_1\sin\theta_1(\epsilon_2\ell_1x+\delta_2\ell_2y)+\gamma_2\sin\theta_2(\epsilon_1\ell_1x+\delta_1\ell_2y)\right]\right.$$

$$\left.\left.+k^2\gamma_1\gamma_2\sin\theta_1\sin\theta_2\right\}\frac{C^m(x,y)}{k^2\gamma_1\gamma_2}\right.$$

$$\text{where } \ell_1=\frac{1}{L_1^2}\qquad \ell_2=\frac{1}{L_2^2} \tag{3.44}$$

The integration with respect to $r_\perp$ is performed after exchanging the integration and summation operations in (3.42) and (3.43) and incorporating the results of (3.44):

$$\Gamma_{12}^{Fh}=H_c\sum_{m=o}^{\infty}\frac{G^m}{m!}\frac{e^{-\frac{k^2}{4}\left(\frac{\bar\alpha^2}{A_1}+\frac{\bar\beta^2}{A_2}\right)}}{\sqrt{A_1A_2}}\left[k^2\gamma_1\gamma_2\sin\theta_1\sin\theta_2\right.$$

$$+2m\left\{\epsilon_1\epsilon_2\ell_1+\delta_1\delta_2\ell_2-\frac{k^2\gamma_1\sin\theta_1}{2}\left(\frac{\ell_1\epsilon_2\bar\alpha}{A_1}+\frac{\ell_2\delta_2\bar\beta}{A_2}\right)\right.$$

$$\left.-k^2\gamma_2\frac{\sin\theta_2}{2}\left(\frac{\ell_1\epsilon_1\bar\alpha}{A_1}+\frac{\ell_2\delta_1\bar\beta}{A_2}\right)\right\}$$

$$\left.+m^2\left\{\frac{k^2\bar\alpha\bar\beta\ell_1\ell_2}{A_1A_2}(\epsilon_1\delta_2+\epsilon_2\delta_1)+\frac{\epsilon_1\epsilon_2\ell_1^2}{A_1^2}(k^2\bar\alpha^2-2A_1)+\frac{\delta_1\delta_2\ell_2^2}{A_2^2}(k^2\bar\beta^2-2A_2)\right\}\right] \tag{3.45}$$

where $H_c = \dfrac{A\, e^{ik(r_1 - r_2)}\, e^{-\Gamma}\, e^{-\frac{k^2}{8}[\alpha^2U^2+\beta^2V^2]}}{8\pi r'^2 r_1 r_2 \gamma_1 r_2}$

and $A_1 = \dfrac{1}{2U^2} + m\ell_1 \qquad A_2 = \dfrac{1}{2V^2} + m\ell_2$

for the Fraunhofer case. For the Fresnel approximation the same computation gives

$$\Gamma_{12}^{Fn} = h_c \sum_{m=o}^{\infty} \frac{G^m}{m!} \frac{\exp\left(-k^2\left[\dfrac{\bar{\beta}^2 a_1 + \bar{\alpha}^2 a_2 + ikP^+\bar{\alpha}\bar{\beta}}{4a_1 a_2 + k^2 P_+^2}\right]\right)}{\sqrt{4a_1 a_2 + k^2 P_+^2}} \Bigg\{ k^2 \gamma_1 \gamma_2 \sin\theta_1 \sin\theta_2$$

$$+m\left[\frac{k^2 \ell_1}{a_1}(\epsilon_2\gamma_1\sin\theta_1 + \epsilon_1\gamma_2\sin\theta_2)\left(\frac{P^+ b}{a_2'} - \bar{\alpha}\right) - 2ik(\delta_2\gamma_1\sin\theta_1 + \delta_1\gamma_2\sin\theta_2)\frac{\ell_2 b}{a_2'}\right.$$

$$\left. + 2\epsilon_1\epsilon_2\ell_1 + 2\delta_1\delta_2\ell_2\right]$$

$$-2m^2\left[\frac{\epsilon_1\epsilon_2\ell_1^2}{a_1^2}\left(a_1 - \frac{k^2\bar{\alpha}^2}{2} + \frac{P^+\bar{\alpha}k^2 b}{a_2'} - \frac{k^2 P^{+2}}{4a_2'^2}\,[2b^2 + a_2']\right)\right.$$

$$\left. - ik(\epsilon_1\delta_1 + \epsilon_2\delta_1)\,\frac{\ell_1\ell_2}{a_1}\left[\frac{\bar{\alpha}b}{a_2'} - \frac{P^+}{2}\left(\frac{2b^2 + a_2'}{a'^2}\right)\right] + \delta_1\delta_2\ell_2^2\left[\frac{2b^2 + a_2'}{a'^2}\right]\right]\Bigg\} \tag{3.46}$$

with $h_c = \dfrac{Ak^2 e^{ik(r_1 - r_2)}\, e^{-\Gamma}\, e^{-\left(\frac{kU\alpha}{2Q_1}\right)^2 + \left(\frac{kV\beta}{2Q_1 W_1}\right)^2 \left(\frac{kU^2 P^+\alpha}{\beta} - i2Q_1^2\right)^2}}{\pi r'^2 r_1 r_2 W_1 k^2 \gamma_1 \gamma_2}$

$$a_1 = \left(\frac{Q_1^2}{2U}\right) + m\ell_1 \qquad a_2 = \left(\frac{Q_2^2}{2V}\right) + m\ell_2 \qquad a' = a_2 + \frac{k^2 P^{+2}}{4a_1}$$

and $b = \frac{1}{2}\left(\frac{P^+\bar{\alpha}k^2}{2a_1} - ik\bar{\beta}\right)$

The coherent component in either approximation is

$$\Gamma_{12\ coh}^{\ j} = \Gamma_{12}^{\ j}{}_{M}\, e^{-\Gamma} \qquad j = \text{Fh or Fn} \tag{3.47}$$

and the covariance from a mirror-like surface is

$$\Gamma_{12\ M}^{\ Fh} = \frac{A^2k^2 e^{-\frac{k^2}{8}[U^2(\alpha^2+4\bar{\alpha}^2)+V^2(\beta^2+4\bar{\beta}^2)]}\, e^{ik(r_1-r_2)} \sin\theta_1 \sin\theta_2}{4\pi^2 r_1 r_2 r'^2}\ , \tag{3.48}$$

for the Fraunhofer case, obtained by taking the m=0 term from (3.45) and letting σ and L_1, L_2 approach zero and infinity, respectively. For the Fresnel approximation we use (3.46) and perform the identical procedure

$$\Gamma_{12\ M}^{\ Fn} = \frac{A^2k^2 e^{ik(r_1-r_2)}\, e^{-\left(\frac{kU\alpha}{2Q_1}\right)^2+\left(\frac{kV\beta}{2Q_1W_1}\right)^2\left(\frac{k^2P^+\alpha}{\beta} - i2Q_1^2\right)^2}}{\pi^2 r_1 r_2 r'^2 W_1 \sqrt{(Q_1Q_2)^2+(2UVkP^+)^2}}$$

$$\times \frac{e^{-\left[k^2\left(\frac{(\bar{\alpha}Q_2U)^2+(\bar{\beta}Q_1V)^2+ik\bar{\alpha}\bar{\beta}U^2V^2}{(Q_1Q_2)^2+(2UVkP^+)^2}\right)\right]} \sin\theta_1 \sin\theta_2}{\pi^2 r_1 r_2 r'^2 W_1 \sqrt{(Q_1Q_2)^2+(2UVkP^+)^2}}\ . \tag{3.49}$$

To get the intensity we let $\mathbf{r}_1$ equal to $\mathbf{r}_2$, (3.45) and (3.46) for the Fraunhofer case,

$$\Gamma_{11}^{Fh} = H_I \sum_{m=o}^{\infty} \frac{g^m}{m!} \frac{e^{-\frac{k^2}{4}\left(\frac{\epsilon^2}{A_1} + \frac{(\cos\theta-\delta)^2}{A_2}\right)}}{\sqrt{A_1 A_2}}$$

$$\times \left[k^2\gamma^2\sin^2\theta_1 + 2m\left\{\epsilon^2\ell_1 + \delta^2\ell_2 + k^2\gamma\sin\theta_1\left[\frac{\ell_1\epsilon^2}{A_1} - \ell_2\,\frac{\delta(\cos\theta-\delta)}{A_2}\right]\right\}\right.$$

$$\left. + m^2\left(\frac{\epsilon^2\ell_1^2}{A_1^2}(k^2\epsilon^2 - 2A_1) + \frac{\delta^2\ell_2^2}{A_2^2}(k^2(\cos-\delta)^2 - 2A_2) - \frac{2k^2\ell_1\ell_2}{A_1A_2}\cos(\theta-\delta)\delta\epsilon^2\right)\right] \tag{3.50}$$

with $H_I = \dfrac{Ae^{-g}}{8\pi(r'r)^2\gamma^2}$

and

$$\Gamma_{11}^{Fn} = h_I \sum_{m=o}^{\infty} \frac{g^m}{m!} \frac{\exp\left\{-k^2\left[\dfrac{\bar{\beta}^2\bar{a}_1 + \bar{\alpha}^2\bar{a}^2 + ikP\bar{\alpha}\bar{\beta}}{4\bar{a}_1\bar{a}_2 + k^2P^2}\right]\right\}}{\sqrt{4\bar{a}_1\bar{a}_2 + k^2p^2}} \left(k^2\gamma^2\sin^2\theta\right.$$

$$+ m\left[\frac{2k^2\ell_1}{\bar{a}_1}\epsilon\gamma\sin\theta_1\left(\frac{\bar{P}\bar{b}}{\bar{a}_2} - \bar{\alpha}\right) - 4ik\delta\gamma\sin\theta_1\ell_2\,\frac{\bar{b}}{\bar{a}_2} + 2\epsilon^2\ell_1 + 2\delta^2\ell_2\right]$$

$$\left. - 2m^2\left[\frac{\epsilon^2\ell_1^2}{\bar{a}_1^2}\left(\bar{a}_1 - \frac{k^2\bar{\alpha}^2}{2} + \frac{\bar{P}\bar{\alpha}k^2\bar{b}}{\bar{a}_2'} - \frac{k^2p^2}{4\bar{a}_2'}\right)[2\bar{b}^2 + \bar{\alpha}_2^2]\right]\right) \tag{3.51}$$

$$-2ik\epsilon\delta\ \frac{\ell_1\ell_2}{\bar{a}_1}\ (\frac{\bar{\alpha}\bar{b}}{\bar{a}_2'}\ -\ \frac{P}{2}(\frac{2\bar{b}^2+\bar{a}_2'}{\bar{a}_2'^2}))+\delta^2\ell_2^2[\frac{2\bar{b}^2+\bar{a}_2'}{\bar{a}_2'^2}]])$$

with $h_I = \dfrac{Ae^{-g}}{\pi^2(r'r)^2\sqrt{16+(kUVP)^2}\ \gamma^2}$

and $\bar{a}_1 = \frac{1}{2U^2}+m\ell_1$

$\bar{a}_2 = \frac{1}{2V^2} + m\ell_2 \qquad \bar{a}' = a_2 + \frac{k^2P^2}{4a_1} \qquad \bar{b} = \frac{1}{2}(\frac{P\bar{\alpha}k^2}{2a_1}-ik\bar{\beta})$

with $P = \dfrac{r'+r}{r'r}$.

Again, the coherent component of the intensity is

$$\Gamma_{11\ coh} = \Gamma_{11\ M}\ e^{-g} \tag{3.52}$$

with $\Gamma_{11\ M}^{Fh} = \dfrac{A^2k^2e^{-\frac{k^2}{2}[U^2\bar{\alpha}^2+V^2\bar{\beta}^2]}}{4\pi^2(r'r)^2}\sin^2\theta_1$ (3.53)

and $\Gamma_{11\ M}^{Fn} = \dfrac{A^2k^2\sin^2\theta_1\exp(-\frac{k^2}{2}[\frac{2(\bar{\alpha}U)^2+2(\bar{\beta}V)^2+ik\bar{\alpha}\bar{\beta}(UV)^2}{1+(kPUV)^2}]}{\pi^2(r'r)^2\sqrt{[16+(kPUV)^2][1+(kPUV)^2]}}$

(3.54)

the covariance can be expressed in terms of its coherent and incoherent component as

$$\Gamma_{12}^{Fh} = \frac{A^2k^2e^{-\frac{k^2}{8}[U^2(\alpha^2+4\bar{\alpha}^2)+V^2(\beta^2+4\bar{\beta}^2)]}\, e^{ik(r_1-r_2)}e^{-\Gamma\sin\theta_1\sin\theta_2}}{4\pi^2e^{12}r_1r_2}$$

$$\cdot\{1+\frac{\pi e^{\frac{k^2}{2}(\bar{\alpha}^2U^2+\bar{\beta}^2V^2)}}{2Ak^2\gamma_1\gamma_2\sin\theta_1\sin\theta_2}\sum_{m=1}^{\infty}\frac{G^m}{m!}\frac{e^{-\frac{k^2}{4}[\frac{\alpha^2}{A_1}+\frac{\beta^2}{A_2}]}}{\sqrt{A_1A_2}}[\quad]\}$$

(3.55)

where the argument in square brackets [ ] is that of (3.45). Similarly, the intensity is

$$\Gamma_{11}^{Fn} = \frac{A^2k^2e^{-\frac{k^2}{2}[U^2\epsilon^2+V^2(\cos\theta-\delta)^2]}\, e^{-g\sin^2\theta_1}}{4\pi^2(r'r)^2}$$

$$\times\ \{1+\frac{\pi e^{\frac{k^2}{2}(U^2\epsilon^2+V^2(\cos\theta-\delta)^2)}}{2Ak^2\gamma^2\sin^2\theta_1}\sum_{m=1}^{\infty}\frac{g^m}{m!}\frac{e^{-\frac{k^2}{4}[\frac{\epsilon^2}{A_1}+\frac{(\cos\theta-\delta)^2}{A_2}]}}{\sqrt{A_1A_2}}[\quad]\}$$

(3.56)

The first term in both expressions is their respective coherent component.

b. Non-Gaussian Surface Autocorrelation in the Farfield

1. Preliminaries

The Fresnel phase approximation result shall not be considered herein, hence there is a need to specify that source and receivers

be in the farfield and the beamwidth be sufficiently narrow. The criteria for farfield for the Tangent Plane methods was developed and discussed by Welton (25) and can be summarized, for the worst case (specular direction) intensity computations he finds that

$$\frac{\sigma}{L} \geq \frac{1.345}{2^{1/2}} \left(1+\frac{rR'}{r_i}\right) \frac{\tan^2(\frac{\phi}{2})}{\sin\theta_i} \quad . \tag{3.57}$$

In the nonspecular direction the criteria is less stringent. For covariance, both receivers must satisfy the above criterion, thus r and θ_i must assume the values of the respective receiver. Furthermore, we limit ourselves to presenting results valid for the surfaces with onmidirectional spectra, hence $L_1=L_2=2^{-1/2}L$.

The same high and low frequency approximation performed in connection with the Standard Model shall also be used here. The term involving the operator and the surface autocorrelation needs to be computed for both the high and low frequency approximations:

$$\begin{aligned} Te^{GC} = \{ & \sin\theta_1 \sin\theta_2 + \frac{G}{k^2\gamma_1\gamma_2} \{\epsilon_1\epsilon_2[S(\chi_x^2)+GS^2(\chi_x)]+\delta_1\delta_2[S(\chi_y^2)+GS^2(\chi_y)] \\ & +(\epsilon_1\delta_2+\epsilon_2\delta_1)[\delta(x_x\chi_y)+GS(\chi_x)\delta(\chi_y)] \\ & +k(\epsilon_2\gamma_1\sin\theta_1+\epsilon_1\gamma_2\sin\theta_2)S(\chi_x)+k(\delta_2\gamma_1\sin\theta_1+\delta_1\gamma_2\sin\theta_2)S(\chi_y)\}\}e^{GC} \end{aligned} \tag{3.58}$$

where $$S(\ ) = \frac{1}{2\pi\sigma^2}\int_{-\infty}^{\infty} d\chi W(\chi)(\ \ )e^{i\chi\cdot r_\perp}$$

and the quantity in parenthesis is always a scalar (magnitude).

2. Slightly Rough Surface: The exponential in (3.58) is expanded. The first 2 terms are retained and (3.58) is substituted into (3.42), the equation corresponding to the Fraunhofer approximation result. The integrations in $\mathbf{r}_\perp$ are peformed to obtain

$$\Gamma_{12}^{Fh}{}_{LF} \doteq \frac{A^2 e^{ik(r_1-r_2)} e^{-\Gamma_e} e^{-\frac{k^2}{8}[\alpha^2U^2+\beta^2V^2]}}{4\pi^2 r'^2 r_1 r_2 \gamma_1 \gamma_2}$$

$$\times \Bigg\{ k^2\gamma_1\gamma_2 \sin\theta_1 \sin\theta_2 e^{-\frac{k^2}{2}(\bar{\alpha}^2U^2+\bar{\beta}^2V^2)}$$

$$+ \frac{G}{(2\pi\sigma^2)} \int_{-\infty}^{\infty} d\chi W(\chi) e^{-\frac{(k\bar{\alpha}+\chi_x)^2}{2}U^2 - \frac{(k\bar{\beta}+\chi_y)^2}{2}V^2} (k^2\gamma_1\gamma_2\sin\theta_1\sin\theta_2 + \epsilon_1\epsilon_2\chi_x^2$$

$$+\delta_1\delta_2\chi_y^2 + (\epsilon_1\delta_2+\epsilon_2\delta_1)\chi_x\chi_y + k(\epsilon_2\gamma_1\sin\theta_1+\epsilon_1\sin\theta_2)\chi_x + k(\delta_2\sin\theta_1+\delta_1\sin\theta_2)\chi_y)$$

$$+ \frac{G^2}{(2\pi\sigma^2)^2} \int_{-\infty}^{\infty} d\chi \int_{-\infty}^{\infty} d\chi' \; W(\chi)W(\chi') e^{-\frac{(k\alpha+\chi_x+\chi_x')^2}{2}U^2 \frac{(k\beta+\chi_y+\chi_y')^2}{2}V^2}$$

$$\times (\epsilon_1\epsilon_2(\chi_x^2+\chi_x\chi_x') + \delta_1\delta_2(\chi_y^2+\chi_y\chi_y') + (\epsilon_1\delta_2+\epsilon_2\delta_1)\chi_x(\chi_y+\chi_y')$$

$$+k(\epsilon_2\gamma_1\sin\theta_1+\epsilon_1\gamma_2\sin\theta_2)\chi_x + k(\delta_2\gamma_1\sin\theta_1+\delta_1\gamma_2\sin\theta_2)\chi_y$$

$$+ \frac{G^3}{(2\pi\sigma^2)^3} \int_{-\infty}^{\infty} d\chi \int_{-\infty}^{\infty} d\chi \int_{-\infty}^{\infty} d\chi'' \; W(\chi)W(\chi')W(\chi'')$$

$$\times e^{-\frac{(k\bar{\alpha}+\chi_x+\chi_x'+\chi_x'')^2}{2}U^2 \frac{(k\bar{\beta}+\chi_y+\chi_y'+\chi_y'')^2}{2}V^2} (\epsilon_1\epsilon_2\chi_x\chi_x' + \delta_1\delta_2\chi_y\chi_y' +$$

$$(\epsilon_1\delta_2+\epsilon_2\delta_1)\chi_x\chi_y') \Bigg\}. \qquad (3.59)$$

The range of validity of (3.59) is that $GC(\mathbf{r}_\perp)<<1$. The intensity is

$$\Gamma_{11}^{Fh}{}_{LF} \doteq \frac{A^2 e^{-g}}{4\pi^2 (r'r)^2 \gamma_2} \{k^2\gamma^2\sin^2\theta_1 e^{-\frac{k^2}{2}[\bar{\alpha}^2U^2+\bar{\beta}^2V^2]}$$

$$+ \frac{g}{2\pi\sigma^2}\int_{-\infty}^{\infty} d\chi W(\chi) e^{-\frac{(k\bar{\alpha}+\chi_x)^2}{2}U^2-\frac{(k\bar{\beta}+\chi_y)^2}{2}V^2}$$

$$\times \quad (k^2\gamma^2\sin^2\theta_1+\epsilon^2\chi_x^2+\delta^2\chi_y^2+2\epsilon\delta\chi_x\chi_y+2k\gamma\sin\theta_1(\epsilon\chi_x+\delta\chi_y))$$

$$+ \frac{g^2}{(2\pi\sigma^2)^2}\int_{-\infty}^{\infty} d\chi \int_{-\infty}^{\infty} d\chi' \; W(\chi)W(\chi') e^{-\frac{(k\bar{\alpha}+\chi_x+\chi_x')^2}{2}U^2-\frac{(k\bar{\beta}+\chi_y+\chi_y')^2}{2}V^2}$$

$$\times \quad (\epsilon^2(\chi_x^2+\chi_x\chi_x')+\delta^2(\chi_y^2+\chi_y\chi_y')+2\epsilon\delta\chi_x(\chi_y+\chi_y')$$

$$+2k\gamma\sin\theta_1(\epsilon\chi_x+\delta\chi_y))$$

$$+ \frac{g^3}{(2\pi\sigma^2)^3}\int_{-\infty}^{\infty} d\chi \int_{-\infty}^{\infty} d\chi' \int_{-\infty}^{\infty} d\chi'' \; W(\chi)W(\chi')W(\chi'')$$

$$e^{-\frac{(k\bar{\alpha}+\chi_x+\chi_x'+\chi_x'')^2}{2}U^2-\frac{(\bar{k}\beta+\chi_y+\chi_y'+\chi_y'')^2}{2}V^2} (\epsilon^2\chi_x\chi_x'+\delta^2\chi_y\chi_y'+2\epsilon\delta\chi_x\chi_y'))\} \quad (3.60)$$

3. Very Rough Surface: The method of stationary phase is employed to evaluate (3.42) with respect to its spatial dependence once (3.58) is substituted in (3.42) and the results from (3.28) and (3.29) are used. In this case, the result

$$\Gamma_{12\ HF}^{Fh} \doteq \frac{A^2 e^{ik(r_1-r_2)} e^{-\frac{GT_o}{2}} e^{-\frac{k^2}{8}[\alpha^2U^2+\beta^2V^2]}}{4\pi^2 r'^2 r_1 r_2 \gamma_1 \gamma_2 B_1 B_2}$$

$$\times \left\{ k^2\gamma_1\gamma_2 \sin\theta_1 \sin\theta_2 e^{-\frac{k^2}{2}\left(\frac{\bar{\alpha}^2U^2}{B_1^2}+\frac{\bar{\beta}^2V^2}{B_2^2}\right)} \right.$$

$$+ \frac{G}{2\pi\sigma^2}\int d\chi W(\chi) e^{-\frac{(k\bar{\alpha}+\chi_x)^2U^2}{2B_1^2}-\frac{(k\bar{\beta}+\chi_y)^2V^2}{2B_2^2}}$$

$$\times \left(\epsilon_1\epsilon_2\chi_x^2+\delta_1\delta_2\chi_y^2+(\epsilon_1\delta_2+\epsilon_2\delta_1)\chi_x\chi_y+k(\epsilon_2\gamma_1\sin\theta_1+\epsilon_1\gamma_2\sin\theta_2)\chi_x\right.$$

$$\left.+k(\delta_2\gamma_1\sin\theta_1+\delta_1\gamma_2\sin\theta_2)\chi_y\right)$$

$$+ \frac{G^2}{(2\pi\sigma^2)^2}\int_{-\infty}^{\infty} d\chi W(\chi)W(\chi') e^{-\frac{(k\bar{\alpha}+\chi_x+\chi_x')^2U^2}{2B_1^2}-\frac{(k\bar{\beta}+\chi_y+\chi_y')^2V^2}{2B_2^2}}$$

$$\left.(\epsilon_1\epsilon_2\chi_x\chi_x'+\delta_1\delta_2\chi_y\chi_y'+(\epsilon_1\delta_2+\epsilon_2\delta_1)\chi_x\chi_y')\right\}. \qquad (3.61)$$

where $B_1 = \sqrt{1-GT_1U^2}$ and $B_2 = \sqrt{1-GT_2V^2}$ are positive roots. This formulation is valid when GC>>1 and the intensity

$$\Gamma_{11\ HF}^{Fh} \doteq \frac{A^2e^{-g}}{B_1B_2 4\pi^2(r'r)^2\gamma^2}\left\{k^2\gamma^2\sin^2\theta_1 e^{-\frac{k^2}{2}\left(\frac{\bar{\alpha}^2U^2}{B_1^2}+\frac{\bar{\beta}^2V^2}{B_2^2}\right)}\right.$$

$$+ \frac{g}{2\pi\sigma^2}\int d\chi W(\chi) e^{-\frac{(k\bar{\alpha}+\chi_x)^2U^2}{2B_1^2}-\frac{(k\bar{\beta}+\chi_y)^2V^2}{2B_2^2}}$$

$$(\epsilon^2\chi_x'+\delta^2\chi_y'+2\epsilon\delta\chi_x\chi_y+2k\gamma\sin\theta_1(\epsilon\chi_x+\delta\chi_y))$$

$$+\frac{g^2}{(2\pi\sigma^2)^2}\int d\chi\int d\chi' W(\chi)W(\chi')e^{-\frac{(k\bar{\alpha}+\chi_x+\chi_x')^2U^2}{2B_1^2}-\frac{(k\bar{\beta}+\chi_y+\chi_y')^2V^2}{2B_2^2}}$$

$$(\epsilon^2\chi_x\chi_x'+\delta^2\chi_y\chi_y'+2\epsilon\delta\chi_x\chi_y')\}. \qquad (3.62)$$

Low and high frequency expressions in the Fresnel approximation could be developed. The algebra is involved and tedius, but not impossible.

C. THE COMPOSITE-ROUGHNESS MODEL (5,6,7)

1. Introduction

The present section deals with a technique that has been successful in studies involving a one-dimensional ocean surface. This is so because it assumes that the surface to which this model applies scatters the incoming wave in two phenomenologically different ways. First, the long wavelength incoming radiation, sees a surface that is locally flat, possibly with non-zero slope, and scatters from it as if though it were a distribution of mirror-like facets. In optics this corresponds to the physical optics domain of radiation scatter and is not new to us since it is formulated by the Helmholtz-Kirchhoff Integral or the Double-Layer Potential Integral discussed previously. Second, the short wavelength incident wave will be scattered diffusely by the ripple which rides on the large

scale undulating surface (see Fig. 3). The ripple has the features of surfaces to which the Method of Small Perturbation applies, such as rapidly changing slopes and small crest-to-trough amplitudes. A theory that applies to surfaces of this type, with two roughness ranges, could be one that merges the Helmholtz-Kirchhoff Integral and the Method of Small Perturbation. It would imply that the scattered wave undergoes Dali-like distortion as predicted by the Helmholtz Integral, but the sharp definition is somewhat lost due to the contribution of the perturbation.

The model being discussed is the Composite-Roughness Model. It applies well to surfaces that can be divided into two scales of roughness, and have most of their energy scattering potential concentrated in the lower regime of the spectrum. However, a problem arises when it is not clear where this spectrum splitting occurs. McDaniel (7) has improved the method by including diffraction corrections. These corrections are also beneficial in reducing the sensitivity of the results to changes in cutoff surface wavenumber.

As with the Tangent-Plane methods this strategy requires the computation of the expectation of the projection of the source wavenumber and the random surface normal. A choice must be made, which usually considers computational simplicity heavily on the averaging technique. But the demands here are not so stringent as in the Tangent-Plane Method since the normal in question is taken to be the slowly varying large-scale roughness normal. The next two

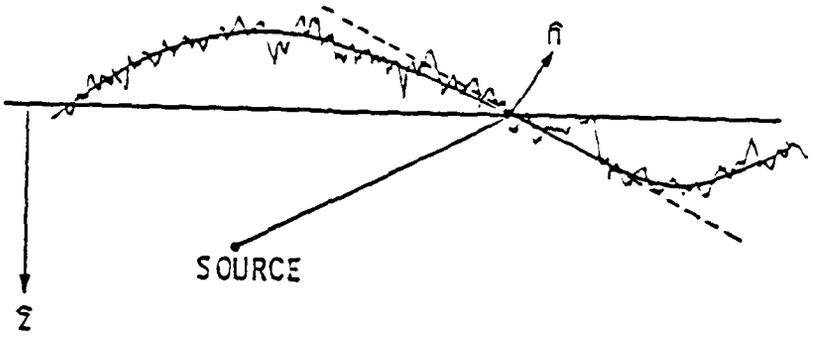

Figure 3. Composite-roughness surface

subsections will present the spatial covariance formulation using the conventional Composite-Roughness Model and diffractive corrections are introduced in the last section.

2. The Conventional Model: the interest is to develop two expressions in the Fraunhofer phase approximation. One will incorporate the function $f(\theta)$ as an approximation to the evaluation of the dot product involving the random normal to the surface. Another expression will use the slope operator instead. The last section shall leave the issue of the dot product behind and shall describe the changes that occur in the model when diffractive corrections as proposed by McDaniel (7) are incorporated.

a. Integration-by-Parts Procedure: Equation (3.10) is our starting point. The autocorrelation function is expressed as a sum of contributions from the spectra of the large scale surface plus the small scale surface spectra.

$$C(\mathbf{r}_\perp) = C_L(\mathbf{r}_\perp) + C_S(\mathbf{r}_\perp) \tag{3.63}$$

where

$$C_L(\mathbf{r}) = \frac{1}{2\pi\sigma^2} \int_0^{\kappa_L} \kappa \, d\kappa \int_0^{2\pi} d\Omega W(\kappa,\Omega)\cos(\chi \cdot \mathbf{r}_\perp)$$

in cylindrical coordinates, with κ_L being the low wavenumber cutoff. Thus, the exponential e^{GC} can be expressed as

$$e^{G(C_L+C_S)} = e^{GC_L}\ [1+GC_S + \frac{G^2}{2!}\ C_s^2 + \ldots] \tag{3.64}$$

so that (3.10) is now

$$\Gamma_{12} = \frac{Ak^2 f_1(\theta) f_2(\theta) e^{ik(r_1-r_2)} e^{-\Gamma} e^{-\frac{k^2}{8}(\alpha^2U^2+\beta^2V^2)}}{8\pi^2 r_1 r_2 r'^2}$$

$$\times \int_{-\infty}^{\infty} dr_\perp D e^{ik(r_\perp \cdot \bar{s})} e^{GC_L}\ [1+GC_S]$$

if we retain up to first order terms in C_S.

The first term of this integral is the contribution from the large-scale surface and shall be separated for convenience. The expression for the covariance is

$$\Gamma_{12} = \frac{Ak^2 f_1(\theta) f_2(\theta) e^{ik(r_1-r_2)} e^{-\Gamma} e^{-\frac{k^2}{8}(\alpha^2U^2+\beta^2V^2)}}{8\pi^2 r_1 r_2 r'^2}$$

$$\times \left(Q_L + \int_{-\infty}^{\infty} dr_\perp D e^{ik(r_\perp \cdot \bar{s})} e^{GC_L} GC_S\right) \tag{3.65}$$

where $$Q_L = \int_{-\infty}^{\infty} dr_\perp D e^{ik(r_\perp \cdot \bar{s})} e^{GC_L}$$

The large-scale surface autocorrelation can be expanded about $r_\perp=0$. The autocorrelation length is assumed to be small and the spectrum is assumed non-directional. Thus,

$$C_L(r_\perp) = \left(\frac{\sigma_L}{\sigma}\right)^2 - \frac{1}{2}\left(\frac{\sigma_x'}{\sigma}\right)^2 x^2 - \frac{1}{2}\left(\frac{\sigma_y'}{\sigma}\right)^2 y^2 \tag{3.66}$$

with σ_L = rms large-scale surface waveheight

σ_x' = the x component of the rms slope-large scale surface

σ_y' = the y component of the rms slope-large scale surface.

Substitution into the explicit form of (3.65) gives

$$\Gamma_{12} \frac{Ak^2 f_1(\theta) f_2(\theta) e^{ik(r_1-r_2)} e^{-\Gamma} e^{-\frac{k^2}{8}(\alpha^2U^2+\beta^2V^2)}}{8\pi^2 r'^2 r_1 r_2}$$

$$\times \left\{ Q_L + e^{G(\frac{\sigma_L}{\sigma})} \int_{-\infty}^{\infty} dy \int_{-\infty}^{\infty} dx\, D e^{ik(\bar{\alpha}x+\bar{\beta}y)} e^{-\frac{G}{2\sigma^2}(\sigma_x'^2 x^2+\sigma_y'^2 y^2)} \right.$$

$$\left. \frac{G}{2\pi\sigma^2} \int_{\ddagger}^{\infty} d\chi\, W(\chi) e^{i\chi\cdot r_\perp} \right\} \tag{3.67}$$

The symbol ‡ indicates that the integrals lower limit corresponds to the cutoff spectral wavenumber.

Integrating over x and y gives

$$\Gamma_{12} = \frac{Ak^2 f_1(\theta) f_2(\theta) e^{ik(r_1 - r_2)} e^{-\Gamma} e^{-\frac{k^2}{8}(\alpha^2 U^2 + \beta^2 V^2)}}{8\pi^2 r'^2 r_1 r_2} \left\{ Q_L + \right.$$

$$\left. + \frac{2Ae}{R_1 R_2} \, G\left(\frac{\sigma_L}{\sigma}\right)^2 \frac{G}{2\pi\sigma^2} \int_{\ddagger}^{\infty} d\chi W(\chi) e^{-\frac{U^2}{2R_1^2}(k\bar{\alpha}+\chi_x)^2 - \frac{V^2}{2R_2^2}(k\bar{\beta}+\chi_y)^2} \right\}$$

$$\text{with} \qquad Q_L = \frac{2Ae}{R_1 R_2} \left(\frac{\sigma_L}{\sigma}\right)^2 e^{-\frac{k^2}{2}\left[\frac{\bar{\alpha}^2 U^2}{R_1^2} + \frac{\bar{\beta}^2 V^2}{R_2^2}\right]} \tag{3.68}$$

$$\text{and} \quad R_1 = \sqrt{1+GU^2\left(\frac{\sigma'_x}{\sigma}\right)^2},$$

$$R_2 = \sqrt{1+GV^2\left(\frac{\sigma'_y}{\sigma}\right)^2} \quad \text{are positive roots.}$$

and the intensity is similar except that the constant in front of (3.68) is replaced by $\frac{Ak^2 f^2(\theta) e^{-g}}{8\pi^2 (r'r)^2}$. The above equation and the resultant equation for intensity are valid so long as $\left(\frac{G\sigma_s}{\sigma}\right)^2 \ll 1$.

In terms of a coherent and incoherent component, (3.68) can be expressed as

$$\Gamma_{12} = \Gamma_{12\ coh} \left\{ 1 + e^{+\frac{k^2}{2}\left[\frac{\bar{\alpha}^2 U^2}{R_1^2} + \frac{\bar{\beta}^2 V^2}{R_1^2}\right]} \right.$$

$$\left. \cdot \frac{G}{2\pi\sigma^2} \int_{\ddagger}^{\infty} d\chi W(\chi) e^{-\frac{U^2}{2R_1^2}(k\bar{\alpha}+\chi_x)^2 - \frac{V^2}{2R_2^2}(k\bar{\beta}+\chi_y)^2} \right\} \tag{3.69}$$

so that $\Gamma_{12\ coh} = \Gamma_{12\ M} e^{-\Gamma}$ as usual and

$$\Gamma_{12\ M} = \frac{A^2k^2f_1(\theta)f_2(\theta)e^{ik(r_1r_2)}e^{-\frac{k^2}{8}(\alpha^2U^2+\beta^2V^2)}e^{G(\frac{\sigma_L}{\sigma})^2}}{4\pi^2r'^2r_1r_2R_1R_2}$$

$$\times\ e^{-\frac{k^2}{2}\left[\frac{\alpha^2U^2}{R_1^2}+\frac{\beta^2V^2}{R_2^2}\right]} \qquad (3.70)$$

The intensity has the same term in { } brackets (the values of $\bar{\alpha}$ and $\bar{\beta}$ are different for intensity) but

$$\Gamma_{11\ coh} = \frac{A^2k^2f^2(\theta)e^{G(\frac{\sigma_L}{\sigma})^2}e^{-\frac{k^2}{2}\left[\frac{\bar{\alpha}^2U^2}{R_1^2}+\frac{\bar{\beta}^2V^2}{R_2^2}\right]}}{4\pi^2(r'r)^2R_1R_2}\ e^{-g} \qquad (3.71)$$

b. Incorporating the Slope Operator:

Recognizing the similarities between the expansion in (3.64) and the one used to obtain (3.59), the result of using the slope-operator in the context of the Composite-Roughness Model can readily be derived using the results of (3.68):

$$\Gamma_{12} = \frac{A^2e^{ik(r_1-r_2)}e^{-\Gamma}e^{-\frac{k^2}{8}[\alpha^2U^2+\beta^2V^2]}e^{G(\frac{\sigma_L}{\sigma})^2}}{4\pi^2r'^2r_1r_2\gamma_1\gamma_2R_1R_2}$$

$$\times\ \left\{k^2\gamma_1\gamma_2\sin\theta_1\sin\theta_2 e^{-\frac{k^2}{2}\left[\frac{\bar{\alpha}^2U^2}{R^2}+\frac{\bar{\beta}^2V^2}{R^2}\right.}\right.$$

AD-A192 489 THE COVARIANCE OF SCALAR FIELDS SCATTERED BY PRESSURE-RELEASE RANDOMLY RO..(U) PENNSYLVANIA STATE UNIV UNIVERSITY PARK APPLIED RESEARCH LAB.. 2/2

UNCLASSIFIED J M RESTREPO ET AL. DEC 87 F/G 20/1 NL

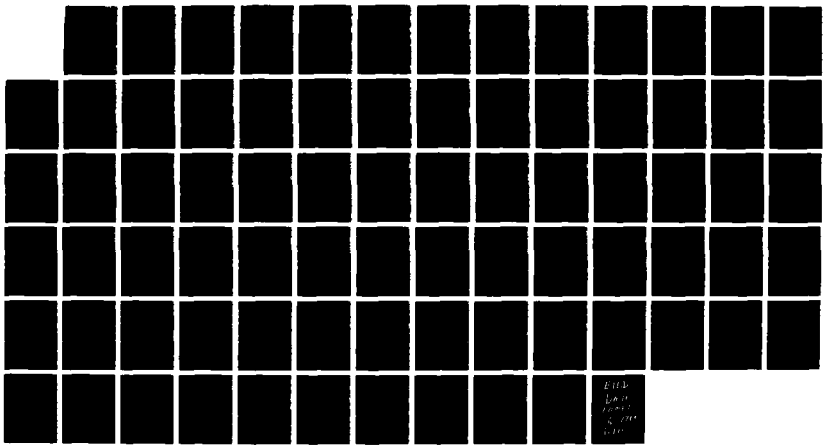

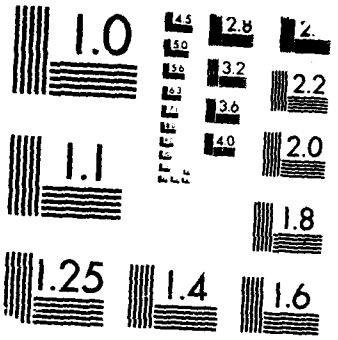

$$+\frac{G}{(2\pi\sigma^2)}\int_{\ddagger}^{\infty} d\chi W(\chi) e^{-\frac{(k\bar{\alpha}+\chi_x)^2V^2}{2R_1^2}-\frac{(k\bar{\beta}+\chi_y)^2V^2}{2R_2^2}} (k^2\gamma_1\gamma_2\sin\theta_1\sin\theta_2+\epsilon_1\epsilon_2\chi_x^2+$$

$$\delta_1\delta_2\chi_y^2+(\epsilon_1\delta_2+\epsilon_2\delta_1)\chi_x\chi_y+k(\epsilon_2\gamma_1\sin\theta_1+\epsilon_1\gamma_2\sin\theta_2)\chi_x$$

$$+ik(\delta_2\gamma_1\sin\theta_1+\delta_1\gamma_2\sin\theta_2)\chi_y)$$

$$+(\frac{G}{2\pi\sigma^2})^2\int_{\ddagger}^{\infty}d\chi\int_{\ddagger'}^{\infty}d\chi\ W(\chi)W(\chi')e^{-\frac{(k\bar{\alpha}+\chi_x'+\chi_x)^2U^2}{2R_1^2}-\frac{(k\bar{\beta}+\chi_y+\chi_y')^2V^2}{2R_2^2}}$$

$$(\epsilon_1\epsilon_2(\chi_x^2+\chi_x\chi_x')+\delta_1\delta_2(\chi_y^2+\chi_y\chi_y')+\epsilon_1\delta_2+\epsilon_2\delta)\chi_x(\chi_y+\chi_y')$$

$$+k(\epsilon_2\gamma_1\sin\theta_1+\epsilon_1\gamma_2\sin\theta_2)\chi_x+k(\delta_2\gamma_1\sin\theta_1+\delta_1\gamma_2\sin\theta_2)\chi_y)$$

$$+(\frac{G}{2\pi\sigma^2})^3\int_{\ddagger}^{\infty}d\chi\int_{\ddagger'}^{\infty}d\chi'\int_{\ddagger''}^{\infty}d\chi''\ W(\chi)W(\chi')W(\chi'')$$

$$\times e^{-\frac{(k\bar{\alpha}+\chi_x+\chi_x'+\chi_x'')^2U^2}{2R_1^2}-\frac{(k\bar{\beta}+\chi_y+\chi_y'+\chi_y'')^2V^2}{2R_2^2}}$$

$$\times(\epsilon_1\epsilon_2\chi_x\chi_x'+\delta_1\delta_2\chi_y\chi_y'+(\epsilon_1\delta_2+\epsilon_2\delta_1)\chi_x\chi_y')\Big\} \qquad (3.72)$$

valid so long $(\frac{G\sigma_s}{\sigma})<<1$. The symbol ‡ indicates that the lower limit of integration is consistent with the lower limit in (3.68).

The intensity is

$$\Gamma_{11} = \frac{A^2 e^{-g} g(\frac{\sigma_L}{\sigma})^2}{4\pi^2(r'r)^2\gamma^2 R_1 R_2}\{k^2\gamma^2\sin^2\theta_1 e^{-\frac{k^2}{2}[\frac{\bar{\alpha}^2U^2}{R_1^2}+\frac{\bar{\beta}^2V^2}{R_2^2}]}$$

$$+\left(\frac{g}{2\pi\sigma^2}\right)\int_{\ddagger}^{\infty} d\chi W(\chi) e^{-\frac{(k\alpha+\chi_x)^2U^2}{2R_1^2}-\frac{(k\beta+\chi_y)^2V^2}{2R_2^2}}$$

$$(k^2\gamma^2\sin^2\theta_1+\epsilon^2\chi_x^2+\delta^2\chi_y^2+2\epsilon\delta\chi_x\chi_y+2k\gamma\sin\theta_1(\epsilon\chi_x+\delta\chi_y))$$

$$+\frac{g}{(2\pi\sigma^2)}\int_{\ddagger}^{\infty} d\chi \int_{\ddagger}^{\infty} d\chi' W(\chi)W(\chi') e^{-\frac{(k\bar{\alpha}+\chi_x+\chi_x')^2U^2}{2R_1^2}-\frac{(k\bar{\beta}+\chi_y+\chi_y')^2V^2}{2R_2^2}}$$

$$(\epsilon^2(\chi_x^2+\chi_x\chi_x')+\delta^2(\chi_y^2+\chi_y\chi_y')+2\epsilon\delta\chi_x(\chi_y+\chi_y')$$

$$+(\frac{g}{2\pi\sigma^2})^3\int_{\ddagger}^{\infty} d\chi \int_{\ddagger'}^{\infty} d\chi' \int_{\ddagger''}^{\infty} d\chi'' W(\chi)W(\chi')W(\chi'')$$

$$e^{-\frac{(k\bar{\alpha}+\chi_x+\chi_x'+\chi_x'')^2U^2}{2R_1^2}-\frac{(k\bar{\beta}+\chi_y+\chi_y'+\chi_y'')^2V^2}{2R_2^2}}$$

$$(\epsilon^2\chi_x\chi_x'+\delta^2\chi_y\chi_y'+2\epsilon\delta\chi_x\chi_y')\} \qquad (3.73)$$

3. Composite-Roughness Model Incorporating Diffractive Corrections

The surface correlation function is partitioned as was done in (3.63), but the expression for the large-scale surface correlation is now

$$\sigma^2 C_L = \sigma_L^2 - \frac{1}{2}[\sigma_x'^2 x^2 + \sigma_y'^2 y^2] + \frac{1}{2\pi}\int_0^{\kappa_L} \kappa d\kappa \int_0^{2\pi} d\Omega W(\kappa,\Omega)\{\cos(\chi\cdot r_\perp)$$

$$-1+\frac{1}{2}(\chi\cdot r_\perp)^2\} \qquad (3.74)$$

Using (3.63) and (3.77), the exponential term in (3.10) is

$$ik(r_\perp\cdot\bar{S}) - \frac{G}{2\sigma^2}[(\sigma_x'\chi)^2+(\sigma_y'^2 y)^2] + \frac{G}{2\pi\sigma^2}\int_0^{\kappa_L}\kappa d\kappa\int_0^{2\pi} d\Omega W(\kappa,\Omega)\{\cos(\chi\cdot r_\perp)-1$$

$$+\frac{1}{2}(\chi\cdot r_\perp)^2\} - G(\frac{\sigma_s}{\sigma})^2 + G\sigma_s^2 C_s(r_\perp). \qquad (3.75)$$

When $G(\frac{\sigma_s}{\sigma})$ is small the above result can be recast as

$$\{ik(r_\perp\cdot s) - \frac{G}{2\sigma^2}[(\sigma_x'x)^2+(\sigma_y'y)^2]\}[1-G^2(1-C(r_\perp)) + \frac{G}{2\sigma^2}((\sigma_x'x)^2+(\sigma_y'y)^2)]. \qquad (3.76)$$

Using (3.75), or (3.76) when applicable, in (3.10) and performing the integrations over $r_\perp$ variables yields an expression that incorporates diffractive corrections and that is less sensitive to the choice of partitioning wavenumber. The result is also attractive because it lacks computational complexity and gives fairly good agreement when its predictions are compared to experiment.

CHAPTER IV

SCATTERING STRENGTH AND COHERENCE

A. SCATTERING STRENGTH

The different models presented in the previous chapter are compared and their behavior analyzed. The aim of the first half of this chapter is to compare the Standard and Slope-Operator Model in general terms, in addition to the three alternatives to the Slope-Operator Model: the Fraunhofer Approximation, the Fresnel Approximation and the case when the random normal $\frac{\partial}{\partial n}$ is approximated by $\frac{\partial}{\partial z}$. To enable comparison, section A examines the scattering strength, defined as

$$S = 10\log_{10} \left(\frac{(r'r)^2}{A} \Gamma_{11}\right) \tag{4.1}$$

involving a flat and a Gaussian surface. Note, however, that the plots shown are normalized to the maximum values. Therefore, the figures show the normalized scattering strength. The second half of the chapter compares the Standard and Slope-Operator models, as they are applied to the measure of coherence (1, p. 498)

$$\gamma_{12} = \frac{\Gamma_{12}}{(\Gamma_{11}\Gamma_{22})^{1/2}} \tag{4.2}$$

when the surface involved is Gaussian. From the three alternatives of the Slope-Operator Model, the Fraunhofer Slope-Operator Model is chosen for comparison to the Standard Model.

1. Flat Surface:

The classical expression for the scattering strength involving a flat surface in the Fraunhofer approximation is

$$S_o = 10\log_{10}\left\{\frac{Ak^2\sin^2\theta}{4\pi^2}\right\} \tag{4.3}$$

and is shown in Figure 4 in the specular case. Equation (3.51), the Slope-Operator Model yields

$$S_{so} = 10\log_{10}\left\{\frac{Ak^2\sin^2\theta}{4\pi^2}\right\}. \tag{4.4}$$

when r' and r become large and the beam very narrow. If the same approximations were possible for the Standard Model (3.20) the result would be

$$S_s = 10\log_{10}\left\{\frac{Ak^2f^2(\theta)}{4\pi^2}\right\} \tag{4.5}$$

For the specular test shown in Figure 4, $f(\theta)$ reduces to $(1+\sin^2\theta)/2\sin\theta$. Figure 5 shows good agreement between the Fraunhofer Slope-Operator, Standard and Figure 4. The plots of Figure 5 show the models without making any approximations. The Fresnel expression will agree with the other two if the above mentioned limiting vaues for r', r and the beam are made. The

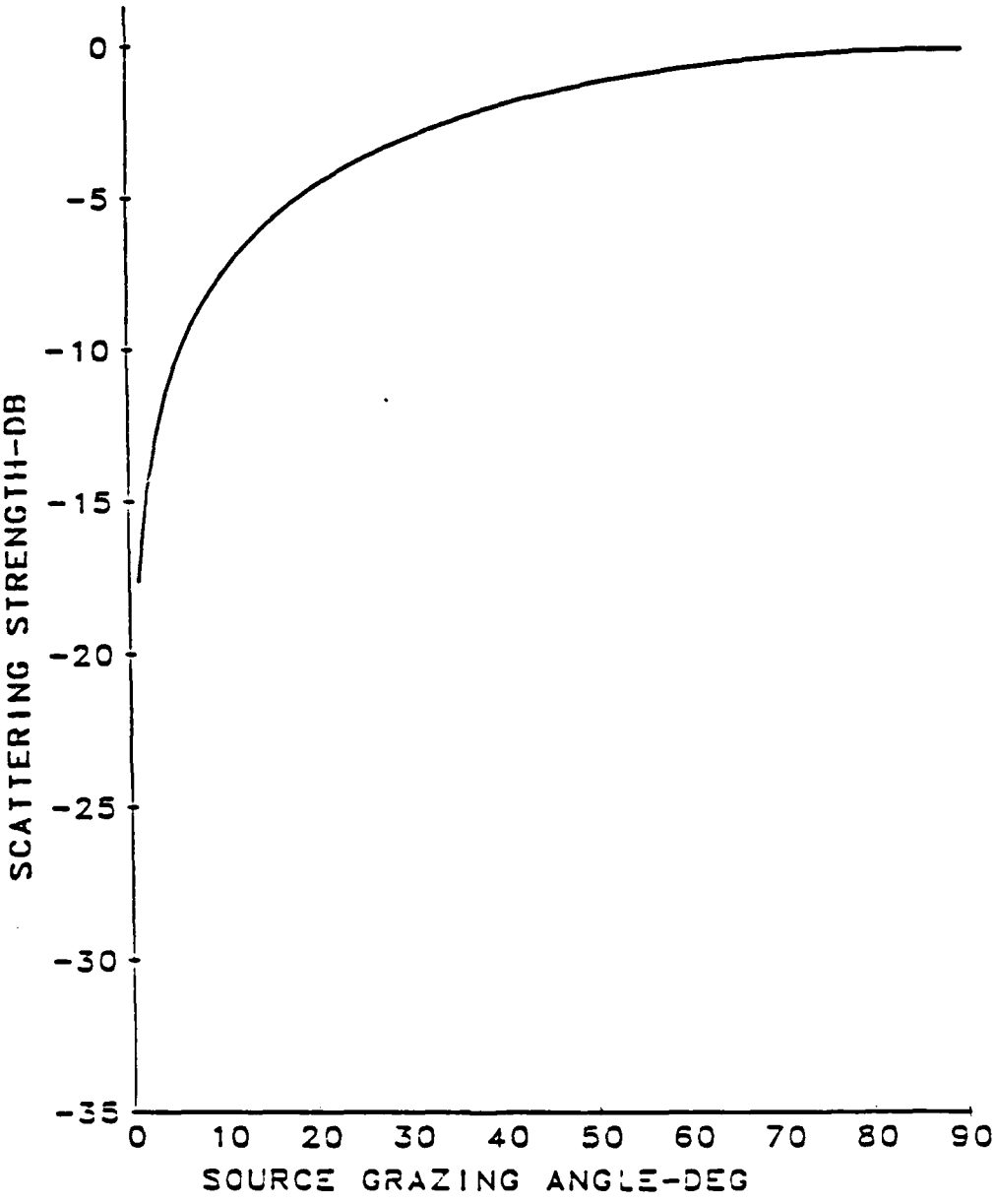

Figure 4. Scattered intensity specular direction in the Fraunhofer approximation. Flat surface. Source at 500 cm frequency is 10 KHz, beamwidth is 3°.

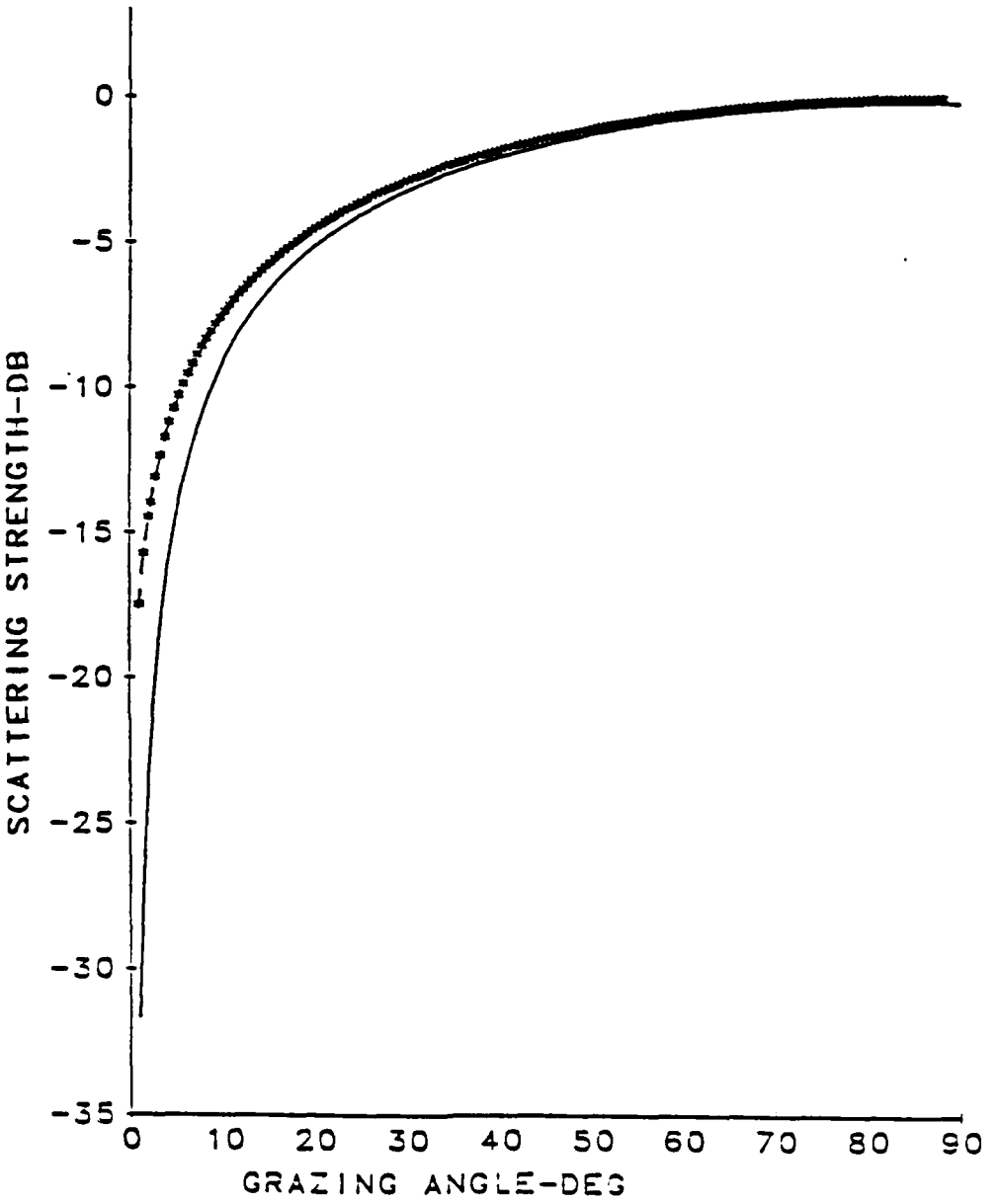

Figure 5. Specular scatter involving Γ_{11M} for Fresnel:_____, Fraunhofer: ***** and standard: -----.

discrepancy between the Standard Model and the Slope-Operator Model in connection to the angular dependence demonstrates how weakly they depend on the functions $f(\theta)$ and $\sin^2\theta$ in the specular case.

For the forward case, the lack of consistency between the two models becomes more obvious. This hypothesis is based not only on the fact that $f(\theta)$ does not simplify to $\sin^2\theta_1$ for all cases, but because by assumption the Standard Model is valid not far from the specular direction. Figure 6 illustrates this point. The Standard Model misbehaves at low and very high receiver grazing angles.

Since the Standard Model is limited to the near specular direction, in the backscatter test it is expected to perform poorly far away from the normal to the mean surface. This is obviously demonstrated in Figure 7. These figures show the backscatter involving a flat surface and a slightly rough Gaussian surface for a source with 3° beamwidth operating at 10 KHz. In this test it is expected that the energy be higher in amplitude and largely concentrated around the normal (source grazing angle of 90°) for the flat surface scatter as shown in Figures 7a an 7b for the Fresnel and Fraunhofer Slope-Operator Models respectively. This is not the case for the Standard Model that is plotted in 7c. This last figure shows good agreement in the normal direction but breaks down for low grazing angles, because the model is used outside its region of validity (see II.B.1).

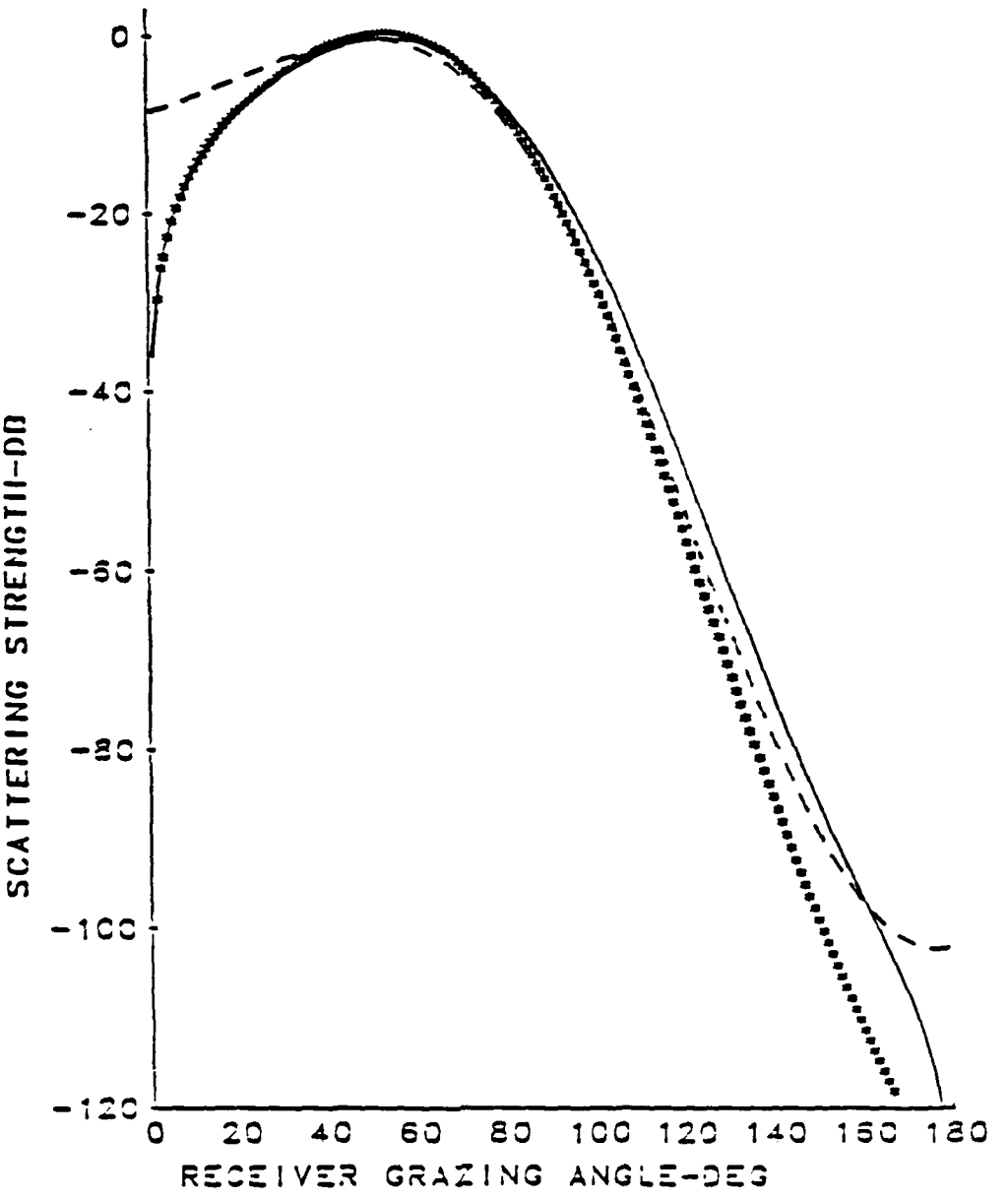

Figure 6. Forward scatter from flat surface at 10 KHz for a source with 3° beamwidth. Fraunhofer slope-operator: ****, Fresnel slope-operator: ____, standard: -----.

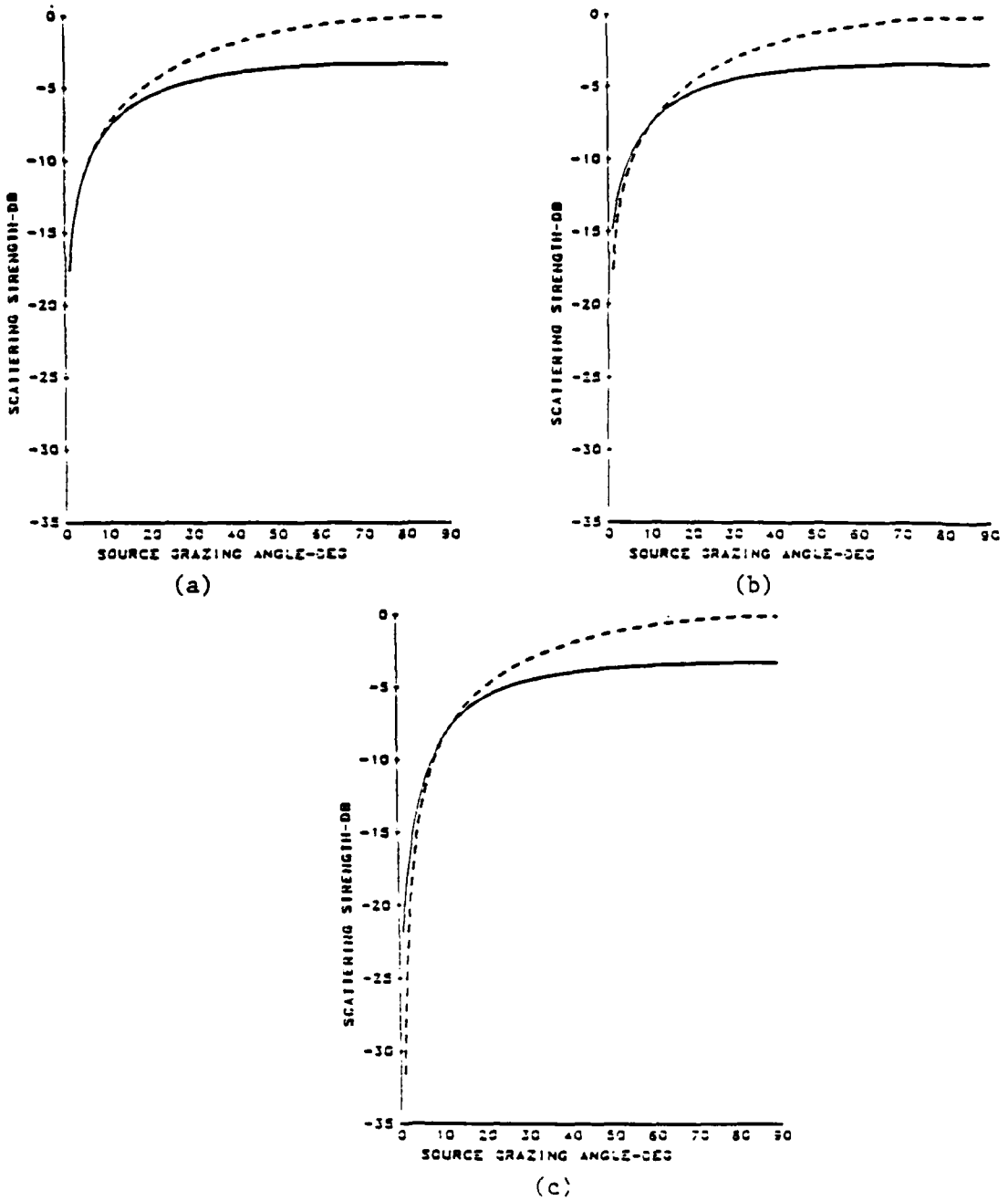

Figure 7. Backscatter from a flat surface: ----, Gaussian surface: ____. (a) standard, (b) Fraunhofer slope-operator, (c) Fresnel slope-operator, 10KHz, 3° beam.

2. Gaussian Surface:

a. Backscatter

Figures 8a, 8b, and 8c correspond to equations (3.51), (3.50), and (3.20), respectively, in the backscatter case. The three figures show good agreement in the prediction of backscatter close to the normal direction. As expected, the low grazing angle regime shows the Fresnel expression yielding demonstrably less backscatter. Near the normal the three models show that the amplitude changes in proportion to the frequency squared, which is implicit in the k^2 that is part of the coherent component of equations (3.51), (3.50), and (3.20).

The effect of changing the rms height of the surface is illustrated in Figures 9a, 9b, and 9c. With an increase in the rms height, the area under the curve becomes wider, as is the case in 9a and 9c, and the overall amplitude drops as seen in all three plots. Again, the Standard Model fails to provide good results far from the normal direction.

Further insight into the way the Standard Model behaves for low source grazing angles is given by Figures 10a, b, c. In these three figures the broken lines represent the coherent component of the backscattered intensity and they can be compared to the solid line which represents the coherent and incoherent components combined. In the Slope-Operator Models the incoherent component contributes to the radiation even at low grazing angles. This is not the case in the

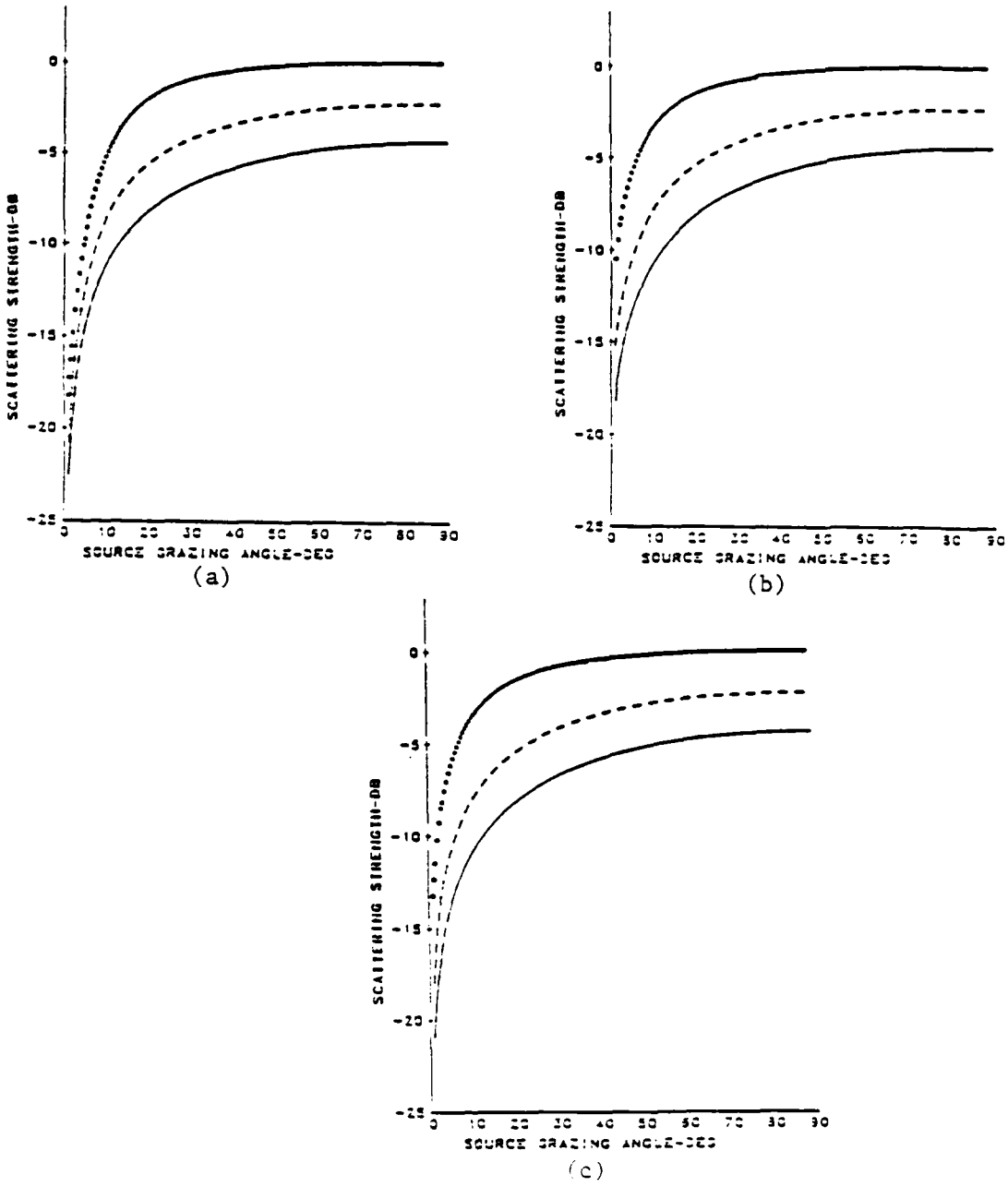

Figure 8. Frequency dependence of backscattered radiation involving Gaussian surface. (a) Fresnel slope-operator, (b) Fraunhofer slope-operator, (c) standard. ____: 5KHz, ----: 7KHz, ****: 12KHz

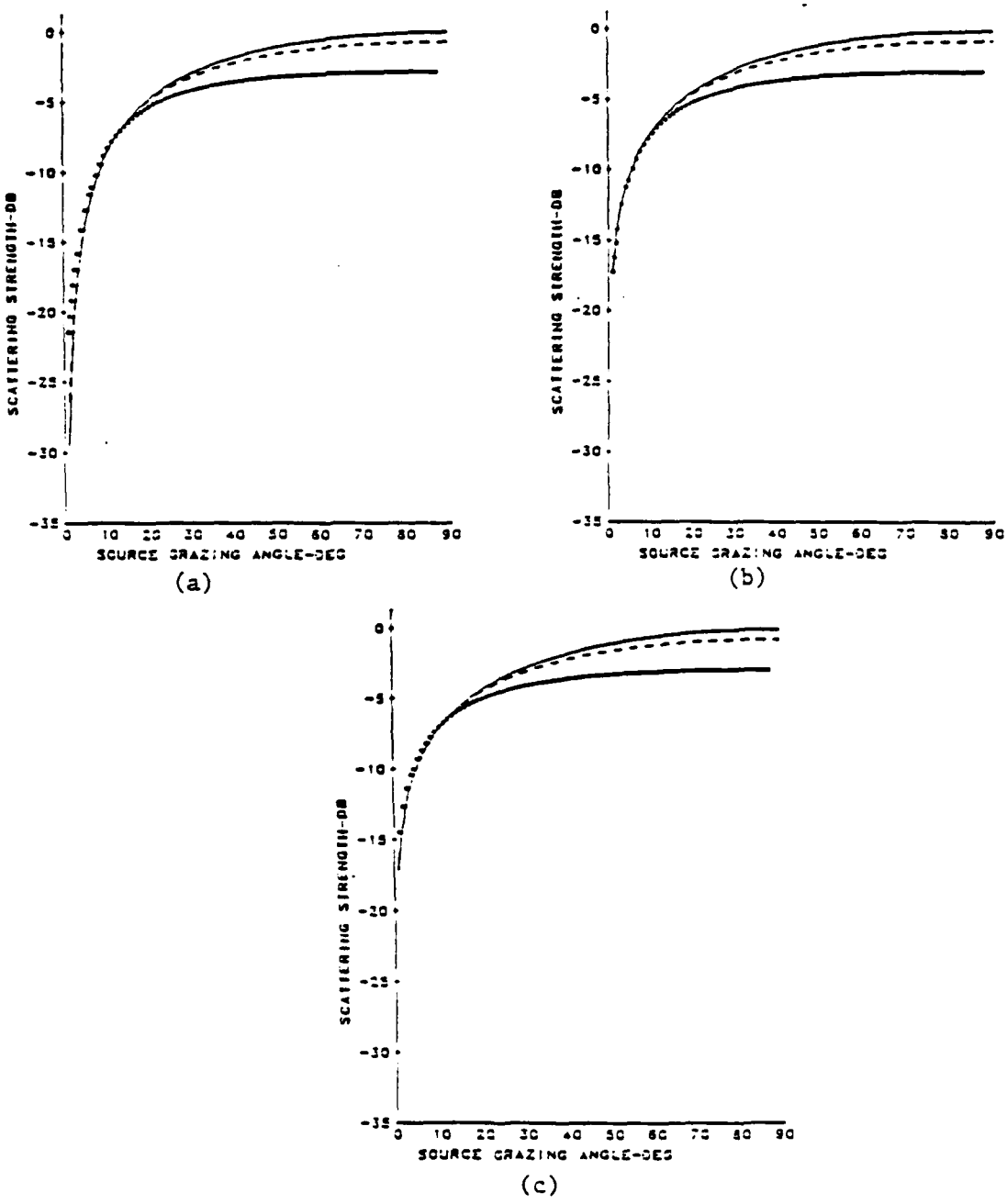

Figure 9. Backscatter. Variation with rms height.
____: 0.5cm, ----: 1.0cm, ****: 2.0cm.
(a) Fresnel slope-operator, (b) standard,
(c) Fraunhofer slope-operator

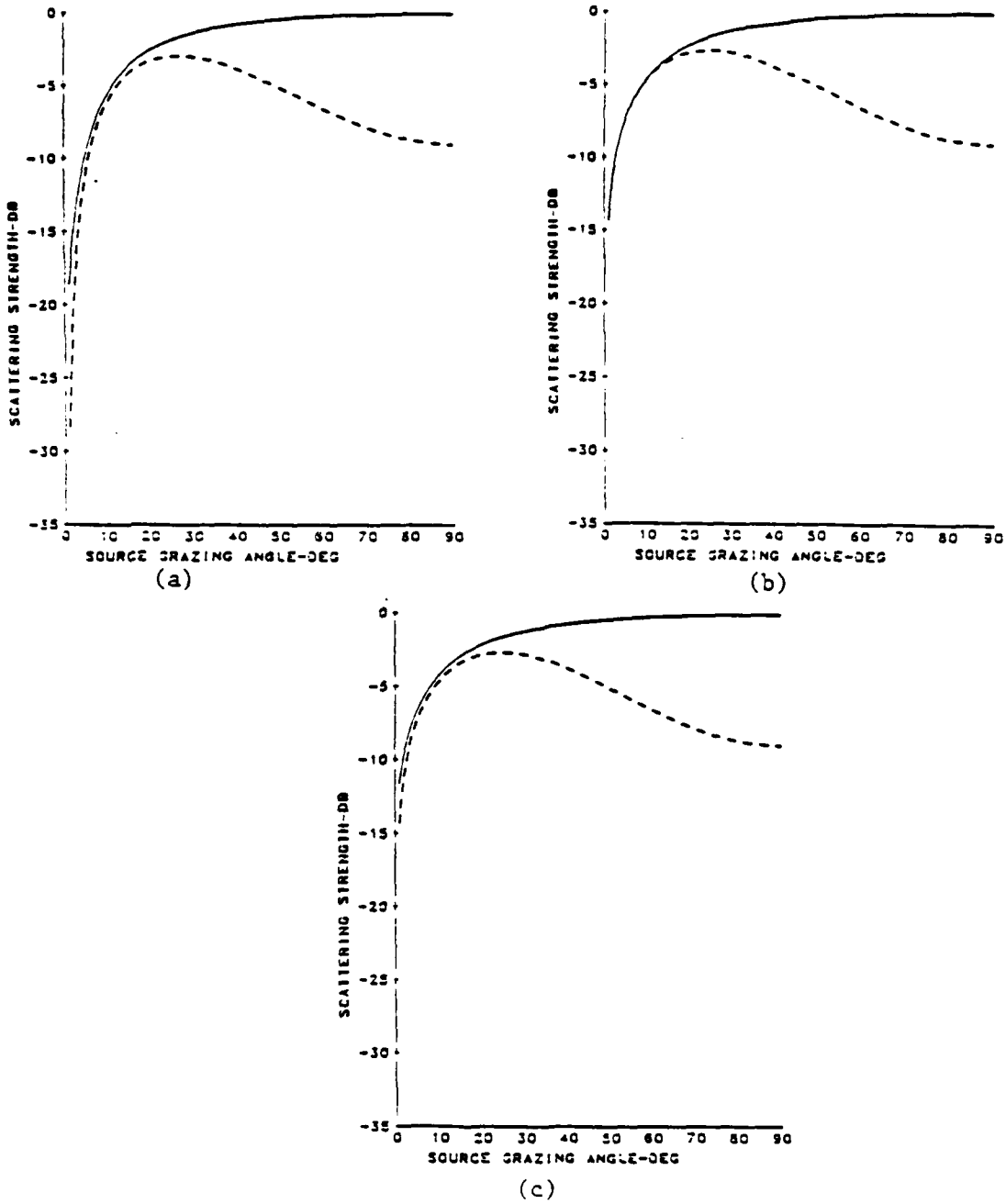

Figure 10. Coherent ---- versus total ____ scattering strength
(a) Fresnel slope-operator, (b) standard,
(c) Fraunhofer slope-operator

Standard Model, for which the radiation is exclusively predicted by the coherent term. The plots correspond to a source operating with a 3° beamwidth at a frequency of 10 KHz. In all the models the incoherent component is the sum of ten terms which is more than adequate for the values to converge for this frequency. In general, the higher the frequency, the more incoherent terms are needed since an expansion of the exponential involving the roughness parameter G was performed in all the models. The result in turn depends on the square of the frequency.

b. Forward Scatter

In the forward scatter test, a source is placed at 500 cm from the surface, at an angle of 45°. The receiver is 200 cm away from the surface. Again, the surface has autocorrelation lengths of 20 cm and an rms height of 2 cm. The scattering strength is expected to peak in the neighborhood of a receiver grazing angle of 45°, corresponding to the specular position.

Figure 11 is the forward scatter, for a source with 30° beam operating at 10 KHz, as predicted by the three models. The peak occurs in the neighborhood of 48°, not at the specular angle. The peak is frequency and beamwidth dependent in all three models and will shift to the specular angle as the frequency or the beamwidth is increased. This shift is apparent in Figures 12a, 12b, and 12c, in which all models exhibit a peak which is further away from the specular angle at lower frequencies.

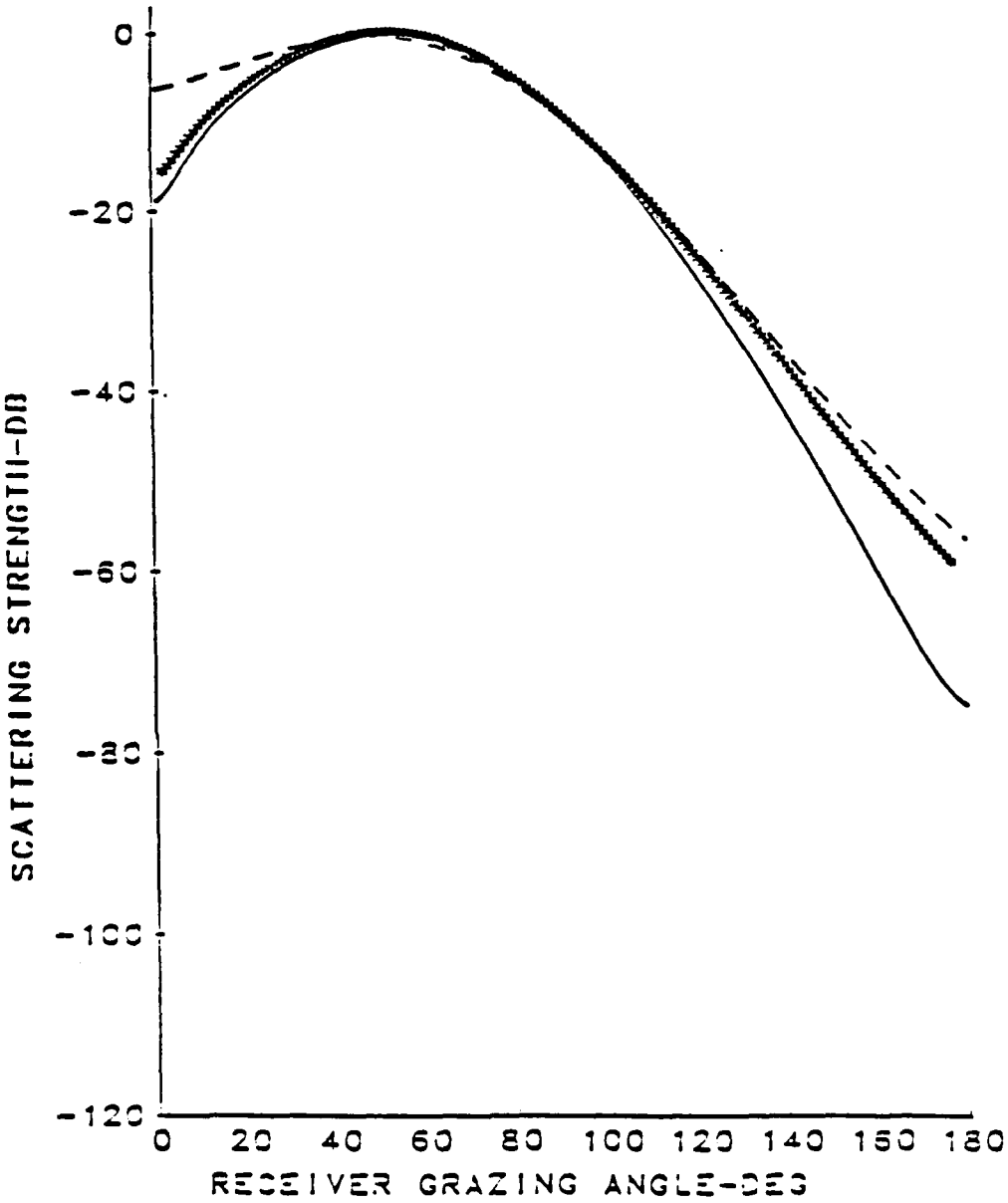

Figure 11. Forward scatter for a source at 500 cm and 45° with a 3° beam and an operating frequency of 10 KHz.
____: Fresnel slope-operator, ----: standard,
****: Fraunhofer slope-operator

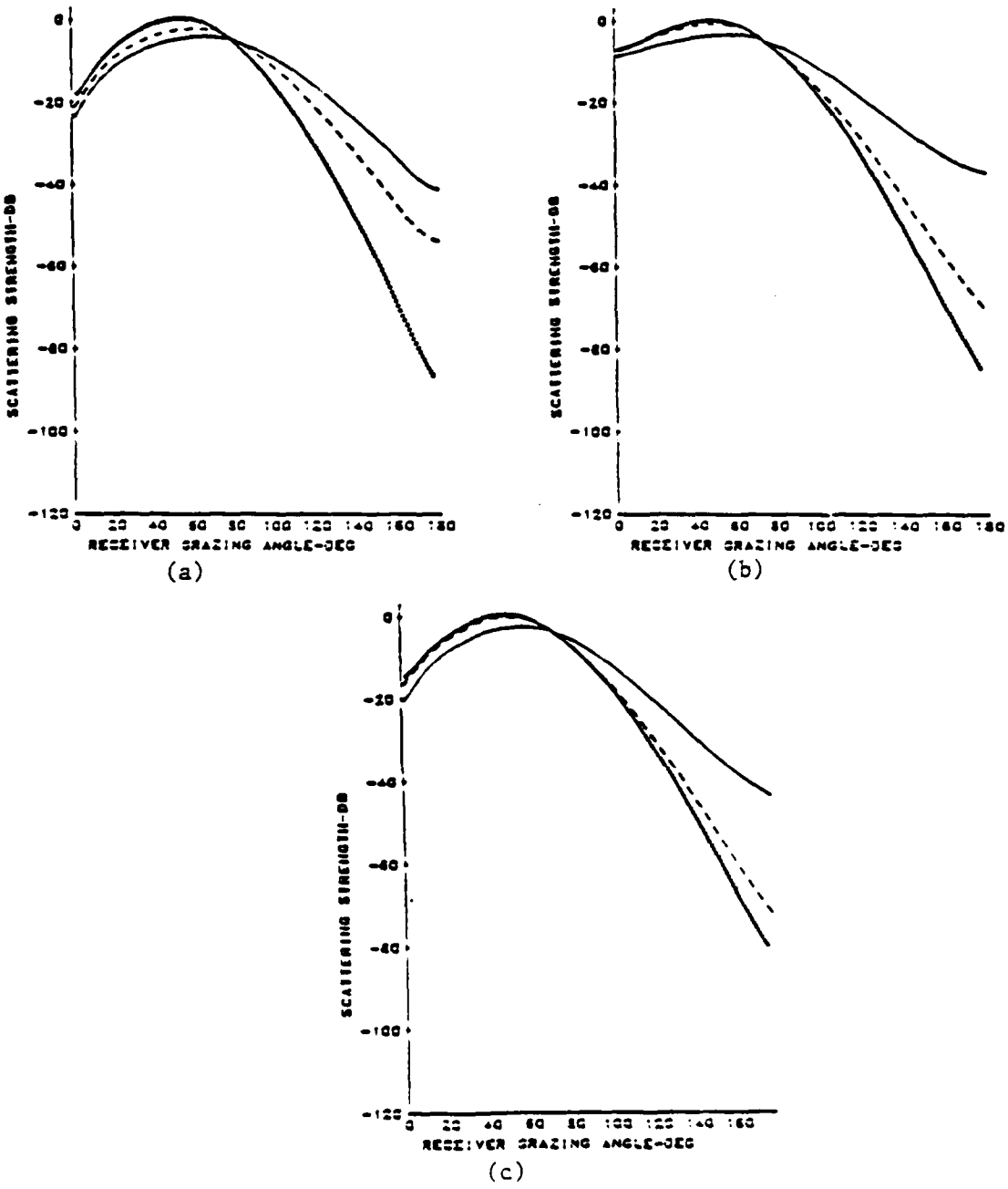

Figure 12. Forward scatter. (a) Fresnel slope-operator, (b) standard, (c) Fraunhofer slope-operator
____: 7KHz, ----: 12KHz, ****: 15KHz

Figures 13a, 13b, and 13c, show the maxima moving away from the specular angle for smaller beamwidths. The plots shown in Figures 14a, b, c hint that the problem lies in the coherent component of equations (3.20), (3.56), and (3.51). Since it involves frequency and beam characteristics and is a function of geometry, the exponential in the coherent term must be causing the phenomenon.

The coherent components of all three models are compared in Figure 15 to show once more that the Standard Model misbehaves for angles far away from the specular direction (80°). This is particularly obvious for shallow receiver angles. A comparison of this figure with number 11 gives an idea of the importance of the incoherent component away from the specular direction.

c. Azimuthal Forward Scatter

In this test the source and surface are as in the previous section, and the receiver is at 200 cm from the surface, the azimuthal angle is allowed to change while the depression angle is held fixed at 45°. The reader is reminded that the forward direction corresponds to an azimuthal angle of 90°, whereas the side and back are at 180° and 270° respectively, as depicted in Figure 2. Figure 16 shows a comparison of the three models. The peak occurs at 90° which corresponds to the specular direction, facing the source. The dip at 270°, in turn, is the antispecular or source position. The three models tend to behave similarly, although the amplitudes do not agree except for when the receiver is in the specular direction where

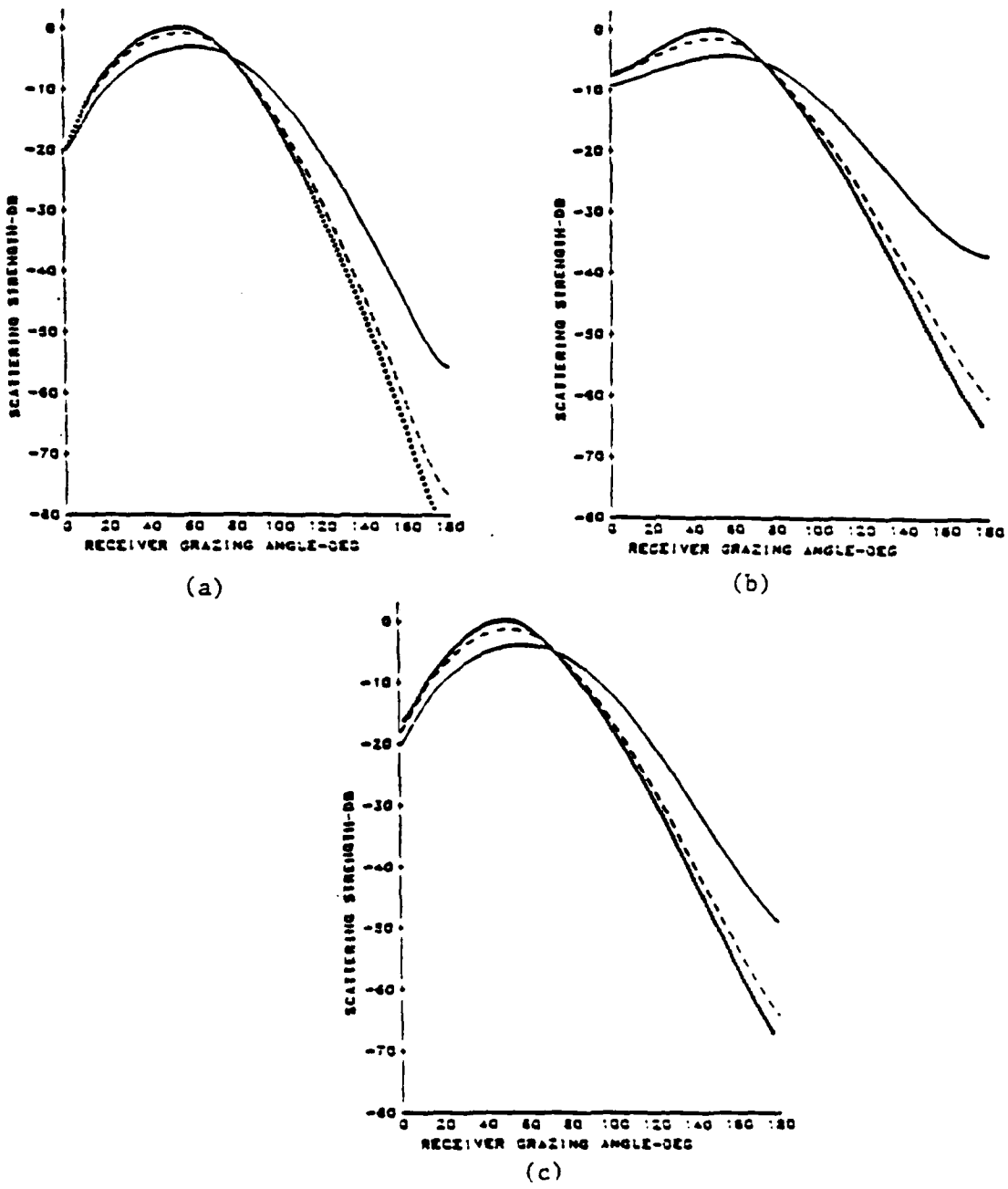

Figure 13. Forward scatter. (a) Fresnel slope-operator, (b) standard, (c) Fraunhofer slope-operator. ____: 5°, ----: 8°, ****: 10° beamwidth for a source operating at 10KHz

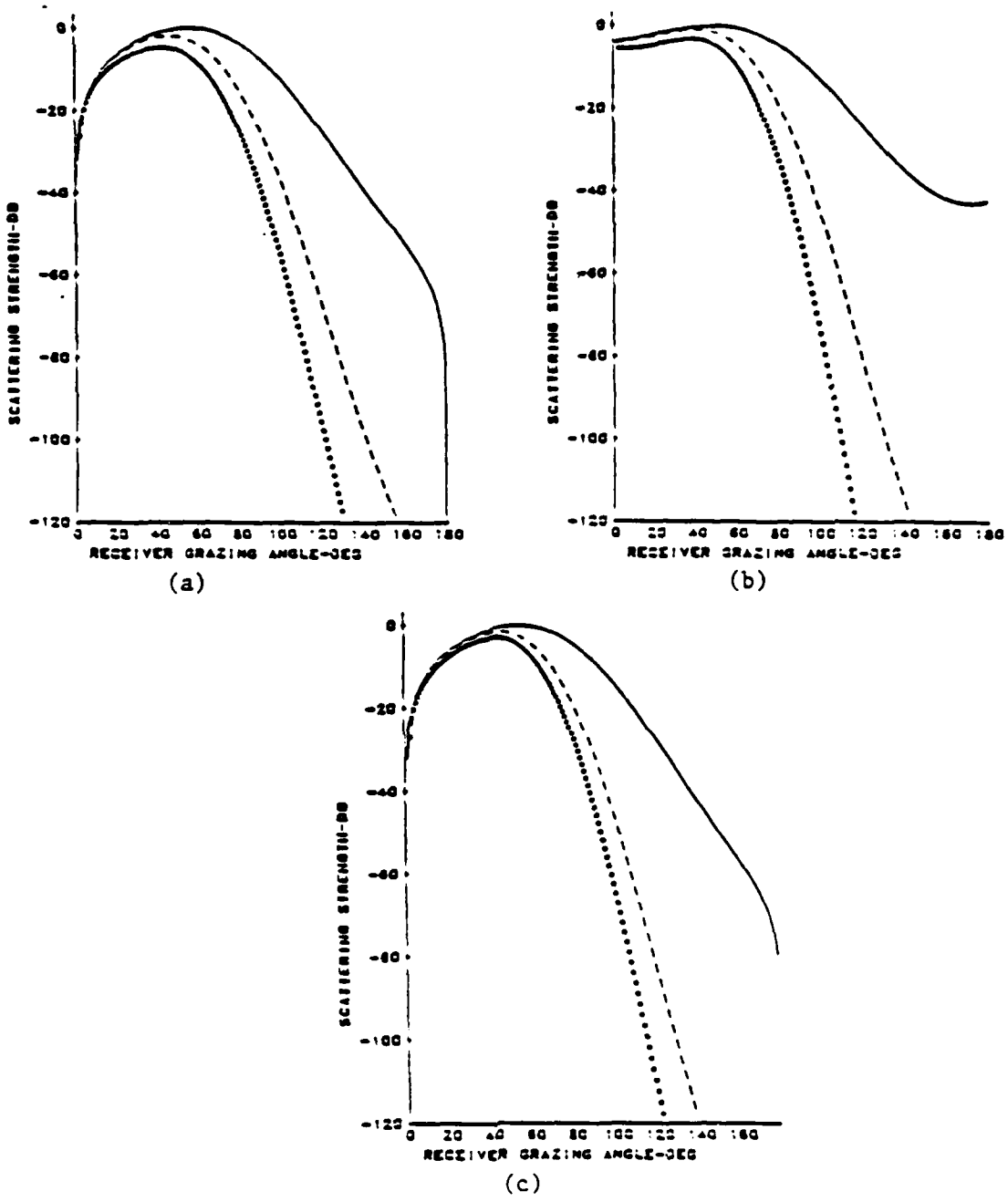

Figure 14. Forward scatter. Coherent component. (a) Fresnel slope-operator, (b) standard, (c) Fraunhofer slope-operator. ____: 7KHz, ----: 12KHz, ****: 15KHz

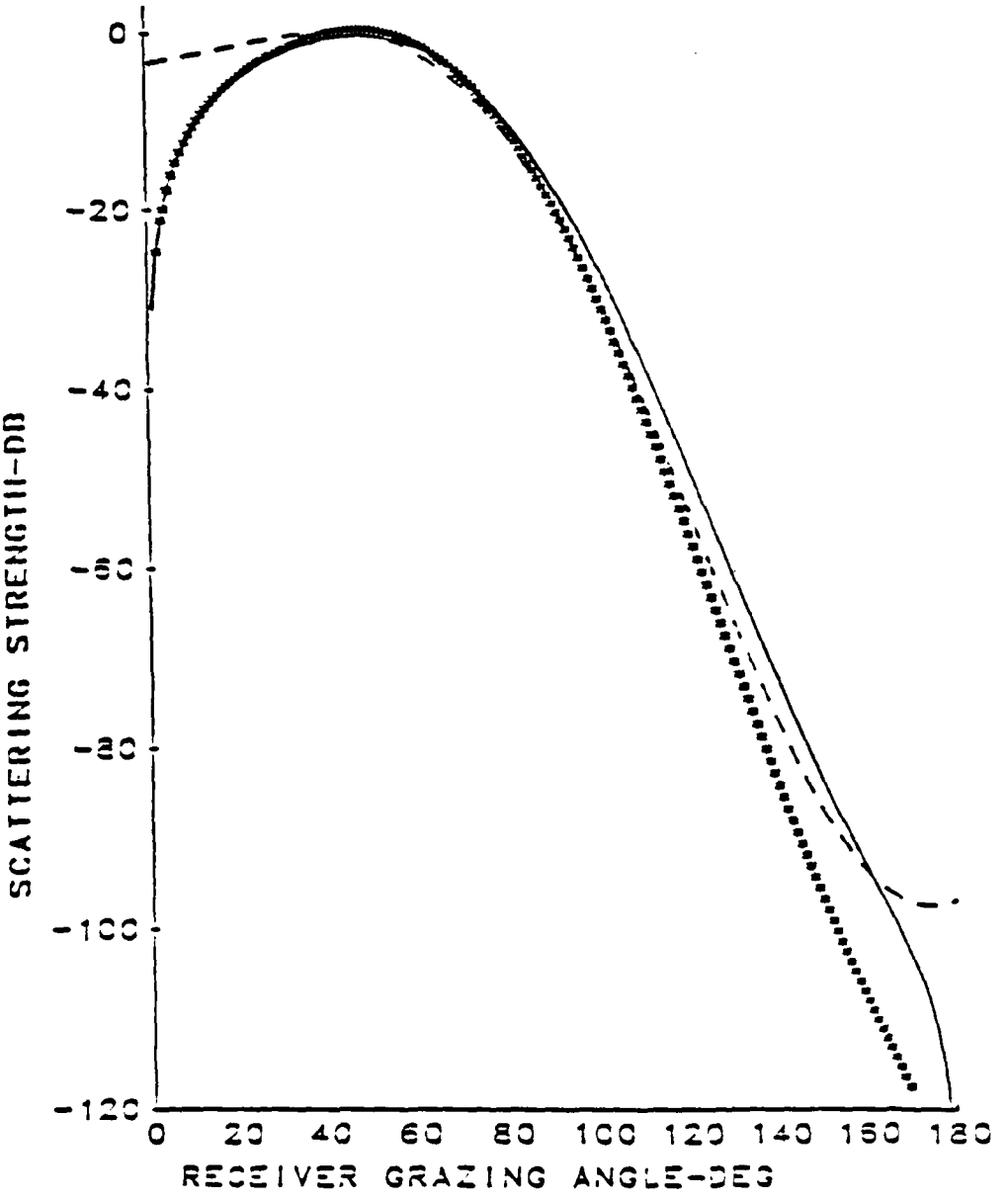

Figure 15. Forward scatter. Coherent component. 3° beam-10KHz source. ____: Fraunhofer slope-operator, ****: Fresnel slope-operator, ----: standard

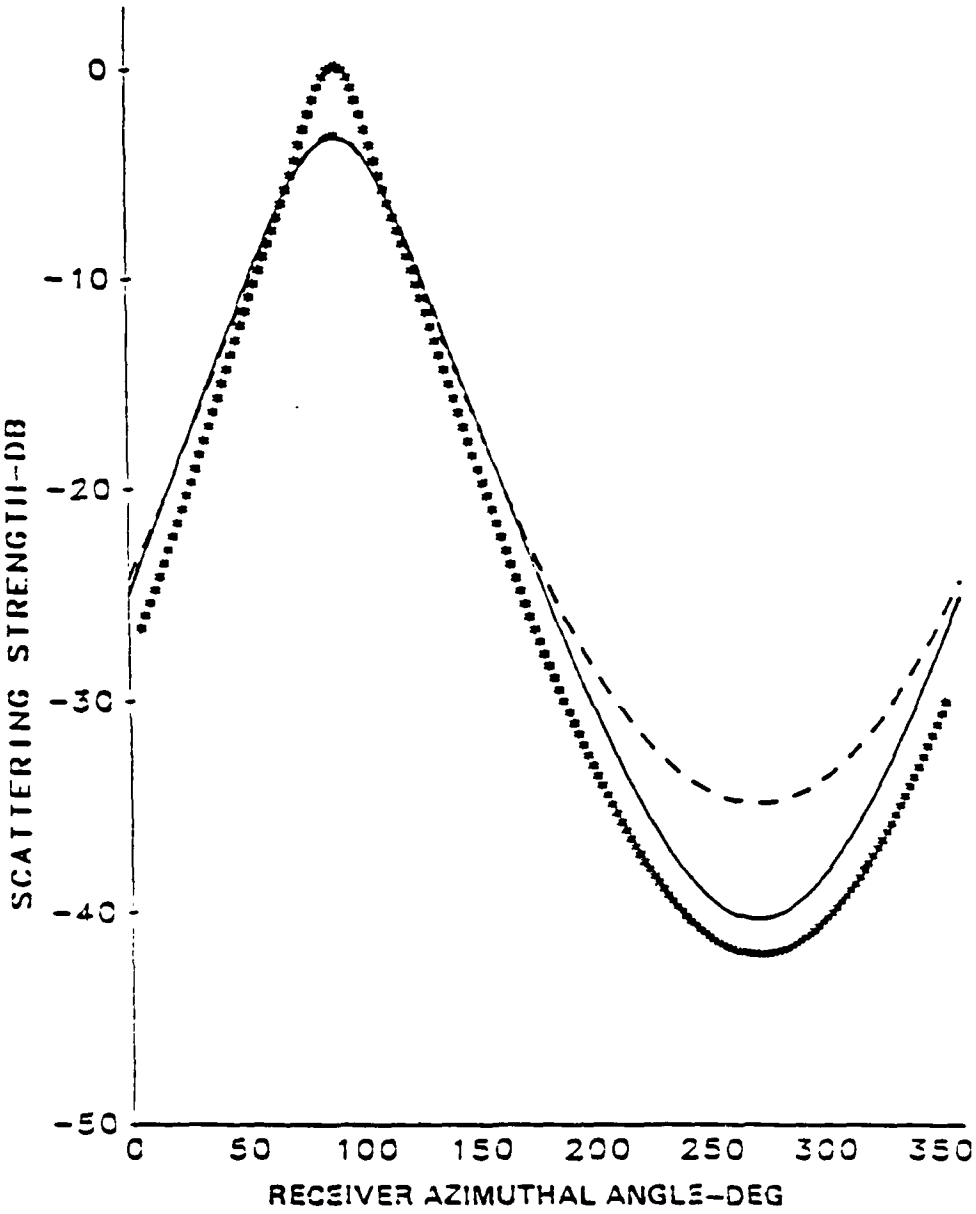

Figure 16. Azimuthal forward scatter. Source at 500 cm, 45° grazing angle. ____: Fraunhofer slope-operator, ----: standard, ****: Fresnel slope-operator.

the Standard and Fresnel result show agreement. Figures 17a, b, c show general qualitative agreement. Changes in the symmetry of the surface affect the predicted scatter in the antispecular direction (270°). When the autocorrelation length parallel to the surface direction is increased, the backscatter drops drastically towards the source and the forward scatter increases somewhat. In the limit of large autocorrelation, this result is logical since in the mirror surface, the scatter is mainly in the forward direction. On the other hand, when the cross-directed autocorrelation length is increased the figures display a narrowing of the forward-directed scatter and an increase in scatter towards the source. If a surface with one-dimensional corrugation is envisioned and a source is directed along the corrugation we would have the limit of the first example. When the source is directed perpendicular to the corrugation we would have the limit of the second example.

d. Summary

The Standard and Slope-Operator models are qualitatively alike, except for low grazing angles. The energy distribution is better described by the Slope-Operator Model than the Standard Model as the surface parameters change, mainly because the energy in the Standard Model is exclusively dominated by the coherent contribution. The coherent component is a good roughness estimator. A different approach to the integration-by-parts or the Slope-Operator is

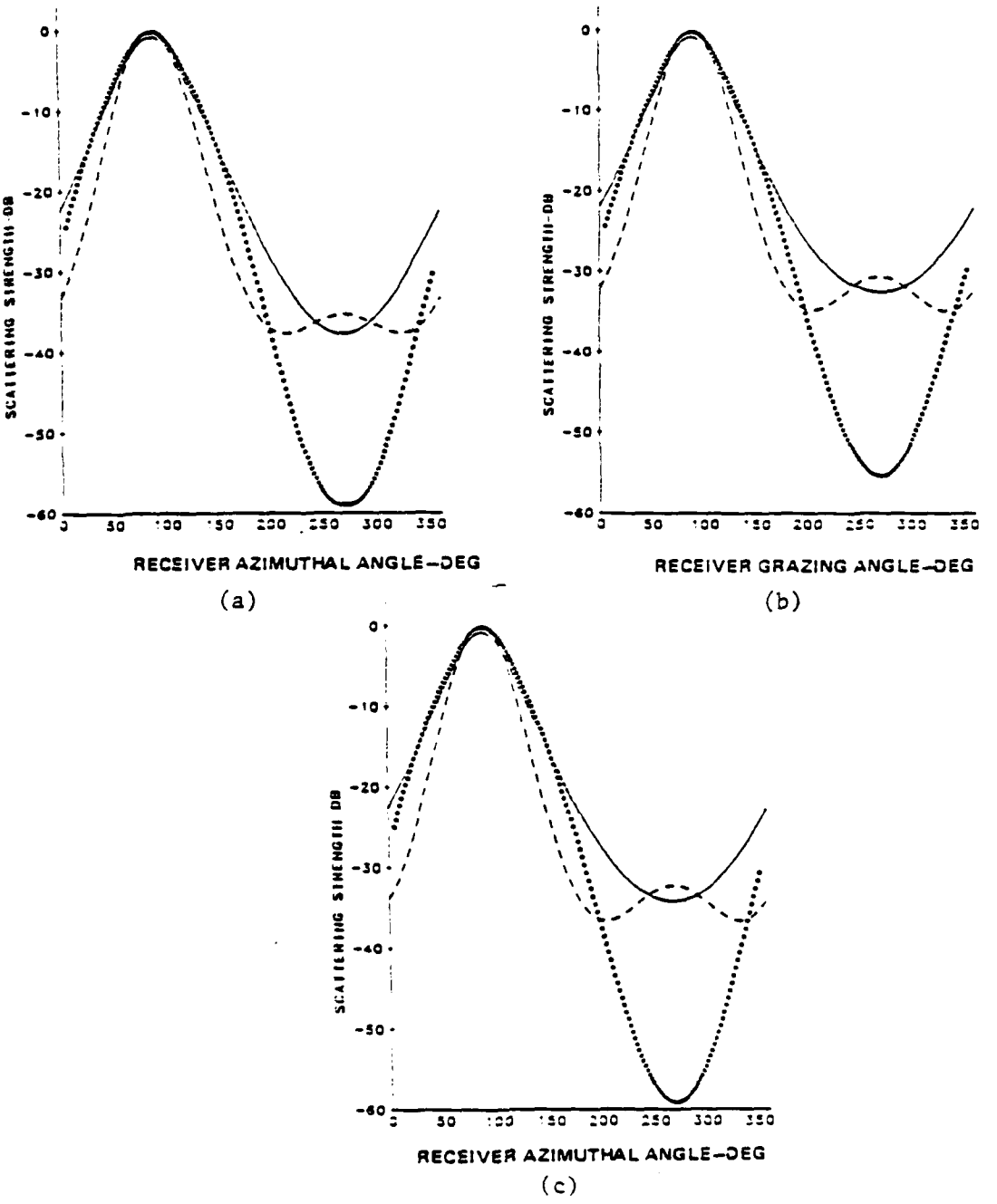

Figure 17. Azimuthal forward scatter. ___: 20,20, ----: 40,20, ****: 20,40cm for the x and y directed autocorrelation lengths respectively. (a) Fraunhofer slope-operator, (b) standard, (c) Fresnel slope-operator.

possible when the surface is only slightly rough. This is done by approximating $\frac{\partial}{\partial n}$ by $\frac{\partial}{\partial z}$, and upon examining the development in analogy to the Slope-Operator Model, assuming ζ_x and ζ_y to be zero in eq. 3.34. The result is identical to the coherent component of 3.45. Thus, a comparison between any of the previously mentioned models with this new approach is one in which the coherent component of the Slope-Operator Model is compared with the full model as well as the Standard approach. The main deficiency of the latter model is that no spectral information is supplied, or required, by the resulting expression. Hence, the approximation is valid in regions where the field is coherent. That comprises a region in the neighborhood of the specular direction for forward scatter and in the normal direction for backscatter. The size of these regions grows as the autocorrelation lengths get large and the rms height gets small.

The significant difference between the two Slope-Operator Models in the far-field occurs at low grazing angle where the Fresnel expression predicts lower energy levels. To answer the question of which model will agree better with experiment, a comparison with data is required. In the following section, among the Slope-Operator formulations, the Fraunhofer expression is chosen to study coherence.

B. COHERENCE

A source operating at 10 KHz with a 3° beam is placed at 200 cm and 45° with respect to the mean insonified surface. The surface

has autocorrelation lengths of 20 cm and an rms height of 2 cm. When one receiver is placed at the source position and another is allowed to move polarly as in Figure 18a, the coherence magnitude varies as shown in Figure 19a when predicted by the Standard and Slope-Operator Models. The peak occurs at 135° which corresponds to the source/fixed-receiver location. If the moving receiver travels azimuthally at a constant depression angle of 45° as per Figure 18b, the magnitude coherence is predicted as plotted in 19b. The coherence is unity at the source location, when the azimuthal angle is 270°.

When the fixed probe is placed 200 cm away from the surface with a depression angle of 45 and a moving receiver travels vertically forming a plane perpendicular to the mean surface, the arrangement is called here a vertical coherence test. Figure 20a illustrates this arrangement. The angle ϕ is set at 90° for the forward scatter direction, 180° for the side scatter direction or 270° for backscatter direction. The results for these three cases appear in Figure 21a, b, c respectively. The peaks occur at a horizontal distance of 141.42 cm, which corresponds to the depth of the fixed probe (i.e., 141.42·sec 45°=200.0). Since r_1 is different from r_2 except at the probe location, the phase of the coherence will be non-zero as shown in Figure 22. This last figure simply reflects the change in phase due to the $k(r_1-r_2)$ imaginary argument in the exponential of eq. 3.45 for the Slope-Operator, and 3.19 for the

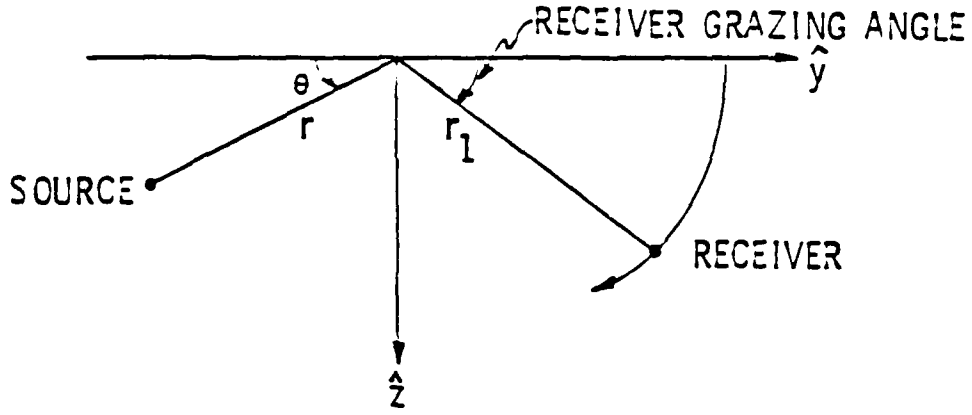

(a)

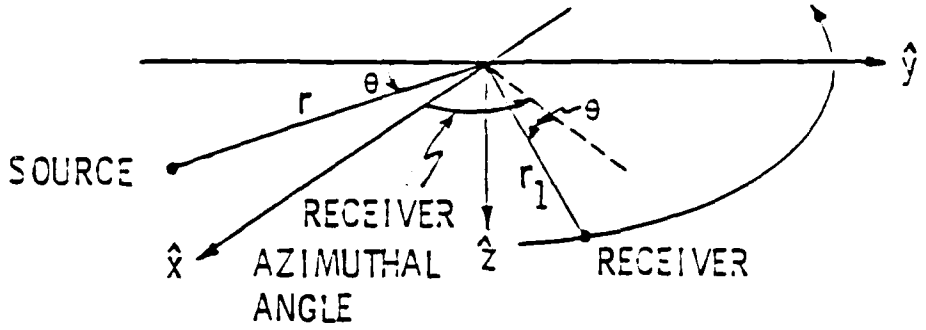

(b)

Figure 18. Geometry for (a) polar coherence, (b) azimuthal coherence

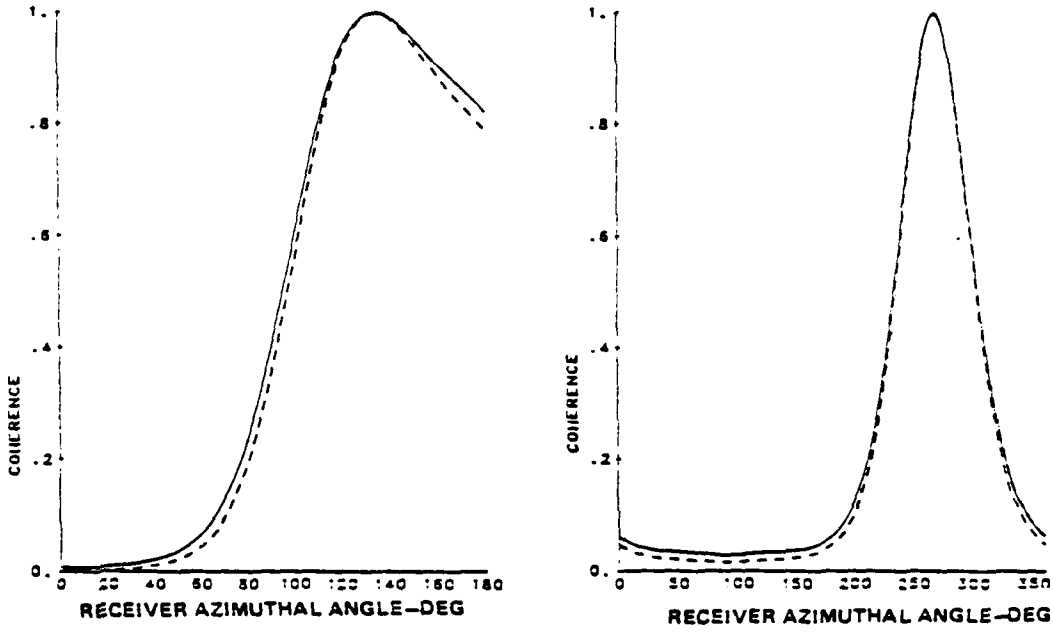

Figure 19. (a) Azimuthal coherence, (b) polar coherence
____: standard, ----: slope-operator

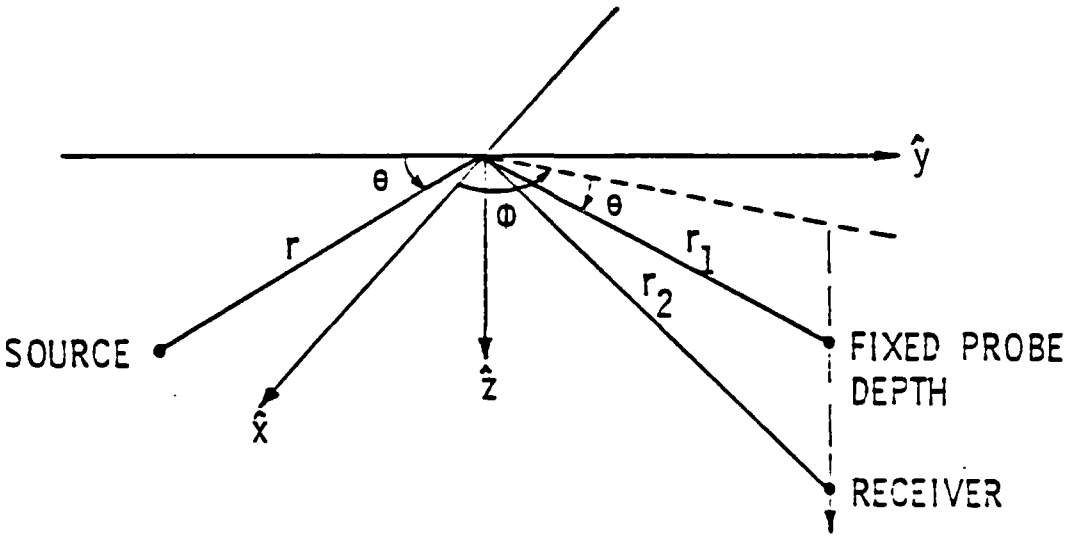

(a)

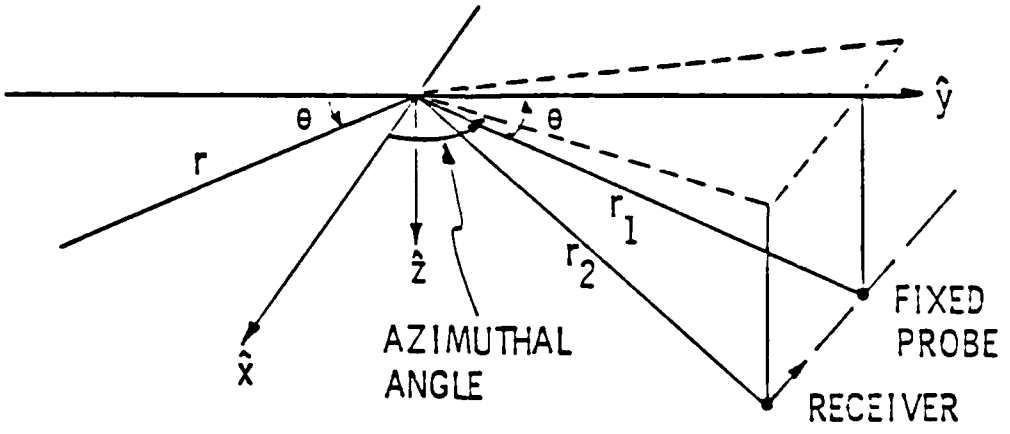

(b)

Figure 20. (a) Vertical coherence geometry, (b) horizontal coherence geometry.

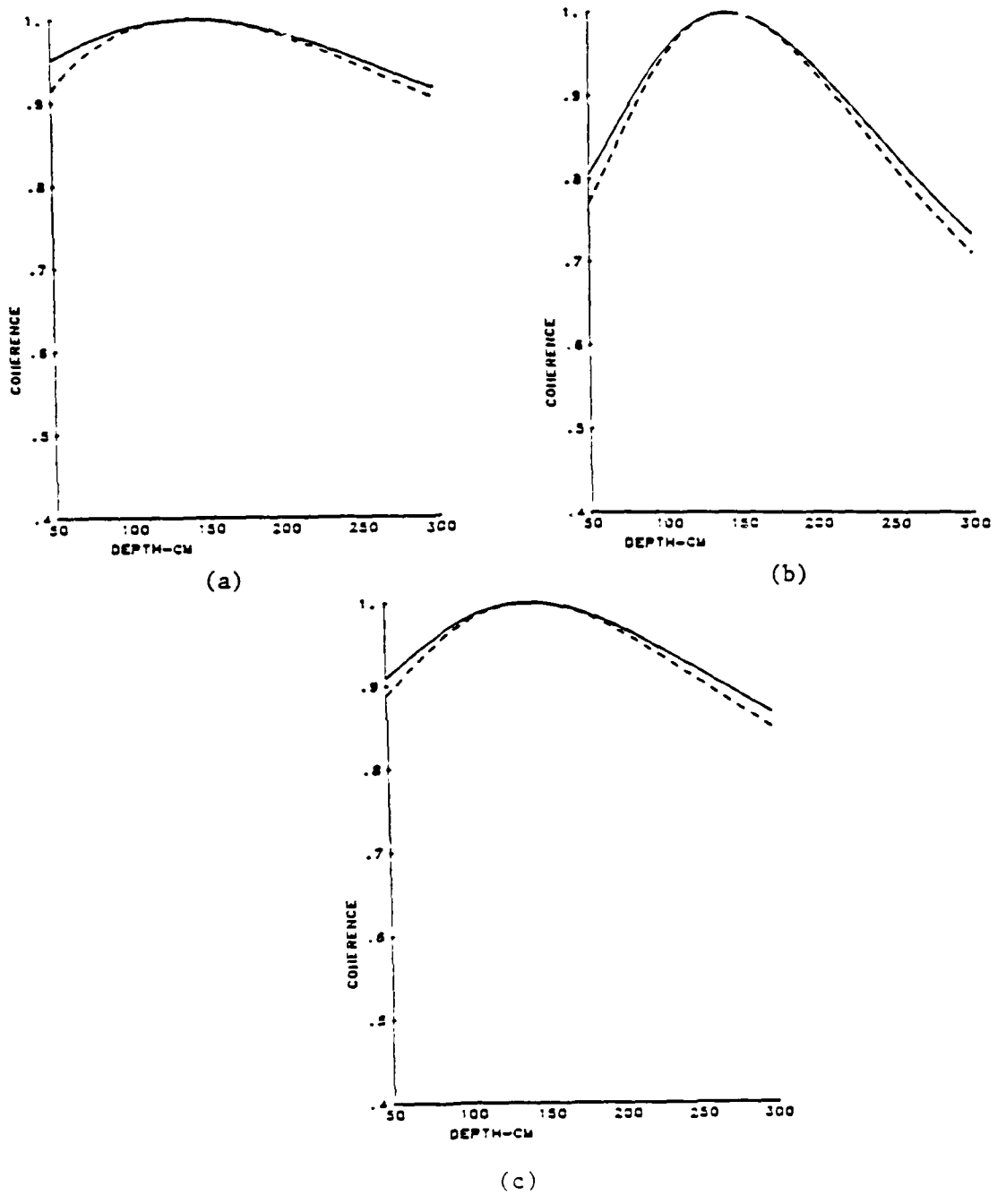

Figure 21. Vertical coherence. ____: standard, ----: slope-operator. (a) forward scatter direction, (b) side scatter direction, (c) back scatter direction.

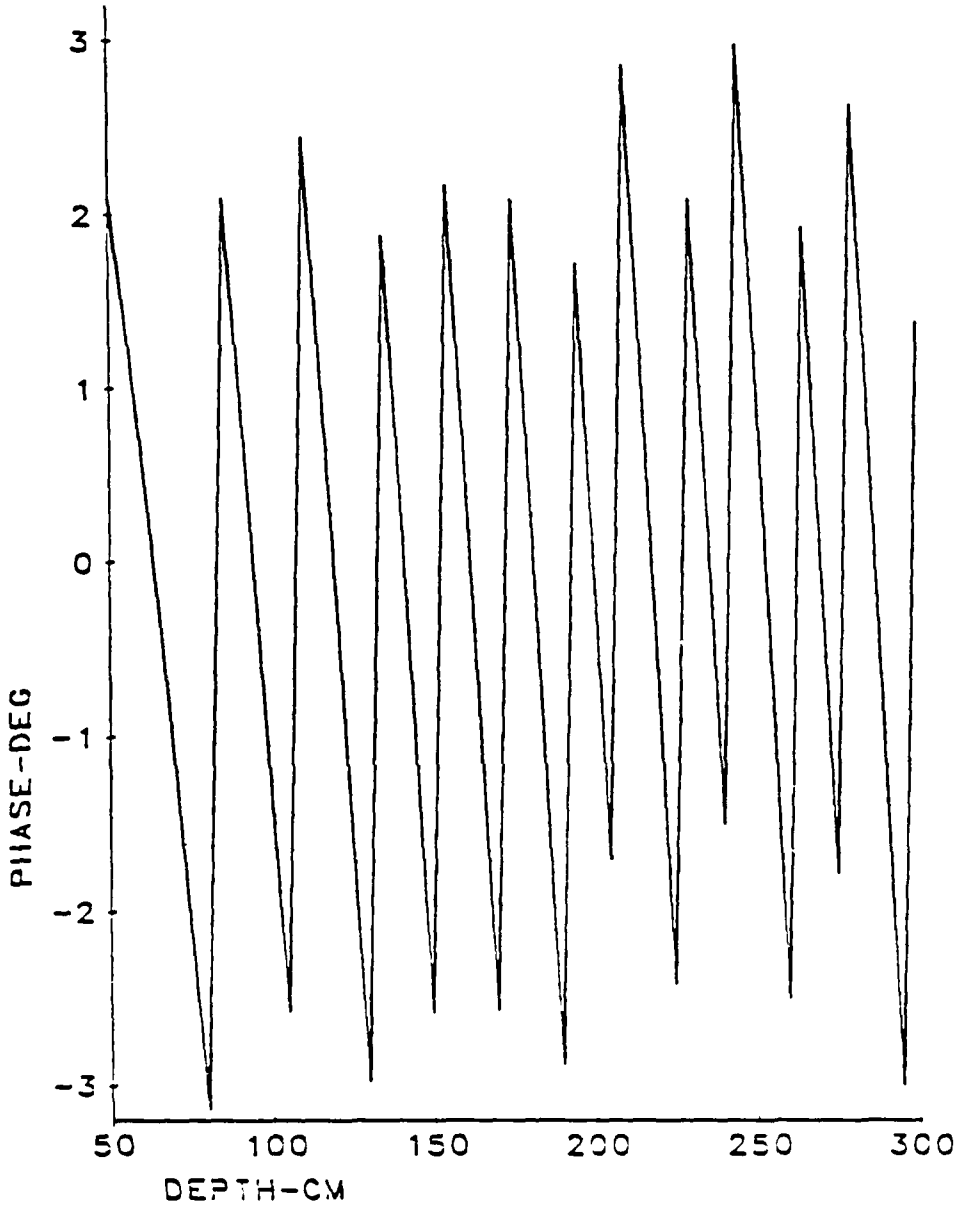

Figure 22. Phase for vertical coherence in the sidescatter direction. Both models.

Standard Case. The horizontal coherence test is illustrated by Figure 20b. The fixed probe is placed at a 45° depression angle, 200 cm away from the surface. The forward, side, and back directions correspond to azimuthal angles 90°, 180°, and 270° respectively (see Figure 2). The moveable receiver travels in straight line parallel to the mean surface within the azimuthal angles shown in Figures 23a, b, c. The coherence is strongly dependent on $\exp\{-\Gamma\}$ from expression (3.45) and (3.19) which is a function of source and receiver depression angles as well as surface roughness. These are factors which strongly affect the vertical coherence, but minimally affect the horizontal coherence, explaining why so little information is provided by the horizontal measurement while the vertical coherence is a good indicator of source direction as well as surface roughness.

The width of the magnitude of the coherence tends to get narrower with an increase in frequency as shown in Figures 24 a,b. The figures show that both models tend to better agreement as the source frequency is increased. On the other hand, better agreement between both models occurs when the beamwidth is decreased. Figures 25 a,b are plots of the coherence as a function of beamwidths for the two models. The coherence curves become narrow with an increase of frequency or beamwidth due to the exponentials involving $-k^2$ as well as $-U^2$ and $-V^2$.

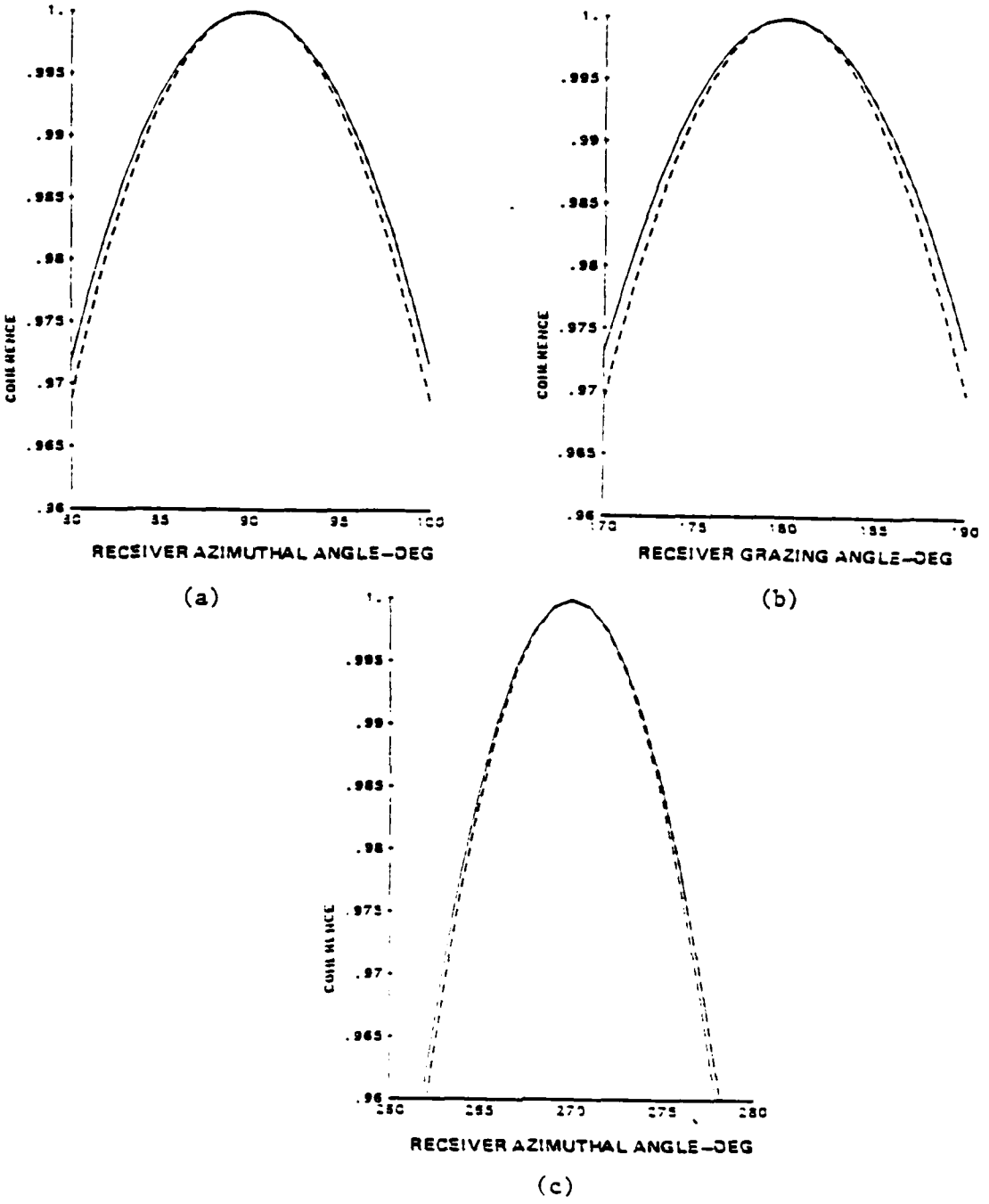

Figure 23. Horizontal coherence ____: standard, ----: slope-operator (a) backscatter direction, (b) side scatter direction, (c) forward scatter direction. Note extremely high resolution of vertical axis when comparing these plots to vertical coherence plots.

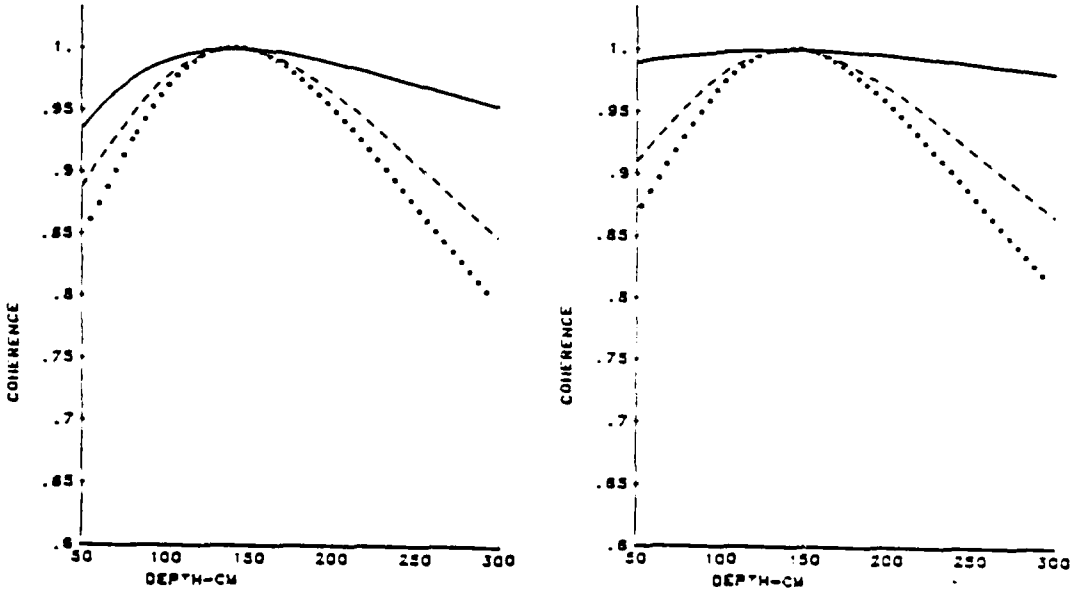

Figure 24. Coherence frequency dependence. ____: 5KHz, ----: 10KHz, ****: 12KHz (a) standard model, (b) slope-operator model

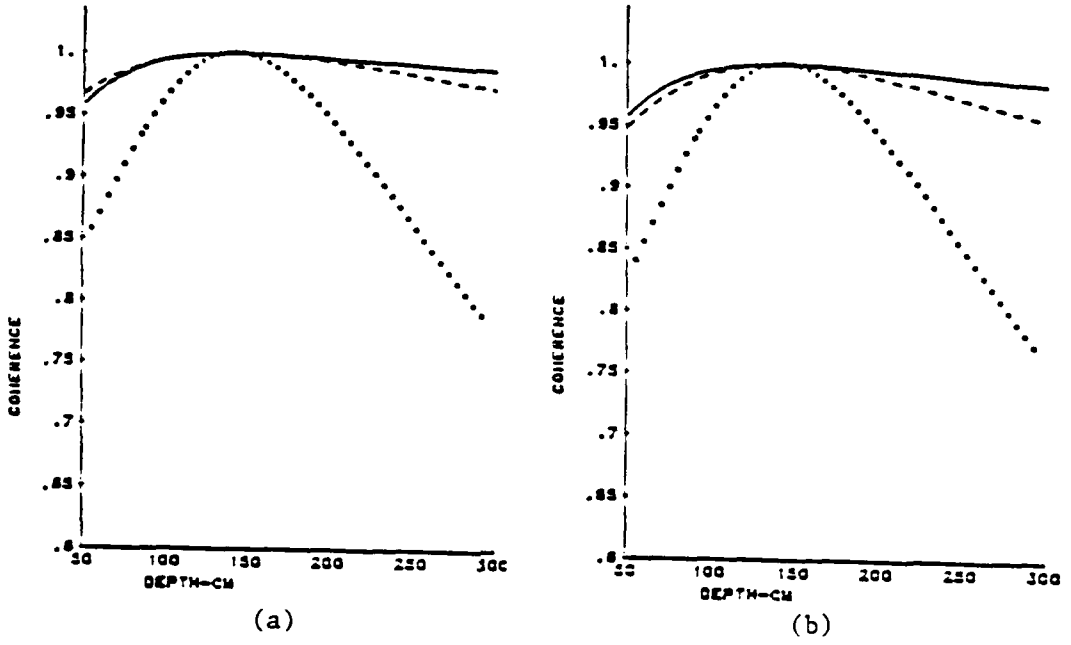

Figure 25. Coherence beamwidth dependence. ____: 3°, ----: 5°, ****: 10° (a) standard model, (b) slope-operator model

The coherence is a function of source position. For example, when the source grazing angle is shallow, U^2 is large so that the coherence is low. This is particularly tue when α and α are non-zero as is the case when the source and receivers are non-coplanar. Coherence is sensitive to variation of the rms height but is best used as an estimator of spectral information. The variation of the coherence with rms height is shown in Figures 26 a,b. Figures 26 c,d show that increasing the autocorrelation length parallel to the source direction will tend to broaden the coherence curves. Changing the cross-directed autocorrelation length does not have any affect on the coherence plots, as is evident in Figures 27 a,b. The best estimator of surface roughness is the coherent component of the intensity, since it is equal to $\langle p \rangle_M \langle p \rangle^*_M e^{-\frac{g_1 \pm g_2}{2}}$, i.e., the coherent intensity reflected from a mirror surface times a "coherence" factor which is a function of surface roughness.

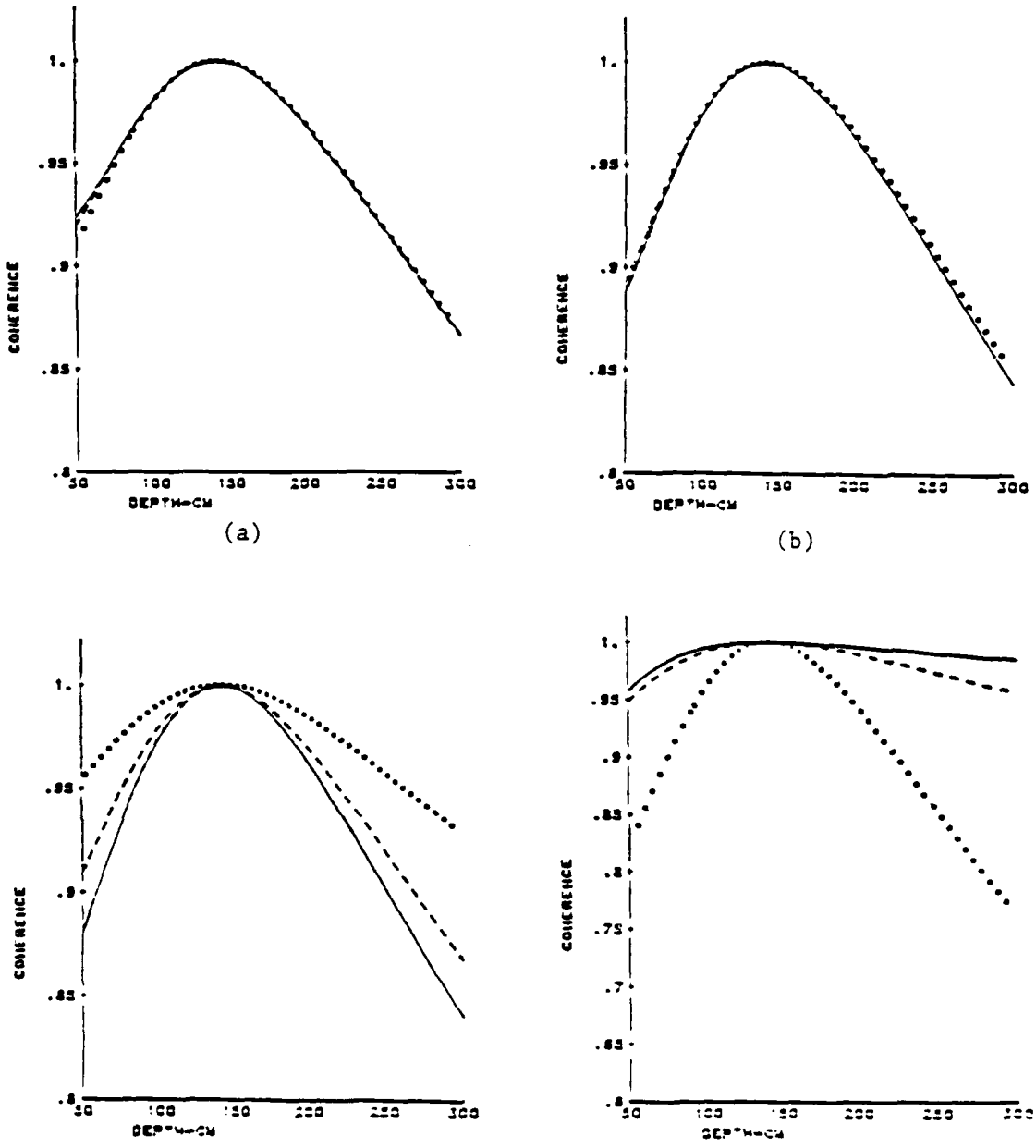

Figure 26. Coherence. (a) dependence on surface rms height, standard model, (b) dependence on surface rms height, slope-operator model ____: .5 cm, ----: 1.0 cm, ****: 2.0 cm, (c) dependence on surface autocorrelation lengths, standard model, (d) dependence on surface autocorrelation lengths, slope-operator model. Cross-directed length fixed at 20 cm, ____: 10 cm, ----: 20 cm, ****: 40 cm for the parallel autocorrelation length.

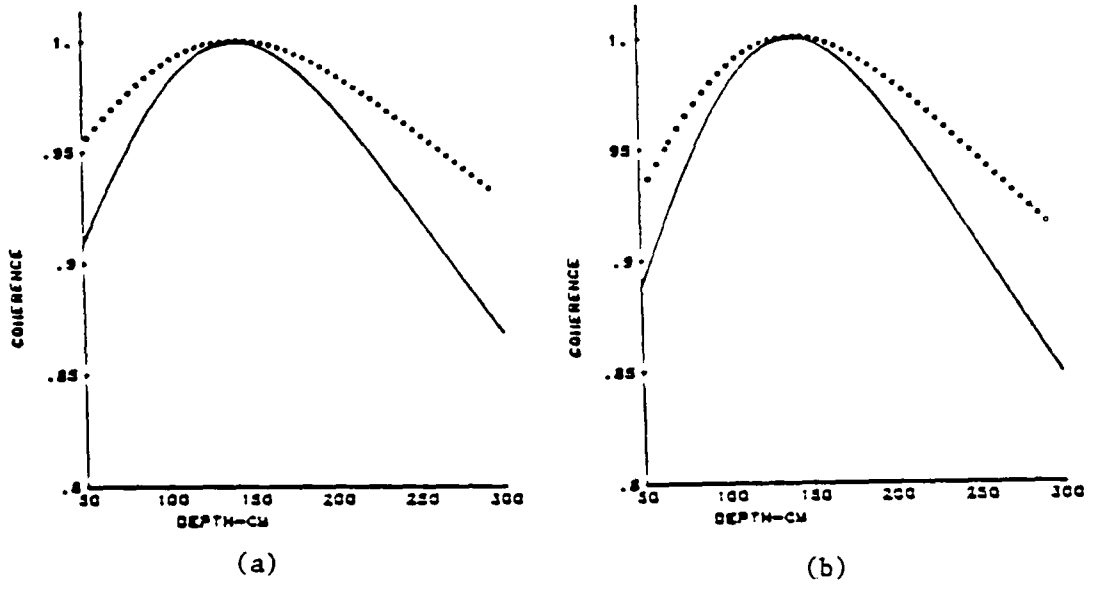

Figure 27. Coherence. Dependence on autocorrelation lengths. ____: 20,20 and 40,20. ----: 20,40 cm for cross-directed and parallel autocorrelation lengths. (a) standard, (b) slope-operator

CHAPTER V

IN-PLANE SCATTER USING THE PIERSON-STACY OCEAN SPECTRUM (42,43)

The aim is to illustrate and compare the far-field results obtained from the models developed in Chapter 3 when the surface involved is the fully developed, non-directional ocean spectrum - see Appendix. For convience we list the most salient changes in the variables owing to the geometry (see Figure 2) and the symmetry in the spectra:

$$f_1(\Theta) = \frac{1+\sin\theta\sin\theta_1}{\sin\theta+\sin\theta_1} \tag{5.1}$$

$$f_2(\Theta) = \frac{1+\sin\theta\sin\theta_2}{\sin\theta+\sin\theta_2} \tag{5.2}$$

Since $\phi_1=\phi_2=\pi/2$ then

$$\alpha_1 = -\epsilon_1 = 0 \qquad \bar{\alpha} = \alpha = 0$$

$$\alpha_2 = -\epsilon_2 = 0 \qquad \bar{\beta} = \cos\theta - \frac{\cos\theta_1+\cos\theta_2}{2}$$

$$\delta_1 = \cos\theta_1 \qquad \beta = -(\cos\theta_1-\cos\theta_2)$$

$$\delta_2 = \cos\theta_2$$

$$\beta_1 = (\cos\theta-\cos\theta_1)$$

$$\beta_2 = (\cos\theta-\cos\theta_2) \tag{5.3}$$

and the spectrum $W(\chi)$ is equal to $S(\kappa)/\kappa$ for the non-directional case.

A. GENERAL CASE

1. Standard Model

a. Slightly Rough Ocean

Implementing the above changes in equations (3.25) and (3.26), the covariance and intensity for in-plane scatter are

$$\Gamma_{12LF} = \Gamma_{12coh} + \frac{GA^2k^2f_1(\Theta)f_2(\Theta)e^{ik(r_1-r_2)-\Gamma-\frac{k^2}{8}V^2\beta^2}}{8\pi^3\sigma^2r_1r_2r'^2} \iint_{-\infty}^{\infty} d\chi_x d\chi_y$$

$$\times \; W(\chi_x,\chi_y)e^{-\frac{1}{2}[\chi_x^2U^2+(k\bar{\beta}+\chi_y)V^2]} \tag{5.4}$$

with $$\Gamma_{12coh} = \frac{A^2k^2f_1(\Theta)e^{-\frac{k^2}{8}[V^2(\beta^2+4\bar{\beta}^2)]}e^{ik(r_1-r_2)}e^{-\Gamma}}{4\pi^2r'^2r_1r_2}$$

and

$$\Gamma_{11LF} = \Gamma_{11coh} + \frac{gA^2k^2f^2(\Theta)e^{-g}}{8\pi^3\sigma^2(r'r)^2} \iint_{-\infty}^{\infty} d\chi_x d\chi_y$$

$$\times \; W(\chi_x,\chi_y)e^{-\frac{1}{2}[\chi_x^2U^2+(k\bar{\beta}+\chi_y)^2V^2]}, \tag{5.5}$$

$$\text{with} \quad \Gamma_{11coh} = \frac{A^2k^2f^2(\Theta)e^{-\frac{k^2}{2}[V^2\bar{\beta}^2]}}{4\pi^2(r'r)^2}.$$

To evaluate the integrals with an omnidirectional spectrum, we perform the change of variables

$$\chi_y = \kappa\cos\Omega$$

$$\chi_x = \kappa\sin\Omega$$

and proceed using polar coordinates. The integral is now

$$e^{-\frac{1}{2}k^2\bar{\beta}^2V^2}\int_0^\infty \kappa d\kappa \int_0^{2\pi} d\Omega W(\kappa,\Omega)e^{-\frac{1}{2}k^2U^2}e^{-\frac{1}{2}[k^2(V^2-U^2)\cos^2\Omega+2k\bar{\beta}\kappa V^2\cos\Omega]} \tag{5.6}$$

Where the omnidirectional spectrum $S(\kappa)/\kappa$ and the angular integration is performed using a procedure outlined by Beckmann (43, p. 195). The expression transforms into

$$2\pi e^{-\frac{1}{2}k^2\bar{\beta}^2V^2}\sum_{m=o}^{\infty}\frac{(\Gamma+\frac{1}{2})}{m!}\left(\frac{(U^2-V^2)}{V^2k\bar{\beta}}\right)^m\int_o^\infty d\kappa\kappa^m I_m(-V^2k\bar{\beta}\kappa)S(\kappa)e^{-\frac{V^2\kappa^2}{2}} \tag{5.7}$$

When $\bar{\beta}$ is zero, the expression takes the form

$$2\pi\sum_{m=o}^{\infty}\frac{\Gamma(m+1)}{m!}\left(\frac{U^2-V^2}{2}\right)^m\int_o^\infty d\kappa\kappa^{2m}S(\kappa)e^{-\frac{1}{2}V^2\kappa^2} \tag{5.7a}$$

The evaluation of (5.4) and (5.5) with (5.7) needs to be performed numerically.

b. Very Rough Ocean

For covariance eq. (3.30) is

$$\Gamma_{12HF} = \frac{A^2k^2f_1(\theta)f_2(\theta)e^{ik(r_1-r_2)} \; e^{-\frac{k^2}{8}[V^2(\beta^2+4\bar{\beta}^2)/B_2^2)]} \; e^{-\frac{G}{2}T_o}}{4\pi^2r'^2r_1r_2B_1B_2} \tag{5.8}$$

and the intensity is thus

$$\Gamma_{11HF} = \frac{A^2k^2f^2(\theta)e^{-\frac{k^2}{2}\left(\frac{\bar{\beta}V}{B_2}\right)^2}}{4\pi^2(r'r)^2B_1B_2} \tag{5.9}$$

with $B_1 = \sqrt{1-GT_1U^2}$

$B_2 = \sqrt{1-GT_2V^2}$

the square roots are to be taken positive. For an omnidirectional spectrum $T_1=T_2=T/\sqrt{2}$, where

$$T = \frac{\partial^2}{\partial r^2}\left\{\frac{1}{2\pi\sigma^2}\int_o^\infty d\kappa \int_o^{2\pi} d\Omega S(\kappa)e^{i\kappa(\sin\Omega\cos\theta+\cos\Omega\sin\theta)}\right\}_{r=o}$$

or

$$T = \frac{1}{2\sigma^2}\int_o^\infty d\kappa\kappa^2S(\kappa) \tag{10}$$

c. Discussion

1. Scattering Strength

A source is placed 500 cm from the ensonified surface and is operating with a 3° beamwidth. The windspeed measured at 1000 cm is 514.4 cm/s (10 knots). This 10 knot wind produces a surface with rms height of 15.8 cm and $-7.1 \cdot 10^{-5}$ for the parameter T, eq. (5.10). Under these conditions the scattering strength varies with source/receiver polar angle for the specular test as shown in Figure 28a. Under the same conditions the backscatter case is illustrated in Figure 28b and for the forward scatter case, 28c. Comparison of the two plots gives an idea of the greater significance of the coherent contribution as the frequency is increased. They also display the phenomenon of a decrease in amplitude and broadening of the curves as the frequency is decreased. Note as well that the amplitude shifts to the specular direction - 45° - as the frequency is increased in the forward scatter test.

If, on the other hand, when the frequency and beamwidth are 10 KHz and 3°, respectively, and the measured windspeed at 1000 cm is 257.2 cm/s, 514.4 cm/s, 771.6 cm/s (corresponding to 5, 10, and 15 knots) the scattering strength will vary as illustrated in Figures 29a, b, c. The primary effects are a broadening and decreasing maximum amplitude with increasing rms height and slope. The forward and backscatter curves show the fundamental shortcoming of the

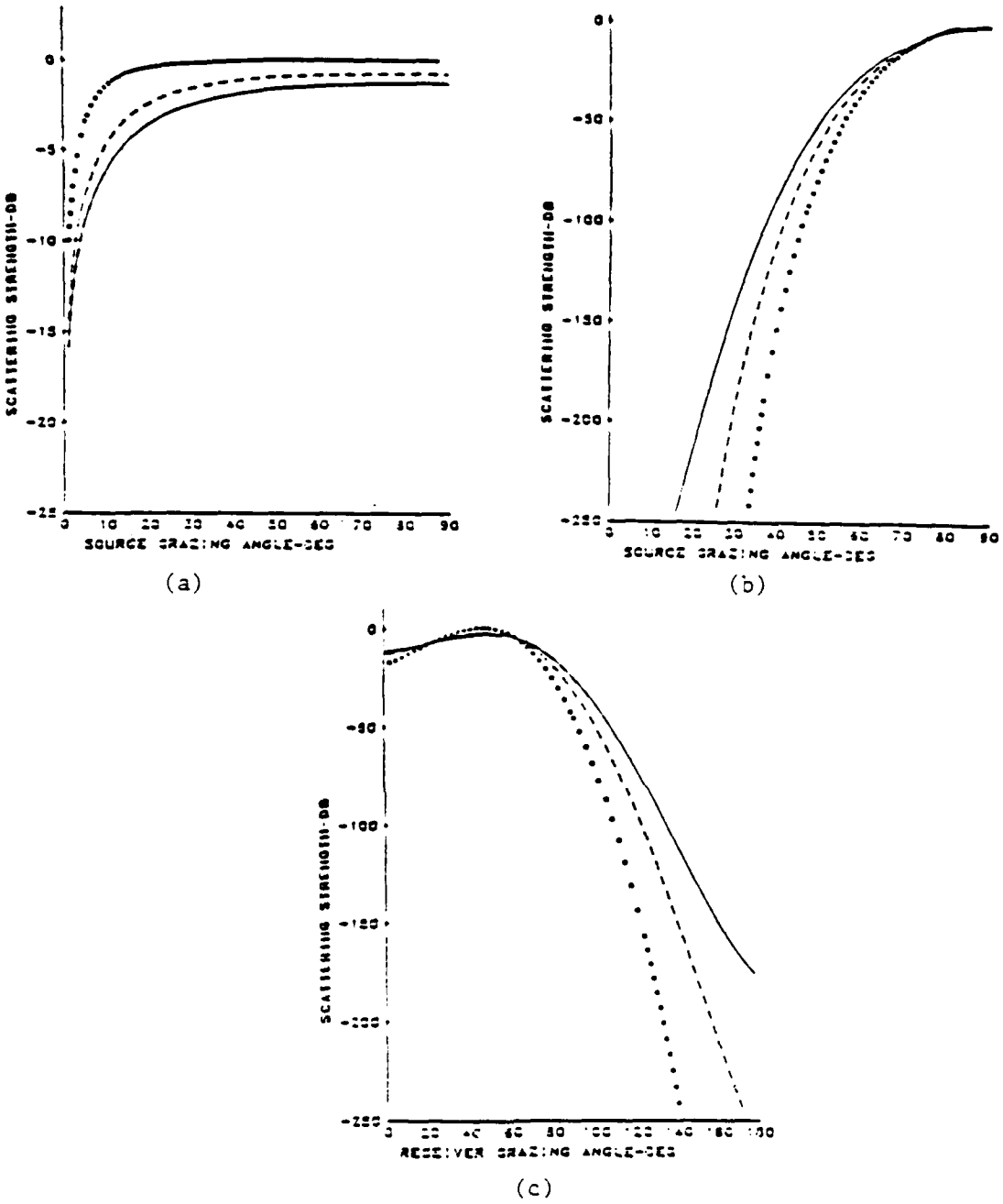

Figure 28. Scattering strength variation with frequency. standard model. (a) specular, (b) backscatter, (c) forward scatter. Windspeed of 1000 cm is 514.4 cm/s ____: 15 KHz, ----: 20 KHz, ****: 50 KHz.

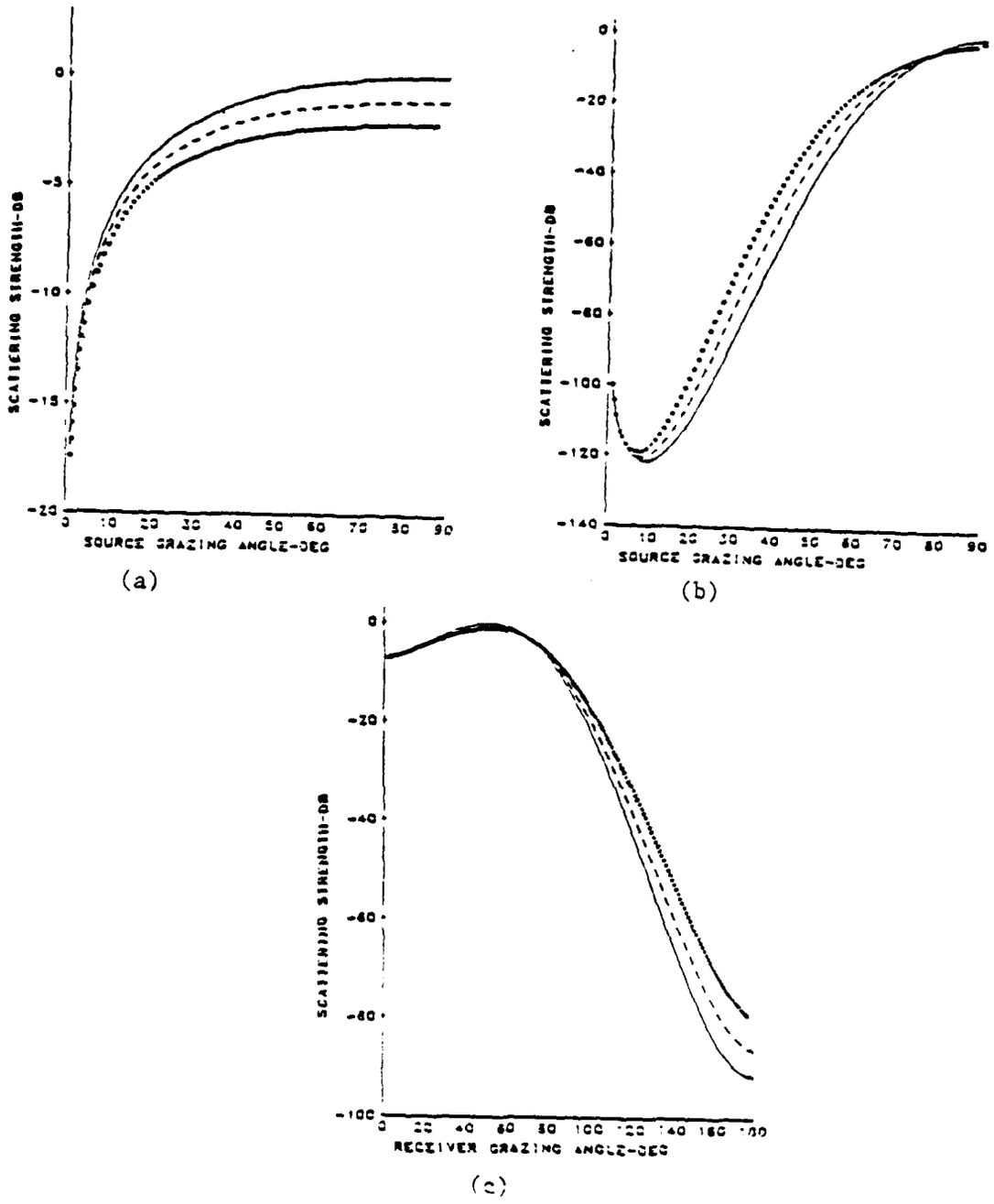

Figure 29. Scattering strength. Variation with windspeed. (a) specular, (b) backscatter, (c) forward scatter, source frequency 10 KHz, 3° beam. ____: 257.2 cm/s, ----: 514.4 cm/s, ****: 771.6 cm/s. ____: σ = 4.0 cm, T = $-6.5 \cdot 10^{-4}$, ----: σ = 15.8 cm, T = $-7.1 \cdot 10^{-5}$, ****: σ = 35.7 cm, T = $2 \cdot 10^{-5}$

Standard Model, namely, the severe misprediction for low grazing angles.

2. Coherence

Figure 30 shows the variation in the vertical coherence as a function of windspeed. the source and a fixed probe are 200 cm away at a depression angle of 45°. The receiver changes in depth from 50 cm to 300 cm. As would be expected, the coherence narrows with an increase in the surface rms slope and height. The coherence tends to narrow as well when the frequency or beamwidth is increased (see Figures 31a, b). The nature of this phenomenon has been discussed in the previous chapter.

B. SPECIAL CASE: WHEN THE SPECTRAL INTEGRALS CONTAIN A GENERALIZED FUNCTION

The integral

$$\int_{-\infty}^{\infty} d\chi_x \int_{-\infty}^{\infty} d\chi_y \; Ne^{-\frac{1}{2}[\chi_x^2 U^2 + \chi_y^2 V^2]} = 1 \qquad (5.11)$$

satifies the equality when U^2 and V^2 are very large and when N is equal to $A/2\pi^2$, because in the limit of very large U^2 and V^2 the integrand is a delta function. This fact can be used to explicitly evaluate some cases that involve an arbitrary spectrum.

In this section the above fact is used to solve the equations, developed in the previous chapter, which involve a non-gaussian spectrum. The Pierson-Stacy spectrum is chosen here because it is an interesting case involving a non-gaussian spectrum belonging to an

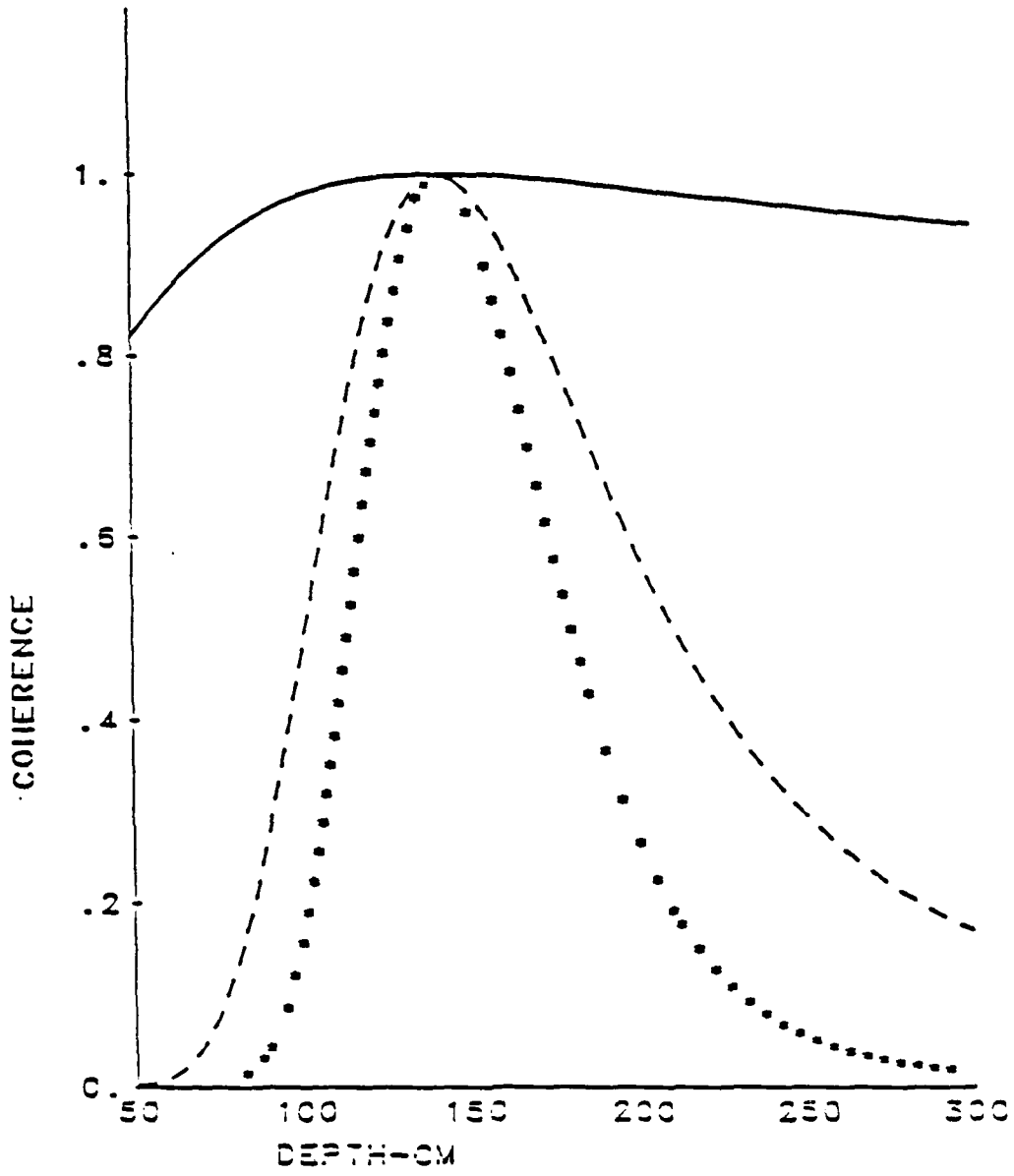

Figure 30. Vertical coherence in the backscatter direction. variation with windspeed. ____: 2.57 cm/s, ----: 514.4 cm/s, ****: 721.6 cm/s measured at 1000 cm. Source at 200 cm at 45° with 3° beamwidth and operating frequency of 10 KHz.

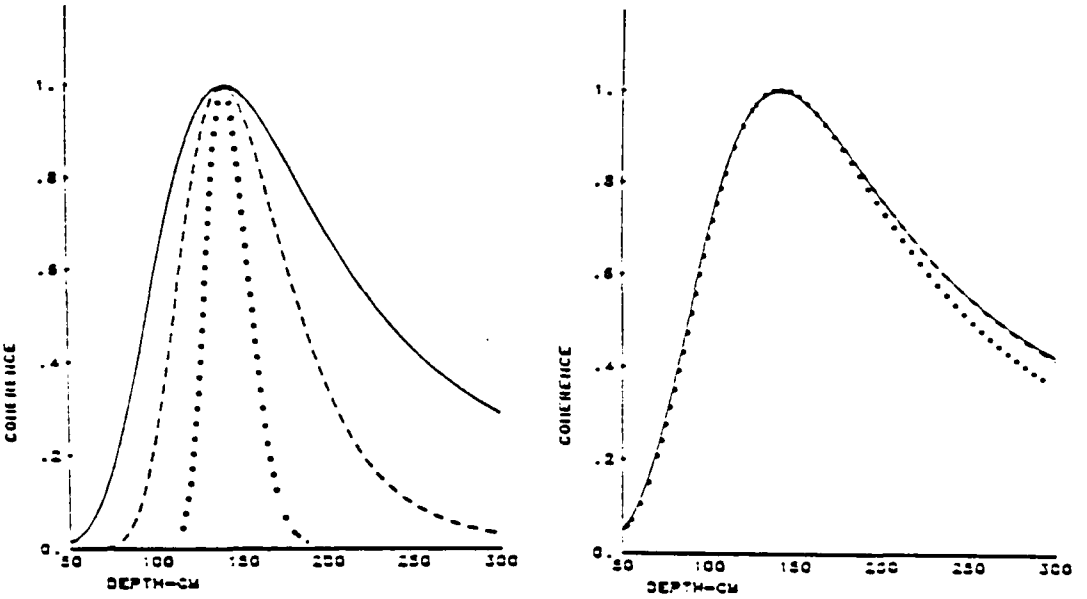

Figure 31. Vertical coherence in backscatter direction (a) variation with frequency. ____: 12 KHz, ----: 20 KHz, ****: 50 KHz, (b) variation with beamwidth ____: 3°, ----: 5°, ****: 10° beam. Wind at 1000 cm above water is 514.4 cm/s

assumed Gaussian height-distributed Dirichlet surface. The in-plane case is considered, as opposed to the general geometry, because the amount of algebraic manipulation is reduced considerably. However, the approximations to be made in this section do not rely on the fact that the source-surface and surface-receiver rays be co-planar.

The integrand in eq. (5.11) is not present in all three models considered in the last chapter in the form presented above. Thus, the constant N shall be different for all three models, depending on the other parameters of the quadratic term in the exponential that behaves delta-like in the above approximation. The parameters U^2 and V^2 are contained in all three models and one must be careful to consider cases of them large not by making the aperture wide but rather, by making the values of the source-surface distance very large in comparison to U and V (see eq. 2.7) while maintaining a very narrow beamwidth. This is because an assumption common to all three models is that the ensonified area dimensions must be comparatively small - see Chapter 2.

1. The Standard and Slope-Operator Models

a. Slightly Rough Surface

Using (3.25) and (3.26) as well as the integration properties of generalized functions, the Standard Model yields

$$\Gamma_{12LF} = \Gamma_{12coh} + \frac{GAk^2 f_1(\theta) f_2(\theta) e^{ik(r_1 - r_2)} e^{-\frac{k^2}{8}\beta^2 V^2} e^{-\Gamma} W(0, |k\tilde{\beta}|)}{4\pi^2 \sigma^2 r'^2 r_1 r_2} \tag{5.12}$$

$$\text{with } \Gamma_{12coh} = \frac{A^2k^2f_1(\theta)f_2(\theta)e^{ik(r_1-r_2)}e^{-\frac{k^2}{8}(\beta^2+4\tilde{\beta}^2)V^2}e^{-\Gamma}}{4\pi^2r'^2r_1r_2}$$

and

$$\Gamma_{11LF} = \Gamma_{11coh} + \frac{gAf^2(\theta)e^{-g}\,W(0,|k\beta|)}{4\pi\sigma^2(r'r)^2} \tag{5.13}$$

$$\text{with } \Gamma_{11coh} = \frac{A^2k^2f^2(\theta)e^{-\frac{k^2}{2}V^2\tilde{\beta}^2}e^{-g}}{4\pi^2(r'r)^2}$$

for the covariance and intensity respectively. W is the cartesian-surface spectrum.

The Slope-Operator Model in the Fraunhofer approximation, Eq. (3.59), gives

$$\Gamma_{12LF} = \frac{Ak^2e^{ik(r_1-r_2)}e^{-\frac{k^2}{8}[\beta^2V^2]}e^{-\Gamma}}{2r'^2r_1r_2\gamma_1\gamma_2}\left\{\frac{A}{2\pi^2}\,\gamma_1\gamma_2\sin\theta_1\sin\theta_2 e^{-\frac{k^2}{2}\tilde{\beta}^2V^2}\right.$$

$$+\frac{G}{2\pi\sigma^2}\,W(0,|k\tilde{\beta}|)[\gamma_1\gamma_2\sin\theta_1\sin\theta_2+\cos\theta_1\cos\theta_2\tilde{\beta}^2-$$

$$(\cos\theta_2\sin\theta_1\gamma_1+\cos\theta_1\sin\theta_2\gamma_2)\tilde{\beta}]$$

$$+\left(\frac{G}{2\pi\sigma^2k}\right)^2\int_{-\infty}^{\infty}d\chi W(\chi)W(-\chi_x;\chi_y-k\tilde{\beta})\chi_y k[(\cos\theta_2\sin\theta_1\gamma_1+\cos\theta_1\sin\theta_2\gamma_2)$$

$$\left.-\bar{\beta}\cos\theta_1\cos\theta_2]\right\} \tag{5.14}$$

and (3.60) yields

$$\Gamma_{11LF} = \frac{Ak^2e^{-g}}{2(r'r)^2\gamma^2}\left\{\frac{A}{2\pi^2}\gamma^2\sin^2\theta_1 e^{-\frac{k^2}{2}\tilde{\beta}^2V^2} + \frac{g}{2\pi\sigma^2}W(0,|k\tilde{\beta}|)\right.$$

$$[\gamma^2\sin^2\theta_1+\cos^2\theta_1\tilde{\beta}^2-2\cos\theta_1\sin\theta_1\gamma\tilde{\beta}]$$

$$\left.+\left(\frac{g}{2\pi\sigma^2k}\right)^2\int d\chi We(\chi)W(-\chi_x,-\chi_y-k\tilde{\beta})\chi_y k[2\cos\theta_1\sin\theta_1\gamma-\tilde{\beta}\cos^2\theta_1]\right\} \tag{5.15}$$

for covariance and intensity. In both equations the highest order correction is neglected.

b. Very Rough Surface

For the Standard Model the covariance and intensity are respectively

$$\Gamma_{12HF} = \frac{A^2k^2f_1(\theta)f_2(\theta)e^{ik(r_1-r_2)}e^{-\frac{k^2}{8}(\beta^2+\frac{4\tilde{\beta}^2}{B_2^2})V^2}e^{-\frac{G}{2}T_o}}{4\pi^2r'^2r_1r_2B_1B_2} \tag{5.16}$$

and

$$\Gamma_{11HF} = \frac{A^2k^2f^2(\theta)e^{-\frac{k^2\tilde{\beta}^2V^2}{2B_2^2}}}{4\pi^2(r'r)^2B_1B_2} \tag{5.17}$$

using (3.30) and (3.31).

The Slope-Operator Model expressions, using (3.61) and (3.62), are

$$\Gamma_{12SF} = \frac{Ak^2 e^{ik(r_1-r_2)}}{2r'^2 r_1, r_2 \gamma_1 \gamma_2} e^{-\frac{k^2}{8}\beta^2 V^2} e^{-\frac{GT_o}{2}} \left\{ \frac{A}{2\pi^2 B_1 B_2} \gamma_1 \gamma_2 \sin\theta_1 \sin\theta_2 \right.$$

$$e^{-\frac{k^2}{2}\frac{\tilde{\beta}^2 V^2}{B_2^2}} + \frac{G}{2\pi\sigma^2} W(0, |k\tilde{\beta}|)[\cos\theta_1 \cos\theta_2 \tilde{\beta}^2 -$$

$$(\cos\theta_2 \sin\theta_1 \gamma_1 + \cos\theta_1 \sin\theta_2 \gamma_2)\tilde{\beta}]$$

$$\left. - \left(\frac{G}{2\pi\sigma^2 k}\right)^2 \int_{\infty}^{\infty} d\chi W(\chi) W(-\chi_x, -\chi_y - k\tilde{\beta}) \chi_y (\chi_y + k\tilde{\beta}) \right\} \qquad (5.18)$$

and

$$\Gamma_{11SF} = \frac{Ak^2}{2(r'r)^2 \gamma^2} \left\{ \frac{A}{2\pi^2 B_1 B_2} \gamma^2 \sin^2\theta_1 e^{-\frac{k^2}{2}\tilde{\beta}^2 \frac{V^2}{B_2^2}} + \frac{g}{2\pi\sigma^2} W(0, |k\tilde{\beta}|) \right.$$

$$\left. [\cos^2\theta_1 \tilde{\beta}^2 - 2\cos\theta_1 \sin\theta_1 \gamma \tilde{\beta}] - \left(\frac{g}{2\pi\sigma^2 k}\right)^2 \int_{-\infty}^{\infty} d\chi W(\chi) W(-\chi_x, -\chi_y - k\tilde{\beta}) \chi_y (\chi_y + k\tilde{\beta}) \right\}$$

(5.19)

With GT_1 and GT_2 very small. The added constants come from the normalization factor required for this particular case.

2. Composite-Roughness Model

The two alternatives: using eq. (3.68), which is the conventional approach, leads to

$$\Gamma_{12} = \frac{Ak^2 f_1(\theta) f_2(\theta) e^{ik(r_1 - r_2)} e^{-\frac{k^2\beta^2V^2}{8}} e^{G(\frac{\sigma_L}{\sigma})^2 - \Gamma}}{2r'^2 r_1 r_2}$$

$$\left\{ \frac{A}{2\pi^2 R_1 R_2} e^{-\frac{1}{2}\left(\frac{k\tilde{\beta}V}{R_2}\right)^2} + \frac{G}{2\pi\sigma^2} W(0, |k\tilde{\beta}|) u(\kappa_L - |k\tilde{\beta}|) \right\} \tag{5.20}$$

for covariance and for intensity

$$\Gamma_{11} = \frac{Ak^2 f^2(\theta) e^{g[(\frac{\sigma_L}{\sigma})^2 - 1]}}{2(r'r)^2} \left\{ \frac{A}{2\pi^2 R_1 R_2} e^{-\frac{1}{2}(\frac{k\tilde{\beta}V}{R_2})^2} + \frac{g}{2\pi\sigma^2} W(0, |k\tilde{\beta}|) u(\kappa_L - |k\tilde{\beta}|) \right\} \tag{5.21}$$

σ_L is the rms height and σ'_x and σ'_y are the rms slopes of the large-scale surface, u is the Heaviside function. The quantity $R_1 R_2$ can be replaced by $G\sigma'_x\sigma'_y/\sigma^2$, a quantity that must remain small for these expressions to be valid.

When the Slope-Operator is incorporated, the integrations in (3.72) and (3.73) yield

$$\Gamma_{12} = \frac{Ak^2 e^{ik(r_1 - r_2)} e^{-\frac{k^2\beta^2V^2}{8}} e^{G(\frac{\sigma_L}{\sigma})^2 - \Gamma}}{2r'^2 r_1, r_2 \gamma_1 \gamma_2} \left\{ \frac{A}{2\pi^2 R_1 R_2} \gamma_1 \gamma_2 \sin\theta_1 \sin\theta_2 \right.$$

$$e^{-\frac{1}{2}\left(\frac{k\beta V}{R_2}\right)^2} + \left(\frac{G}{2\pi\sigma^2 k}\right) W(0, |k\tilde{\beta}|) [\gamma_1 \gamma_2 \sin\theta_1 \sin\theta_2 + \delta_1 \delta_2 \tilde{\beta}^2 -$$

$$(\delta_2 \sin\theta_1 \gamma_1 + \delta_1 \sin\theta_2 \gamma_2)] u(\kappa_L - |\tilde{k}\beta|)$$

$$+\left(\frac{G}{2\pi\sigma^2 k}\right)\int_{\ddagger}^{\infty} d\chi W(\chi)W(-\chi_x,-\chi_y-k\tilde{\beta})\chi_y k[(\delta_2\sin\theta_1\gamma_1+\delta_1\sin\theta_2\gamma_2)$$

$$-\delta_1\delta_2\beta]u(\kappa_L-|k\tilde{\beta}|)\Big\} \qquad (5.22)$$

and

$$\Gamma_{11F} = \frac{Ak^2 e^{g[(\frac{\sigma_L}{\sigma})^2-1]}}{2(r'r)^2\gamma^2}\left\{\frac{A\gamma^2}{2\pi^2 R_1 R_2}\sin^2\theta_1\, e^{-\frac{1}{2}\left(\frac{k\beta V}{R_2}\right)^2} + \frac{g}{2\pi\sigma^2}W(0,|k\tilde{\beta}|)\right.$$

$$[\gamma^2\sin^2\theta_1+\cos^2\theta_1\tilde{\beta}^2-2\cos\theta_1\sin\theta_1\gamma\tilde{\beta}]u(\kappa_L-|k\tilde{\beta}|)$$

$$\left.+\left(\frac{g}{2\pi\sigma^2 k}\right)^2\int_{\ddagger}^{\infty} d\chi W(\chi)W(-\chi_x,-\chi_y-k\tilde{\beta})\chi_y k(2\cos\theta_1\sin\theta_1\gamma-\cos^2\theta_1\tilde{\beta})u(\kappa_L-|k\tilde{\beta}|)\right\} \qquad (5.23)$$

3. Discussion

The spectral part of the above equations can be recast in cylindrical polar coordinates, which is more convenient than cartesian when the surface is omni-directional. In that case the following changes occur:

$$\chi_x = \kappa\sin\Omega$$

$$\chi_y = \kappa\cos\Omega$$

$$W(0,|k\tilde{\beta}|) = \frac{S(|k\tilde{\beta}|)}{|k\tilde{\beta}|}$$

$$d\chi W(\chi) = \kappa d\kappa d\Omega\,\frac{S(\kappa)}{\kappa},$$

and $W(-\chi_x, -\chi_y - k\bar{\beta}) = \frac{S(\eta)}{\eta}$

where $\eta = \sqrt{\kappa^2 + 2\kappa k\bar{\beta}\cos\Omega + k^2\bar{\beta}^2}$, the positive root.

The spectral integrals will span over κ from 0 to infinity and Ω from 0 to 2π, except in the Composite-Roughness Model, in which the span of κ is from κ_L to infinity.

Figures 32 a and b are plots of the backscattered and forward scattered scattering strength as per equation (5.17). In these computer runs the source and receiver were set at 1000 cm from the ensonified surface. The wind 1000 cm above the surface was 514.4 cm/s and the source was given a 1° beamwidth. In the forward scatter test the source had a 45° depression angle. It is apparent in Figure b that far away from the specular direction, i.e., for receiver angles greater than 120° or so, the model begins to fail and the effect is more severe for lower frequencies. The reason for this is that for small U and V, the source wavenumber k must be large in order for the conditions kV>>1 and kU>>1 to prevail.

A comparison of the prediction of equation (5.17) with that of (5.19) in the backscatter test case is shown in Figures 33a and b. These are, respectively, the Standard Model and the Slope-Operator Model for source/receiver distance of 1000 cm, 1 degree beam and 20 KHz. The wind is 514.4 cm/s at 1000 cm above the surface. The Slope-Operator Model and the Composite-Roughness Model using equation (5.21) are compared next in Figures 34a and b. In this case the source is 70

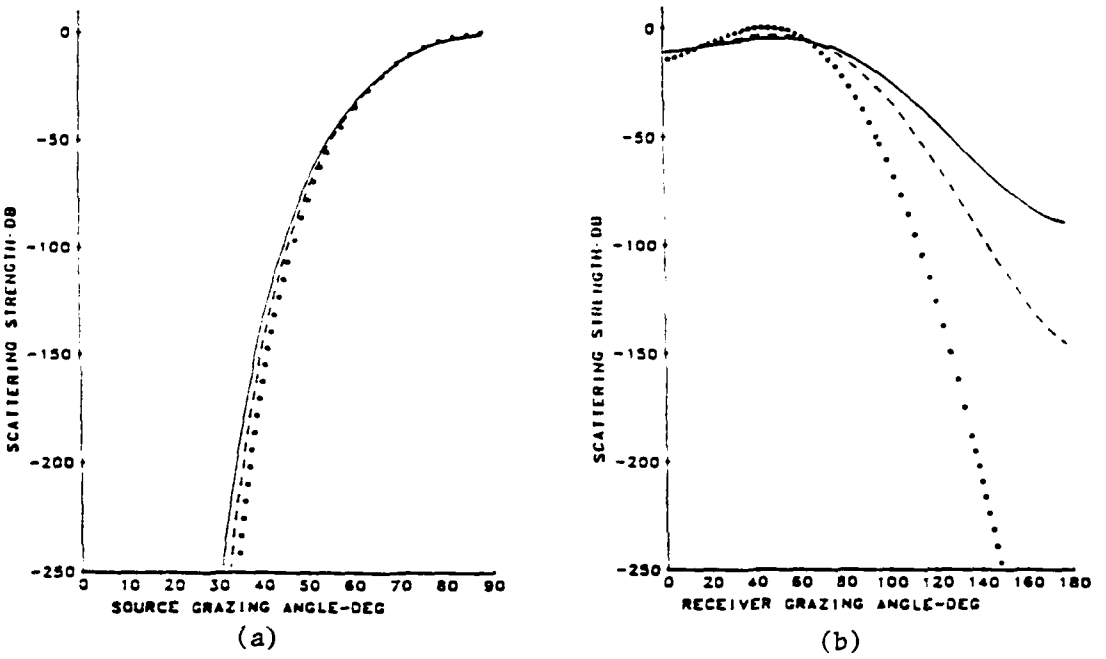

Figure 32. Scattering strength. Eq. (5.17) (a) backscatter, (b) forward scatter. Receiver/source at 1000 cm. 1° beamwidth. Wind at 1000 cm is 514.4 cm/s. ____: 15 KHz, ----: 20 KHz, ****: 50 KHz.

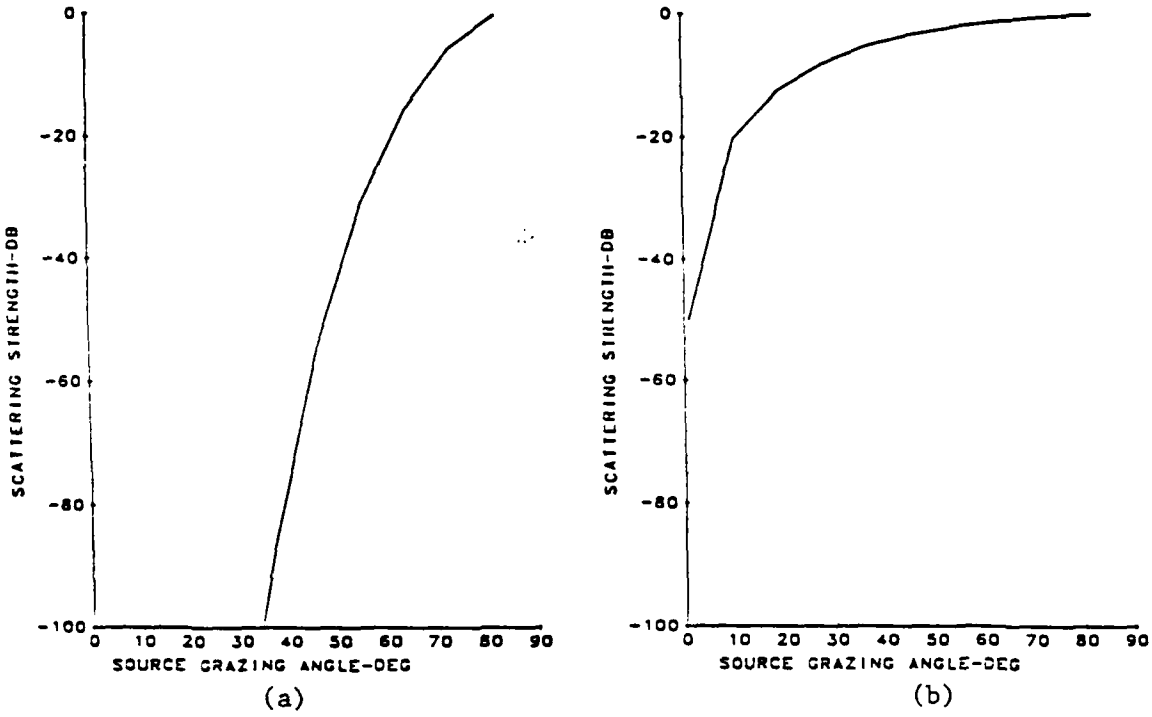

Figure 33. Backscatter. (a) Eq. (5.17) standard model, (b) eq. (5.19) slope-operator model. 20 KHz 1° beamed source. Wind at 1000 cm is 514.4 cm/s

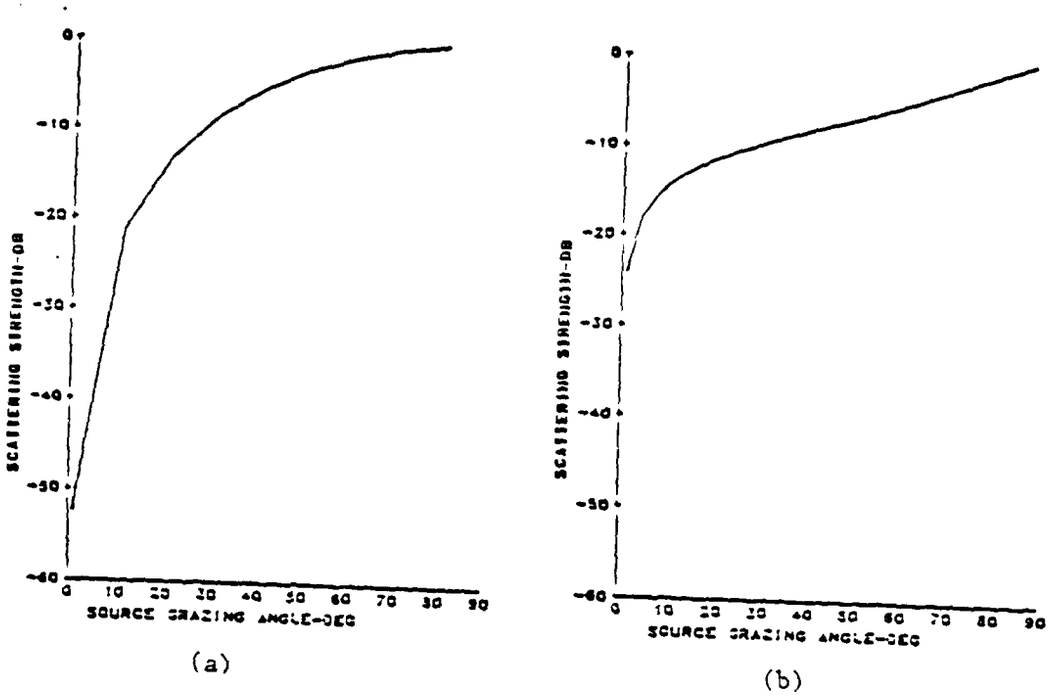

Figure 34. Backscatter. Source at 70 cm operating at 10 KHz with 1° beam. Wind at 1000 cm is 514.4 cm/s, (a) slope-operator model, (b) conventional composite-roughness model.

cm away and all other parameters discussed above are held fixed. Figure 34b shows the characteristic Bragg resonance dip in the backscatter plots, which are typical of the experimental findings. The dip is more noticeable when the beamwidth is narrow - see Figures 35a and b.

Figures 35a, b, and 34b have all been plotted using a quarter source wavenumber value for spectral cutoff value κ_L. The choice of cutoff is not at all given by the theory itself. Figures 36a, b, and c show the variation in the backscatter with choice of cutoff wavenumber. In these figures the frequency is 10 KHz and the choice of κ_L is (a) equal to the source wavenumber, (b) .8 times the wavenumber, (c) 0.25 times the wavenumber.

Another feature of the Composite-Roughness Model as per equations (5.21) and (5.23) is that care must be exercised in order to not operate out of the bounds of the regime of validity. Assuming the beamwidth is small, the four conditions that must be satisfied are:

(a) $GC_s \ll 1$, which leads to $G\frac{\sigma_s^2}{\sigma^2} \ll 1$. This permits the series expansion of the exponential involving GC_s and the retention of the first two terms.

(b) $\sigma_L''^4 R^4 \ll 24\sigma_L^2 - 12\sigma_L'^2 R^2$, where R is a radial distance on the insonified area. In order for the Taylor series expansion of the large-scale surface autocorrelation to remain valid, eq. (3.66), the terms higher than second order must be insignificant compared to those retained.

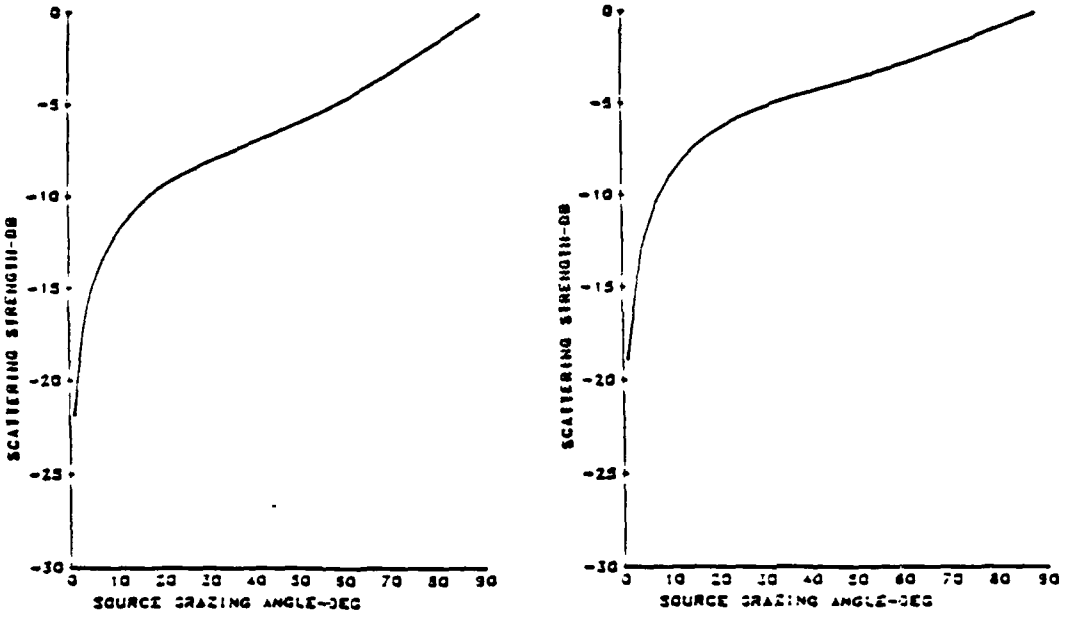

Figure 35. Conventional composite-roughness model. Backscatter for a source at 70 cm from surface. 10 KHz source with (a) 1° beamwidth, (b) 3° beamwidth. Wind at 1000 cm is 514.4 cm/s.

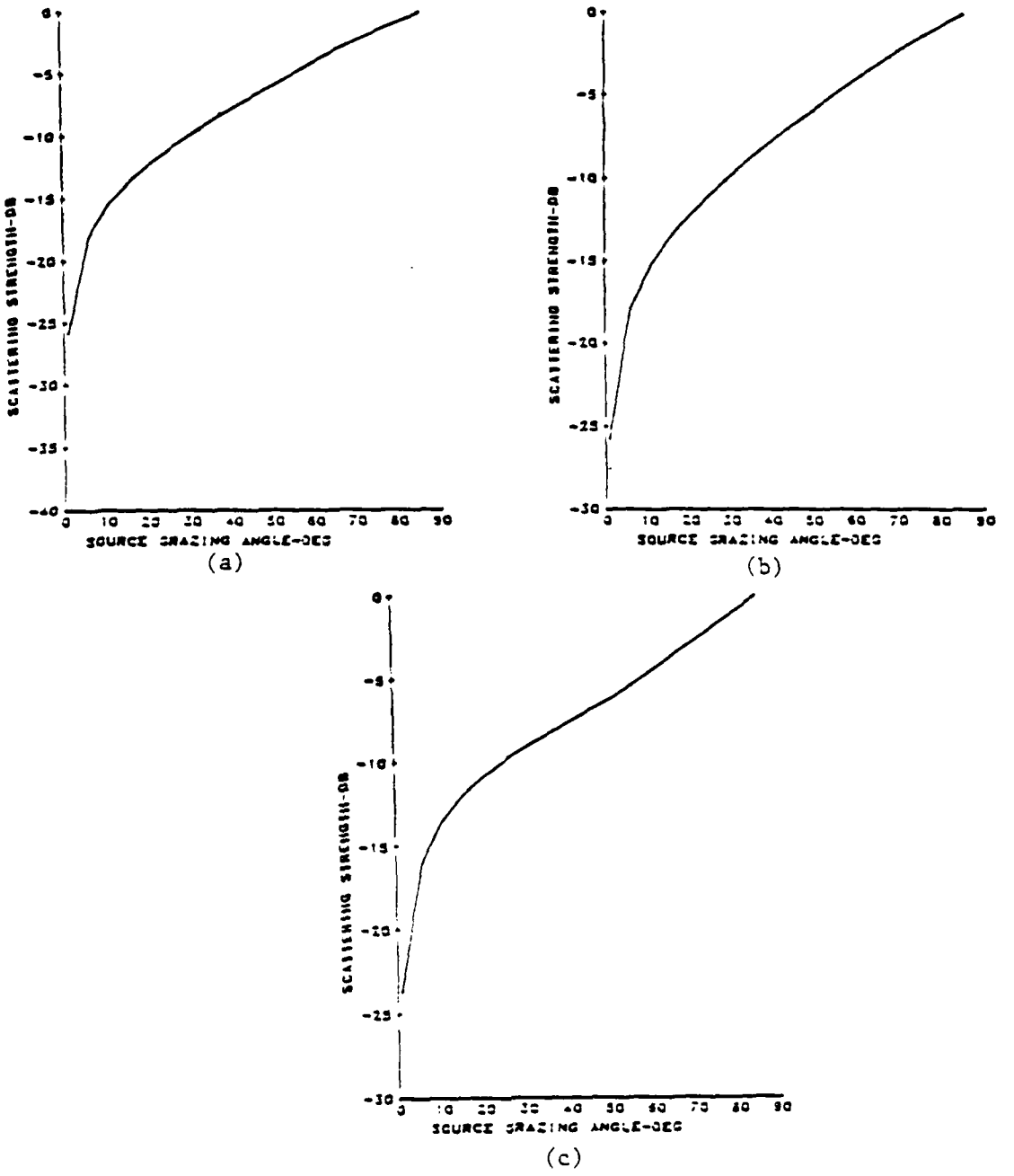

Figure 36. Backscatter. Composite-roughness model-conventional (a) κ_L = 1 wavenumber, (b) κ_L = 0.8 wavenumber (c) κ_L = 0.2 wavenumber.

(c) U and V must be of comparable or smaller size than R. This is necessary because an early assumption of the TPM was that the integral over the entire surface was the same as the integral over the insonified portion due to the minute contribution of the integrand outside of this region. As well, it is necessary for the quadratic terms in the spatial integrations of (3.70) to be such that $U^{-2} >> G\sigma_x'^2/\sigma^2$ and $V^{-2} >> G\sigma_y'^2/\sigma^2$ in order to permit the integration over all space.

(d) Related to the generalized function integration, it is necessary that $V^{-2}+4k^2\sin^2\theta\sigma_y'^2 << 1/2$ and $U^{-2} +4k^2\sin^2\theta\sigma_x'^2 << 1/2$ because the delta-like integration becomes possible when $2R_2^2/V^2 << 1$ and $2R_1^2/U^2 <<1$.

The Pierson-Stacy report on ocean spectra (42) is to the author's knowledge the best study available in the open literature. The report is not considered to be a definitive study on the subject owing to the fact that it is a compilation of reports made by several investigators who considered limited surface wavenumber ranges in different experimental conditions, using a wide range of measuring techniques. In fact, most investigators agree that a thorough and reliable study on the ocean spectrum would be welcomed, but the task has not been performed due to the challenges involved with the measurement of spectra in the open sea.

This chapter has been devoted mainly to the in-plane case, hence the use of the omnidirectional spectrum $W(\chi) = S(\kappa)/\kappa$. The non-coplanar case would be most interesting and general, if the directional

spectrum is utilized instead of the omnidirectional one used here. This would require making none of the geometrical simplifications used in the in-plane situation, as well as the incorporation of angular variation in the spectrum function.

Angular variation in the spectrum would be expressed in the form

$$W(\kappa,\Omega) = S(\kappa)F(\kappa,\Omega) \tag{5.29}$$

with $S(\kappa)$ being the non-directional function used in this study and $F(\kappa,\Omega)$ most researchers aegree has a general form

$$F(\kappa,\Omega) \propto G(s)|\cos\tfrac{1}{2}(\Omega-\Omega')|^{2s} \tag{5.30}$$

where s is a function of κ such that $F(\kappa,\Omega)$ tends to a narrower and higher amplitude angular distribution (44) and G(s) is a normalization function such that the integral over all wavenumber space of equation (5.29) is one. The constant Ω' is aligned with the mean wind velocity direction.

The surface autocorrelation can be a function of time as well. This implies that the surface has a well defined temporal dependence and that the covariance will be space as well as time dependent. The autocorrelation function can have an envelope which travels in time with same group velocity. A case in point (38, p. 518) would be the wind-blown water waves, for which the autocorrelation can be

$$C \doteq \exp\left[\frac{-(\frac{Y}{u} - \tau)^2}{T^2}\right] \cos\left[\Omega(\frac{Y}{v} - \tau)\right] \exp(-bx^2) \qquad (5.31)$$

where the waves are moving in the $\hat{y}$ direction with phase velocity v and angular frequency Ω. The envelope travels with group velocity u and is coherent within an approximate range τ in time. In the $\hat{x}$ direction it dies off by virtue of the paramater b, the length of each crest.

In this type of highly organized surface states, the spatial and temporal components of the autocorrelation are not separable. In a confused sea, the waves travel in all directions and we would expect the spatial correlation function to be isotropic, as was assumed in this study, and that the spatial and temporal components be separable.

CHAPTER VI

SUMMARY AND SUGGESTIONS FOR FURTHER STUDY

In this study two different philosophies for representing the scattered field when a randomly-rough surface is involved have been presented. The MSP is simple, adequate when the roughness is very slight. It doesn't rely on the Kirchhoff approximation and will tolerate steep slopes. The scatter is diffuse, whereas the TPM consider it more of a distortion. The TPM does not handle steep slopes but can work well with rough surfaces. The drawbacks of the latter are the use of the Kirchhoff approximation as well as cumbersome mathematics.

Within the TPM, several variants have been presented. The Standard Model, simplest of all, is ill behaved for angles far from the specular direction because the incoherent component makes bad estimates of its contribution and because an assumption in the integration-by-parts techniques is that the angular dependence is a function which is nearly constant so that that it can be removed from the integral.

The other extreme in complexity is the Slope-Operator Model, which is shown to behave properly for all grazing angles. This model is compared when the surface is slightly rough to the case when the

gradient of the normal of the surface is approximated by $\partial/\partial z$. In effect this is a comparison between the full model and the coherent component itself and the two obvious shortcomings are that the latter does not incorporate any spectral information, nor does it apply to other than low frequency cases. The Slope-Operator model is presented using both the Fraunhofer and Fresnel phase approximation. The Fresnel case is more complicated and presents no more information than the Fraunhofer model in the farfield. In principle the Fraunhofer case will diverge in the specular direction if no source beampattern is used. This is because the integral over the ensonified area is assumed to be the same as the integral between minus and plus infinity, since the integrand with a Gaussian beampattern restricts significant contributions to the ensonified area. The Fresnel approximation presented in this study is derived using the binomial expansion. This alternative is admittedly poor when compared to a power series expansion in the phase but is considerably easier to implement.

Lastly, the MSP and TPM are effectively merged in the Composite-Roughness Model. It is rather easy to implement and offers good results when the surface spectra can be divided into two distinct regimes. However, the model is very sensitive to the choice of spectral partitioning when it is not apparent where the division in the spectrum is to be made.

Expressions for the covariance and intensity were developed. The coherent component of the intensity is shown to be a good estimator of

surface roughness. Spectral content turns up in the incoherent component. The covariance of the field is shown to be analogous to the mutual covariance quantity whereas the intensity is the same as the self-covariance.

No attempt was made to conduct an in-depth coherence study, but several examples were provided so that the models can be compared and some qualitative features of coherence calculations can be highlighted. The coherence is shown to drop with increasing beamwidth and frequency. This feature is useful in interferometric partial coherence studies. When the Fraunhofer phase approximation is used, the coherence phase is determined solely by the wavenumber times the difference in magnitude of the distances between the surface and the two receivers. The point was made that the horizontal coherence tends to vary very little compared to the vertical coherence because the random processes considered are a function of vertical coordinates. Coherence is a good estimator of source localization and it provides considerable spectral information.

Although partial coherence is a well-developed theory in the field of optics, in acoustics, a comprehensive theory encompassing the fundamental notions is yet to be formulated. The acoustics community would undoubtedly welcome a monograph in this area.

In optical coherence studies, rapidity of phase fluctuations is the primary challenge, whereas in acoustics the difficulty is that near perfect shadows are unattainable in an important frequency range. These aspects, along with the distinctly different near-field characteristics and the polarization, must be dealt with differently in acoustics.

Reliable experimental data on coherence measurements involving Gaussian surfaces as well as the ocean surface is needed in order to make an assessment of the validity of the several models presented in this study. Exact numerical evaluation of equations (2.1) and (2.2) would permit an analysis of the validity and interaction of the many assumptions and approximations made in this study, as well as a means of comparing the two equations for similarity in results. A difficult but necessary project is the measurement of the ocean spectra under more controlled and consistent conditions. The tabulation of the surface autocorrelation could be performed as once did Fortuin and deBoer (12), Latta (45), and Mellen (46) with the outdated Roll-Fisher and Neumann-Pierson spectra.

Time dependence can be introduced in the problem, so that a model for spatial and temporal covariance can be formulated. Time coherence would enable the determination of finite spectral width of the scattering surface and surface movement, in addition to surface autocorrelation "movement." The directional spectrum and full geometric implementation would be most useful in this case.

A logical and extremely useful continuance of this work would be: (1) the quantitative analysis of the sensitivity of the models to field

fluctuations, (2) the importance of higher-order multiple scatter terms to coherence calculations, (3) the contribution of multiple scatter to field flucations, and (4) the development of covariant expressions that are valid in the near-field.

Derivation of expressions for higher-order moments (which are less sensitive to inhomogeneities in the media) is required for a theory of partial coherence, particularly if the general theory for Gaussian as well as non-Gaussian surfaces is formulated. Though higher order moments do not provide any new information if the surface is Gaussian, they do so, however, for non-Gaussian surfaces. The theory underlying non-Gaussian surface statistics can be found in Beckmann's paper (38).

REFERENCES

1. Born, M., Wolf, E., Principles of Optics, The MacMillan Company, New York, 1959.

2. Issakovich, "Scatter of Waves from a Statistically rough Surface," Zh, Eksp. Teor, Fiz 23, 1952, pp. 305-3125.

3. Eckart, C., "The Scattering of Sound from the Sea Surface," J. Acoust. Soc. Am., 22, 1953, pp. 566-570.

4. Rice, S. O. "Reflection of Electromagnetic Waves from Slightly Rough Surfaces," Commun. Pure Appl. Math, 4, 1951, pp. 351-378.

5. Kur'yanov, B. F., "The Scattering of Sound at a Rough Surface with Two Types of Irregularity," Sov. Phys. Acoust., 8, 1963, pp. 252-257.

6. McDaniel, S. T., Gorman, A. D., "An Examination of the Composite-Roughness Scattering Model," J. Acoust. Soc. Am., 73, 1983, pp. 1476-1485.

7. McDaniel, S. T., "Diffractive Corrections to the High Frequency Kirchhoff Approximation," J. Acoust. Soc. Am., 79, 1986, pp. 952-957.

8. Clay, C. S., Medwin, H., "Dependence of Spatial and Temporal Correlation of Forward Scattered Underwater Sound on the Surface Statistics II Experiment," J. Acoust. Soc. Am., 47, 1970, pp. 1419-1429.

9. Gulin, E. P., Malychev, K. I., "Spatial Correlation of Amplitude Fluctuations of a Continuous Tone with a Reflection from Ocean Surface Waves," Sov. Phys. Acoust., 4, p. 428.

10. Gulin, E. P., Malychev, K. I., "Experiments in the Spatial Correlation of the Amplitude and Phase Fluctuations of Acoustic Signals Reflected from a Rough Ocean Surface," Sov. Phys. Acoust., 10, p. 365.

11. Neklyudov, V. I., Chuprov, S. D., "Spatial and Frequency Correlation of the Amplitude Fluctuations of Sound Signals," Sov. Phys. Acoust., 19, p. 255.

12. Fortuin, L., deBoer, J. G., "Spatial and Temporal Correlation of the Sea Surface," J. Acoust. Soc. Am, 49, 1971, pp. 1677-1679.

13. Bass, F. G., Fuks, I. M., Wave Scattering from Statistically Rough Surfaces, Pergamon Press, New York, 1979.

14. Clay, C. S., Medwin, H., "Dependence of Spatial and Temporal Correlation of Forward Scattered Underwater Sound on the Surface Statistics I Theory," J. Acoust. Soc. Am., 47, 1970, pp. 1412-1418.

15. Gulin, E. P., "The Correlation of Amplitude and Phase Fluctuations in Sound Waves Reflected from a Statistically Rough Surface," Sov. Phys. Acoust., 8, 1963, pp. 335-339.

16. Parkins, B. E., "Coherence of Acoustic Signals Reradiated from the Time Varying Surface of the Ocean," J. Acoust. Soc. Am., 45, 1969, pp. 119-123.

17. Kinney, W. A., Clay, C. S., "The Spatial Coherence of Sound Scattered from a Wind-driven Surface: Comparison between Experiment, Eckart Theory, and the Facet-ensemble Method," J. Acoust. Soc. Am., 75, 1984, pp. 145-148.

18. Pierson, W. J., The Theory and Applications of Ocean Wave Measuring Systems At and Below the Sea surface on the Land from Aircraft and from Spacecraft, NASA Contract, Rep. CR-2646, NASA, Washington, DC, 1976.

19. Strutt, J. W. (Lord Rayleigh), The Theory of Sound, The MacMillan Co., London, Vol. II, Section 272, London.

20. Rice, R. O., "Reflection of Electromagnetic Waves from Slightly Rough Surfaces," Com. Appl. Math, 4, 1951, pp. 351-378.

21. Mandel'shtan, L., The Roughness of Free-Liquid Surfaces," Collection Izd-vo AN55R, 1948, pp. 246-260.

22. Brekhovskikh, L., Lysanov, Yu, Fundamentals of Ocean Acoustics, Springer-Verlag, Berlin, 1982.

23. Tamoikin, V. V., Fraiman, A. A., "The Statistical Properties of a Field Scattered by a Rough Surface," Izv VUZ, Radiofizika, 11, 1968, pp. 56-56. [English translation in Radiophysics and Quantum Electronics, 11, 1968, pp. 31-36.]

24. Jackson, J. D., Classical Electrodynamics, John Wiley & Sons, New York, 1975.

25. Welton, P. J., "A Theoretical and Experimental Investigation of the Scattering of Acoustic Waves by Randomly Rough Surfaces," ARL UT 75-30, Report, 1975.

26. Kellogg, O. D., Foundations of Potential Theory, Dover, New York, 1954.

27. Pogorzelski, W., Integral Equations and Applications, Pergamon Press, Oxford, 1966.

28. Colton, D., Kress R., Integral Equation Methods in Scattering Theory, John Wiley, New York, 1983.

29. Maue, A. N., "On the Formulation of a General Scattering Problem by Means of an Integral Equation," J. Phys., 126, 1949, pp. 601-618.

30. Morse, P. M., Feshbach, H., Methods of Theoretical Physics, Vol. I, McGraw-Hill, New York, 1953.

31. Wagner, R. J., "Shadowing of Randomly Rough Surfaces," J. Acoust. Soc. Am., 41, 1967, p. 138.

32. Tolstoy, I., Clay, C. S., Ocean Acoustics, McGraw-Hill, New York, 1966.

33. McDonald, J. F., Spindel, R. C., "Implications of Fresnel Corrections in a Non-Gaussian Surface Scatter Channel," J. Acoust. Soc. of Am., 1979, pp. 290-303.

34. Melton, D. R., Horton, C. W., "Importance of the Fresnel Correction in Scattering from a Rough Surface, I. Phase and Amplitude Fluctuation, II. Scattering Coefficient," J. Acoust. Soc. Am., 1979, pp. 290-303.

35. Brekhovskikh, L. M., "Diffraction of Waves by Irregular Surfaces," Zh. Eksp. Teor. Fiz, 24, Part I and II, 1952, pp. 275-304.

36. Boyd, M. L., Deavenport, R. L., "Forward and Specular Scattering from a Rough Surface: Theory and Experiment," J. Acoust. Soc. Am., 53, 1973, pp. 791-801.

37. Grobner, W., Hofreiter, N., Integraltafel Zweiterteil Bestimute Integrale, Springer-Verlag, 1950.

38. Clay, C. S., Medwin, H., Acoustical Oceanography, Wiley Interscience, John Wiley, New York, 1977.

39. Ruffine, R., "Note on the Scattering of Waves by Rough Surfaces," IEEE Trans., AP 12, 1964, p. 802.

40. Parkins, B. E., "Omnidirectional Scattering of Acoustic Waves by Rough, Imperfectly Reflecting Surfaces," J. Acoust. Soc. Am., 41, 1967, pp. 126-134.

41. Middelton, D., An Introduction to Statistical Communication Theory, McGraw-Hill, New York, 1960.

42. Pierson, W. J., Stacy, R. A., The Elevation Slope and Curvature Spectrum of a Wind Roughened Sea Surface, NASA Contract, Rep. (R-24), NASA, Washington, DC 1973.

43. Beckmann, P., Spizzichino, A., The Scattering of EM Waves from Randomly Rough Surfaces, Pergamon Press, New York, 1963.

44. Mitsuyasu, H., Tasai, F., et al., "Observations of the Directional Spectrum of Ocean Waves Using a Cloverleaf Buoy," Journal of Physical Oceanography, 5, 1975, pp. 750-760.

45. Latta, G. E., "On the Autocorrelation Functions of Wind Generated Ocean Waves," Zeit. Math. Phys., 9, 1968, pp. 575-586.

46. Mellen, R. H., "Directional Correlation Functions of the Sea Surface, J. Acoust. Soc. Am., 1974, pp. 1084-1085.

47. Beckmann, P., "Scattering by Non-Gaussian Surfaces," IEEE Antennas and Propagation, 1973, pp. 169-175.

48. McCammon, D. F., Personal Communication (September 1986).

APPENDIX

THE PIERSON-STACY SPECTRUM

The non-directional ocean wavenumber elevation spectrum is included here for convenience. This summary has been extracted word for word from a summary prepared by McCammon (48) on the subject of the Pierson-Stacy (42) Reports.

This wavenumber elevation spectra is non-directional with the units of cm^3 and is related to the RMS waveheight by

$$\langle \sigma^2 \rangle = \int_0^\infty W(K)dK. \tag{A.1}$$

The spectral equations for each region are

(1) Pierson Moskowitz region

$$W_1(K) = \alpha \exp[-B/K^2]/(2K^3). \tag{A.2}$$

(2) Stacy region

$$W_S(K) = (2.04x10^5+1.02x10^4U_*)\exp[-79.2K^{1/2}]/K^{1/2} \tag{A.3}$$

(3) Kitaigorodskii region

$$W_2(K) = \alpha/(2\beta^{1/2}K^{5/2}). \tag{A.4}$$

(4) Leykin-Rosenberg range

$$W_3(K) = W_4(K_3)(K/K_3)^q. \tag{A.5}$$

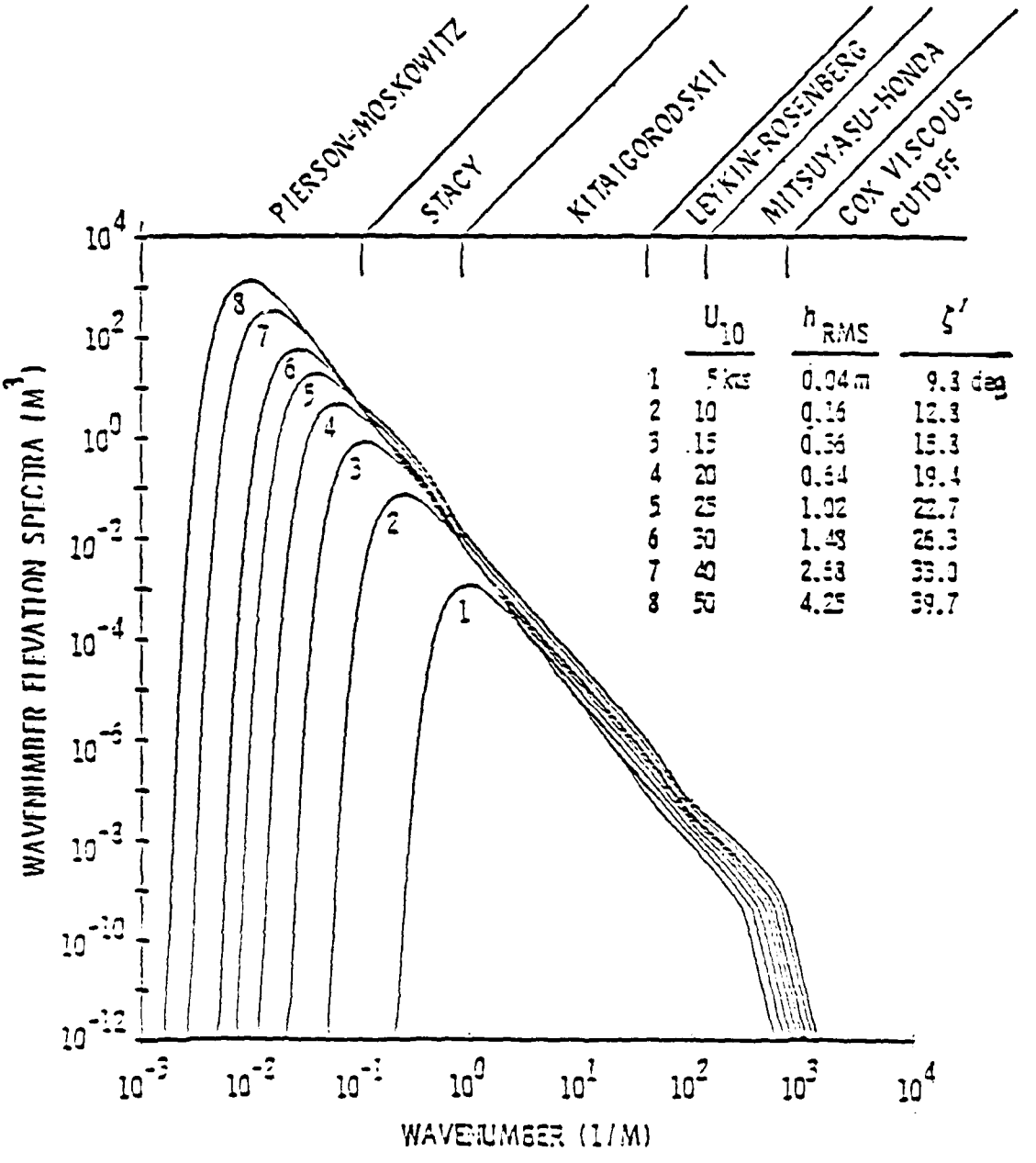

Figure A.1 Pierson wavenumber elevation spectrum.

(5) Mitsuyasu-Honda range

$$W_4(K) = 0.875(2\pi)^{p-1}(1+3\tau K^2)/(g^{(p-1)/2}(K+K^3\tau)^{(p+1)/2}). \quad (A.6)$$

(6) Cox viscous cutoff range

$$W_5(K) = 7.04\times10^{-3}\ U_*^3/K^9. \quad (A.7)$$

where $\alpha = 8.1\times10^{-3}$

$\beta = 0.74\ g^2/U^4_{19}$,

$q = 51.71/U_*^2$,

$p = 5.0 - \log_{10}[U_*]$,

$\tau = 7.58\times10^{-2}$,

$g = 980.$

These regions are linked together in K space as

$$W(K) = \begin{cases} W_1(K) & 0<K<K_i \\ \max\{W_S(K), W_1(K)\} \text{ if } U_* \geq 35.8 \text{ else use } W_1(K) & K_i<K<K_1 \\ \max\{W_S(K), W_2(K)\} \text{ if } U_* \geq 75.76 \text{ else use } W_2(K) & K_1<K<K_2 \\ W_3(K) & K_2<K<K_3 \\ \min\{W_4(K), W_5(K)\} & K_3>K \end{cases}$$

where

K_i - $0.702g/U_{19}^2$,

K_1 - $51.71/U_*^2$,

K_2 - 0.359,

K_3 - 0.942,

U_{19} - wind speed at 19.5 m,

U_* - friction velocity obtained from the equations,

$$U_z = U_* \ln(z.z_o)/0.4,$$

$$z_o = 0.684/U_* + 4.28\text{x}10^{-5}U_*^2 - 0.0443.$$

The units of these equations are CGS, W(K) is given in cm^3, K in cm^{-1}, U_{19} in cm/sec.

END

DATE

FILMED

6-1988

DTIC